



HAL
open science

Aero-acoustic sources localization and high resolution imaging

Jad Abou Chaaya

► **To cite this version:**

Jad Abou Chaaya. Aero-acoustic sources localization and high resolution imaging. Other. Centrale-Supélec, 2015. English. NNT : 2015CSUP0016 . tel-01346461

HAL Id: tel-01346461

<https://theses.hal.science/tel-01346461>

Submitted on 19 Jul 2016

HAL is a multi-disciplinary open access archive for the deposit and dissemination of scientific research documents, whether they are published or not. The documents may come from teaching and research institutions in France or abroad, or from public or private research centers.

L'archive ouverte pluridisciplinaire **HAL**, est destinée au dépôt et à la diffusion de documents scientifiques de niveau recherche, publiés ou non, émanant des établissements d'enseignement et de recherche français ou étrangers, des laboratoires publics ou privés.



CentraleSupélec



N d'ordre : 2015-16-TH

CentraleSupélec

ÉCOLE DOCTORALE STITS

"Sciences et Technologies de l'Information, des Télécommunications et des Systèmes"

THÈSE DE DOCTORAT

DOMAINE : STIC

Spécialité : Traitement du signal

Soutenue le 30/06/2015

par:

Jad ABOU CHAAYA

Localisation de sources aéroacoustiques et imagerie à haute résolution

Aero-acoustic sources localization and high resolution imaging

Composition du jury :

ANTONI Jérôme	INSA Lyon	Professeur des universités	(Rapporteur)
FORSTER Philippe	Université Paris Ouest	Professeur des universités	(Président du jury)
MARCOS Sylvie	L2S, CNRS	Directeur de Recherche	(Directeur de thèse)
PICHERAL José	L2S, CentraleSupélec	Professeur associé	(Encadrant)
WANG Yide	Polytech Nantes	Professeur des universités	(Rapporteur)

Dedication

I dedicate this work to the person who sacrificed all of his time and energy for his wife and children. I devote my thesis to you Georges hoping it will make you look down from heaven and smile at what your son has achieved ! As I promised father, this is the beginning but not the end.

Abstract

One challenging issue in the array signal processing applications, is the localization of spatially distributed sources in vicinity of the array. The acoustic imaging application consists in mapping the positions and power of the sources by using an array of microphones aiming to reduce the contribution of noisy source in automobile and aircraft industries. However, as far as we know, methods for localizing and power estimating the sources based on their spatial extension are not really studied in the literature of acoustic imaging field. The present thesis is then motivated by this challenge.

Firstly, we extend the Coherently Distributed (CD) model and the Distributed Signal Parameter Estimator (DSPE) to the near-field case (NF-DSPE). The NF-DSPE requires the knowledge of the angular spread distribution of the sources, therefore, we propose a Joint Angle, Distance, Spread and Shape Estimator called JADSSE. It provides accurate estimation even when the angular spread shape distribution is unknown or imperfectly known and improves Direction of Arrival (DOA) separation of the CD sources.

Secondly, we extend the Decoupled DSPE (DDSPE) to near-field, yielding the NF-DDSPE. This method is based on decoupling the estimation of the DOA and the range from the estimation of the angular spread. The NF-DDSPE method allows to estimate the DOAs and ranges of CD sources without knowing their angular shape distributions. However when the angular spread is required, we propose the DADSSE which consists in using JADSSE with NF-DDSPE to successively estimate the DOA, the range of the source and then its spread and shape distribution.

Thirdly, considering the setup parameters of the Renault wind tunnel application, we build up the CD model considering the Cartesian coordinates and the two dimensional spatial spread of the source. Then, our previously proposed estimators are adapted to the two dimensional Cartesian case. Next, we propose two approaches for source power estimation. The first one uses the Generalized Beamforming pseudo-spectrum and the second one is a least square estimator based on the array correlation matrix. Both of the methods overcome the challenge of estimating weak power sources. Results show, on one side, the limitation of considering point source estimators for distributed sources, and on another side, the shape impact on the distributed source localization and on their power estimation.

Finally, the previously proposed methods are used on the Renault real data. Results show that the main contributing sources appear with the point and distributed source estimators with a slight variation for this latter. However, using the distributed source based estimators: i) we can show the presence of new CD sources; ii) we offer the spread and shape estimation to improve the characterization of these sources; iii) we detect overlapped aero-acoustic CD sources with NF-DSPE and JPSSE; iv) we increase the dynamic power range estimation to detect both weak and powerful sources. We provide a tool for a better mapping of the aero-acoustic sources by accounting the positions, spread, power and shape estimations.

Résumé

La localisation de sources distribuées à proximité de l'antenne présente un défi des applications du traitement d'antenne. L'imagerie acoustique présente une application intéressante qui consiste à déterminer les positions et les puissances de sources aéro-acoustiques à l'aide d'un réseau de microphones. L'objectif est de réduire la contribution des sources bruyantes dans les industries de transport comme les automobiles et les avions. Néanmoins, les méthodes de localisation et d'estimation de puissance des sources qui présentent un étalement spatial n'étaient pas vraiment étudiées dans le domaine de l'imagerie acoustique. D'où la motivation qui mène aux travaux de cette thèse.

D'abord, on étend le modèle de source Distribuées Cohérente (DC) et l'estimateur Distributed Signal Parameter Estimator (DSPE) en champ proche sous le nom de NF-DSPE. Cet estimateur exige la connaissance à priori sur la forme de distribution de la dispersion de la source, la raison qui nous motive à proposer une estimation conjointe de l'angle, la distance, la dispersion et la forme de la source nommée JADSSE. Cette méthode fournit des estimations précises même en absence de l'information sur la forme de la distribution qui décrit la dispersion de la source et améliore la séparation des Directions D'Arrivées (DDA) des sources DC.

Ensuite, on généralise l'estimateur DSPE en champ proche, le NF-DDSPE. La méthode est basée sur le découplage de l'estimation de la DDA et de la distance de l'estimation de la dispersion angulaire. Le NF-DDSPE permet l'estimation des DDA et des distances des sources DC sans la connaissance a priori des formes des distributions angulaires. Pourtant, afin d'estimer la dispersion de la source, on propose le DADSSE qui consiste à utiliser le JADSSE et le NF-DDSPE pour estimer successivement la DDA, la distance de la source et ensuite la dispersion et la forme de la distribution.

Puis, tenant compte de la configuration de l'application de la soufflerie de Renault, on construit le modèle de source DC considérant l'extension spatiale bidimensionnelle de la source paramétré en coordonnées Cartésiennes. Les estimateurs proposés antérieurement sont reformulés pour le cas bidimensionnelle Cartésien. Après, on propose deux approches pour l'estimation de la puissance des sources: la première exploite le pseudo-spectre de la formation de voies généralisées et la deuxième repose sur un estimateur de moindres carrés basé sur la matrice de corrélation de l'antenne. Les deux méthodes surmontent le défi d'estimer les sources moins puissantes. Les résultats montrent, d'un côté, l'inconvénient d'utiliser des estimateurs supposant des sources ponctuelles pour des sources distribuées, et d'un autre côté, l'avantage de considérer la forme de la source sur la localisation et l'estimation de la puissance.

Finalement, les méthodes proposées sont utilisées sur les données réelles de Renault. Nos résultats montrent que les principales sources aéro-acoustiques apparaissent avec les estimateurs de source ponctuelle et distribué. Cependant, utiliser des estimateurs basés sur l'étalement de la source (source distribuée): i) permet de localiser des nouvelles sources; ii) offre une estimation de la dispersion et de la forme pour améliorer la caractérisation de ces sources; iii) détecte des sources aéro-acoustiques très proches; iv) augmente la gamme d'estimation des puissances pour détecter à la fois les sources faibles et dominantes. En conclusion, on fournit un outil pour une meilleure cartographie des sources aéro-acoustiques qui considère l'estimation de la position, l'étalement, la puissance et la forme.

Contents

1	Introduction	1
1.1	Context	1
1.1.1	Applications	2
1.1.2	Problem Statement and Motivation	2
1.2	Main Contributions	4
1.3	Thesis Structure	6
1.4	Author's Publications	7
2	Modeling and Localizing Distributed Sources	9
2.1	Signal Models	10
2.1.1	Point Source Model	10
2.1.2	Discrete Distributed Model	12
2.1.3	Continuous Distributed Model	14
2.2	Classical Estimators	18
2.2.1	Classical Beam Forming	18
2.2.2	Generalized Beam Forming	20
2.3	High Resolution Estimators	21
2.3.1	Standard MUSIC	23
2.3.2	Generalized MUSIC for Distributed Sources	23
2.4	Near Field (NFE)	24
2.4.1	Near Field Estimator	25
2.4.2	Near Field Side Works	26
2.5	Conclusion	26
3	Estimator with Unknown Angular Spread Shape	27
3.1	Introduction	27
3.2	Signal Model of CD Source in Near-Field	28
3.3	Proposed Estimators	30
3.3.1	Near Field-DSPE	30

3.3.2	Joint Angle Distance Spread Shape Estimator (JADSSE)	31
3.4	Numerical Results	32
3.4.1	Criterion Analysis	32
3.4.2	JADSSE Performance	33
3.4.3	Performance versus SNR	37
3.4.4	Reconstruction of Angular Shape Distribution	39
3.4.5	Performance Versus the Angular Spread and Shape Parameters	41
3.4.6	Performance Versus DOA Separation	42
3.5	Conclusion	44
4	Decoupled Estimation of the DOA and Angular Spread of CD Sources	47
4.1	The DDSPE Method in Far-Field	48
4.1.1	Decoupling the Generalized Steering Vector in Far-Field	48
4.1.2	The ULA Particular Case	49
4.1.3	Decoupled DSPE	50
4.2	DDSPE Generalized to the Near-Field Case	52
4.2.1	Decoupling the Generalized Steering Vector in Near-Field	52
4.2.2	The Near-field DDSPE (NF-DDSPE)	54
4.2.3	Decoupled Angle Distance Spread and Shape Estimator (DADSSE)	55
4.3	Simulations Results	55
4.3.1	Mixture of Uniform Coherently Distributed (UCD) Sources	56
4.3.2	Mixture of Overlapping UCD and GCD Sources	58
4.3.3	Resolution of Mixed CD Sources	62
4.3.4	A Mixture of Raised-Cosine and Uniform CD Sources	63
4.4	Conclusions	64
5	Localization Estimators for Two Dimensional CD Sources	67
5.1	Problem Formulation	68
5.2	Modeling of Aero-acoustic Signal Source Propagation	69
5.2.1	Two Dimensional CD Source	69
5.2.2	2D Spatial Distributions	71
5.2.3	2D Signal Modeling for CD Sources	74
5.3	Classical Estimators	77
5.3.1	Near Field-CBF (NF-CBF)	77
5.3.2	Near Field-GBF (NF-GBF)	77
5.3.3	Near Field Estimator	78
5.4	Proposed Estimators	78
5.4.1	Near Field-DSPE	78

5.4.2	Joint Position Spread Shape Estimator (JPSSE)	79
5.5	Power Source Estimators	79
5.5.1	CBF and GBF Power Estimators	79
5.5.2	Least Square (LS) Subspace Based Power Estimators	80
5.6	Synthetic Data for Source Imaging	81
5.6.1	Simulation Parameters	81
5.6.2	Methods Comparison and Reconstruction of Shape Distributions	82
5.7	Performance Analysis	88
5.7.1	Performance Versus SNR and Snapshots	89
5.7.2	Performance Versus Source Spread Δ and Shape β	92
5.8	Conclusion	92
6	Aero-acoustic Source Imaging	95
6.1	Wind Tunnel Experimentation	96
6.1.1	Configuration Setup for Real Data	96
6.2	Comparison of The Localization Methods	100
6.3	Influence of the Spread Distribution Shape	105
6.3.1	Localization	106
6.3.2	Spatial Power Distribution	106
6.4	Conclusions	107
7	Conclusions and Perspectives	111
7.1	Conclusions	111
7.2	Perspectives	113
	References	118

List of figures

2.1	Localization principle of a point source in far-field with ULA.	10
2.2	Localization of a distributed source in far-field	15
3.1	Localization of a distributed source in near-field	29
3.2	Plot of the cost function S for the Multi RCCD sources scenario at SNR=20dB. For each estimator S is plotted versus the DOA θ , spread Δ and for fixed parameters r_1, β_1 : $S(\Delta, \theta; r_1, \beta_1)$. True parameters for the first RCCD source: $\theta_1 = 0^\circ, \Delta_1 = 6^\circ, r_1 = 25\lambda$ and $\beta_1 = 0.5$, for the second RCCD source: $\theta_2 = 16^\circ, \Delta_2 = 16^\circ, r_2 = 25\lambda$ and $\beta_2 = 0.5$. Markers represent the maximum positions in the above criteria for the couple $(\hat{\Delta}, \hat{\theta})$. (\square : JADSSE, \diamond : NF-DSPE using uniform shape, \circ : NF-DSPE using Gaussian shape, ∇ : NF-DSPE using Butterworth shape).	34
3.3	Root Mean Square Error of the estimated parameters $\hat{\theta}, \hat{\Delta}, \hat{r}$ and $\hat{\beta}$ versus SNR for the first RCCD source in the mixed RCCD scenario. True parameters $\theta_1 = 0^\circ, \Delta_1 = 8^\circ, r_1 = 30\lambda$ and $\beta_1 = 0$	35
3.4	Root Mean Square Error of the estimated parameters $\hat{\theta}, \hat{\Delta}, \hat{r}$ and $\hat{\beta}$ versus SNR for the second RCCD source in the mixed RCCD scenario. True parameters $\theta_2 = 30^\circ, \Delta_2 = 10^\circ, r_2 = 25\lambda$ and $\beta_2 = 1$	36
3.5	Root Mean Square Error of the DOA parameter $\hat{\theta}$ versus SNR for the 3 sources. True DOAs $\theta_1 = 0^\circ, \theta_2 = 30^\circ$ and $\theta_3 = 60^\circ$	38
3.6	Root Mean Square Error of the distance parameter \hat{r} versus SNR for the 3 sources. True distances $r_1 = 30\lambda, r_2 = 25\lambda$ and $r_3 = 30\lambda$	40
3.7	Reconstruction of the angular spread distribution $\hat{h}(\phi)$	41
3.8	Reconstruction of the angular spread distribution $\hat{h}(\phi)$. True DOAs [$\theta_1 = 0^\circ, \theta_2 = 7^\circ$].	42
3.9	Root Mean Square Error of DOA $\hat{\theta}$ for Raised Cosine source at SNR=20dB. True parameters $\theta = 10^\circ$ and $r = 25\lambda$	43

3.10	Root Mean Square Error of DOA $\hat{\theta}$ versus δ_{θ} for both UCD sources at SNR=20dB. True parameters $\theta_1 = 0^\circ$ $\theta_2 = \theta_1 + \delta_{\theta}$, $\Delta_1 = 5^\circ$, $\Delta_2 = 8^\circ$ and $r_1 = r_2 = 25\lambda$	45
4.1	Root Mean Square Error versus SNR for two UCD sources. True parameters $\theta_1 = 0^\circ$ $\theta_2 = 30^\circ$, $\Delta_1 = 5^\circ$, $\Delta_2 = 15^\circ$ and $r_1 = 30\lambda$, $r_2 = 25\lambda$. (Note that for NF-DSPE the angular shape distribution is known).	57
4.2	Reconstruction of the true $h(\phi)$ and estimated angular spread distribution $\hat{h}(\phi)$ for JADSSE and NF-DSPE(Unif) at SNR=40dB	59
4.3	Root Mean Square Error versus SNR for two UCD sources. True parameters $\theta_1 = 0^\circ$ $\theta_2 = 7^\circ$, $\Delta_1 = 5^\circ$, $\Delta_2 = 8^\circ$ and $r_1 = 30\lambda$, $r_2 = 25\lambda$	60
4.4	Reconstruction of the angular spread distribution $\hat{h}(\phi)$	62
4.5	Root Mean Square Error of DOA $\hat{\theta}$ versus δ_{θ} for both UCD sources at SNR=20dB. True parameters $\theta_1 = 0^\circ$ $\theta_2 = \theta_1 + \delta_{\theta}$, $\Delta_1 = 5^\circ$, $\Delta_2 = 8^\circ$ and $r_1 = 30\lambda$, $r_2 = 25\lambda$	63
4.6	Root Mean Square Error versus SNR for RCCD(with $\beta = 1$) & UCD sources. True parameters $\theta_1 = 0^\circ$ $\theta_2 = 30^\circ$, $\Delta_1 = 7^\circ$, $\Delta_2 = 8^\circ$ and $r_1 = 30\lambda$, $r_2 = 25\lambda$	65
4.7	Root Mean Square Error versus SNR for RCCD(with $\beta = 1$) & UCD sources. True parameters $\theta_1 = 0^\circ$ $\theta_2 = 30^\circ$, $\Delta_1 = 7^\circ$, $\Delta_2 = 8^\circ$ and $r_1 = 30\lambda$, $r_2 = 25\lambda$	66
5.1	Configurations of Wind Tunnel Platform.	70
5.2	The two dimensional Gaussian spatial distribution with a spatial extension $\Delta = 10cm$	72
5.3	The 2D Separable Kernel RC given for shape value $\beta = 0$	73
5.4	The 2D Separable Kernel RC given for shape value $\beta = 0.5$	74
5.5	The 2D symmetrical RC given for shape value $\beta = 0$	75
5.6	The 2D symmetrical RC given for shape value $\beta = 0.5$	75
5.7	Array geometry in the the plane $z_0 = 4.5m$	81
5.8	The sum of spatial distribution of 2D-CD sources weighted by the power for each source. Each sub-figure represents the plot with true or estimated positions and powers.	85
5.9	Spatial power distribution of 2D-CD sources with true and estimated positions and powers.	86
5.10	Root Mean Square Error of \hat{x} versus SNR for the three sources. True positions $x_1 = 0.75m$, $x_2 = 1m$ and $x_3 = 0.3m$	90

5.11	Root Mean Square Error of \hat{x} versus snapshots for the three sources. True positions $x_1 = 1m$ and $x_2 = 0.3m$	91
5.12	Root Mean Square Error of \hat{x} versus spread Δ and shape β for the 2D-RC source. True positions $x_1 = 0.3m$ and $y_1 = 0.6m$	92
6.1	Back-look of the experimentation	97
6.2	Overlook of the experimentation	98
6.3	3D Wind tunnel experimentation	99
6.4	The estimated source position are compared on the grid of the car with the methods: CBF, NFE, NF-DSPE with Gaussian shape and NF-DSPE with unifrom shape.	100
6.5	The CBF criterion of 32 point sources on the vehicle with the estimated positions depicted with a black diamond marker.	102
6.6	The NFE criterion of 32 point sources on the vehicle with the estimated positions depicted with a black point marker.	102
6.7	The NF-DSPE with unifrom shape criterion of 32 CD sources on the vehicle with the estimated positions depicted with a green square marker where the dashed green circle represents the source spread. In this figure we plot the criterion for the spreads 5,10,15,20 cm.	103
6.8	The NF-DSPE with unifrom shape criterion of 32 CD sources on the vehicle with the estimated positions depicted with a green square marker where the dashed green circle represents the source spread. In this figure we plot the criterion for the spreads 25,30,35,40 cm.	104
6.9	The estimated source position are compared on the grid of the car with the following methods: NF-DSPE(G), NF-DSPE(U) and JPSSE. The first NF-DSPE(G) and NF-DSPE(U) methods are used with either equal or different spreads over x and y . For the third JPSSE method, we only considers the equal spreads case.	106
6.10	Spatial power distribution plots of 32 CD sources using NF-DSPE(U) and NF-DSPE(G) with circular symmetric shape on the vehicle with the estimated positions, spreads and powers expressed in dB (in white numbers).	108
6.11	Spatial power distribution plot of 32 CD sources using NF-DSPE(G) and NF-DSPE(G) with elliptical shape on the vehicle with the estimated positions, spreads (in dashed red line) and powers expressed in dB (in white numbers).	109

6.12 Spatial power distribution plots of 32 CD sources using JPSSE on the vehicle with estimated positions, spreads (in dashed magenta line), shapes and powers expressed in dB (in white numbers). 110

List of Tables

4.1	Summarizing Parameter values of the framework with two UCD sources.	56
4.2	True and estimated parameters of the Multi - UCD sources scenario at SNR=40 dB.	58
4.3	Summarizing Parameters values of the framework with two UCD & GCD sources.	58
4.4	True and estimated parameters of the mixed GCD & UCD sources scenario at SNR=40 dB. Recalling that the estimated $\hat{\Delta}_1$ models a different extension given the distribution used by the estimator. For example, the spread for JADSSE represents the extension given at the mid-height of the distribution whereas for NF-DSPE(Gauss) it depicts the standard deviation.	61
4.5	Summarizing parameters values of the framework with two UCD & RCCD sources.	63
5.1	True and estimated parameters of Multi-sources.	84
5.2	True and estimated parameters for the synthetic Multi-sources scenario (position, spread and shape). All sources frequencies are equal to $f_0 = 1\text{KHz}$ and SNR=-0.65dB. The color is used to provide a better values examination (red:2D-GCD, green:2D-UCD and magenta:2D-RCCD). However, symbols near estimator are also used to a better referring for the estimator in Fig.5.9.	87
5.3	Sources configurations considered for the performances analysis versus the snapshots.	91

List of Notations

θ	Direction Of Arrival (DOA)	\sum	Summation
M	Sensors number	$\mathbb{E}[\cdot]$	Expectation
m	Sensor index	$[\cdot]^T$	Transpose
q	Sources number	$[\cdot]^H$	Conjugate transpose
t	Time variable	$[\cdot]^*$	Complex conjugate
i	Source Index	$ \cdot $	Modulus
m	Sensor index	$\ \cdot\ $	Euclidean norm
j	Term imaginary unit	\simeq	Approximately equal
f_0	Signal central frequency	\odot	Element wise product
g_m	Sensor gain	$\Re\{\cdot\}$	Real operator
d	Inter-sensor distance in wavelength unit (λ)	$\mathcal{N}(0, 1)$	Normal PDF
c	Wave Celerity	\mathbb{R}	Set of real numbers
σ^2	Noise variance/power	δ	Kronecker delta
L	Sanpshots (temporal observations)	\cos	Cosinus function
l	Sanpshots index	\sin	Sinus function
σ_θ	Angular extension (for discrete model)	$\exp(\cdot)$	Exponential function
N	Rays number	$\arg \max$	Argument of the maximum
n	Ray index	$\text{rank}(\cdot)$	Matrix rank
k, l, i, \dots	Subscripts used for indexing	$\text{diag}(\cdot)$	Diagonal matrix
ϑ, ϕ, ϕ'	Angular variables	$\text{Ker}(\cdot)$	Kernel (or null space)
Δ	Spread parameter	$\text{Tr}(\cdot)$	Trace of a matrix
λ_i	The i -th eigenvalue	\hat{x}	Estimated value of x
r	Range (distance) parameter	$\mathcal{O}(x)$	Terms of order x
β	Shape parameter	$\mathcal{F}\{\cdot\}$	Fourier transformation
ϵ	Small number	$\underline{\Lambda}$	Eigenvalues matrix
σ_s^2	Source Signal variance/power	$\underline{\mathbf{E}}_s$	Signal subspace matrix
Δ_x, Δ_y	Spread parameter over x or y	$\underline{\mathbf{E}}_n$	Noise subspace matrix
$\underline{\mathbf{k}}(\theta)$	wave vector	$\underline{\mathbf{A}}$	Steering vectors matrix
$\underline{\mathbf{r}}_m$	Position vector of the m -th sensor	$\underline{\mathbf{C}}$	Generalized steering vectors matrix
$\underline{\mathbf{x}}$	Observation vector	$\underline{\mathbf{R}}_x$	Observation correlation matrix
$\underline{\mathbf{s}}$	Signal vector	$\underline{\mathbf{R}}_s$	Signal correlation matrix
$\underline{\mathbf{n}}$	Noise vector	$\underline{\mathbf{R}}_n$	Noise correlation matrix
$\underline{\mathbf{a}}$	Steering vector	$\underline{\mathbf{I}}$	Identity matrix
$\underline{\mathbf{c}}$	Generalized Steering Vector (GSV)	$\underline{\mathbf{X}}$	Observation matrix
$\underline{\mathbf{p}}$	Source vector position	$\underline{\mathbf{S}}$	Signal matrix
$s(t)$	Received signal	$\underline{\mathbf{N}}$	Noise matrix
$x_m(t)$	Observation of the m -th sensor		
$\tau_m(\theta)$	Wave-front delay		
$n_m(t)$	Noise of the m -th sensor		
$\bar{s}(t)$	Received signal		
$\tilde{\theta}(t)$	Ray angular deviation from θ		
$h(\phi)$	Angular spread distribution		
$h(x, y)$	Spatial spread distribution		
$S(\theta)$	Criteria (cost function)		

Acknowledgments

A brave man acknowledges the strength of others. *Veronica Roth*

The following manuscript presents the fruit of my research work during the last three years at *CentraleSupélec*¹. This achievement involves the support of many people that contributed either on the physical, moral or spiritual side. Therefore, to remember and acknowledge their support it is an important matter to reserve a couple of words for them.

I will allow myself to dedicate, in the first place, my acknowledgment to Georges and Amal who inspired, encouraged and provided me the full moral support to continue my doctoral studies. Unfortunately, my father Georges left our family during the first year of my PhD journey where I was obliged to suspend my doctoral thesis for more than six months to handle many responsibilities. After this period I re-started/continued my research and teaching activities in France to successfully finish my PhD today. Georges, sometimes there is no way to thanks or payback some people for their endless love. I am offering you my work to perpetuate your excellent memory. Amal, your endless efforts and sacrifices are rising the best men and women of the future, may God bless you.

I would like to address my acknowledgment to the ex-chairman of the Signals and Electronic Systems department, Stéphane FONT, who supported the start and the going back of my doctoral studies.

My sincere acknowledgments goes to José PICHERAL and Sylvie MARCOS who supervised and directed my PhD thesis. I thanks them for believing in me to continue my PhD after the difficult circumstances that i faced. Sylvie and José, I appreciate your kindness and endless encouragement to finish what I have started. Your scientific and professional implications oriented the thesis towards significant and valuable results. I am also grateful for your guidance that buildup my research vision.

¹School of engineering (AKA Supélec)

I express all my gratitude to professor Philippe FORSTER to have granted me the honor of chairing the jury of my defense. I also thank him for the valuable scientific discussions that were very interesting concerning the theoretical performance aspect for my research works.

I would like to particularly thank professor Jérôme ANTONI for having reviewed and reported my thesis very carefully. Also, I appreciate him for supplying a list of constructive comments for the future studies and analysis concerning the experimental data and for the improvement of my report.

I would like to thank professor Yide WANG for having agreed to report my thesis. I especially appreciated the perspectives which he proposed to my research works and the fruitful discussion that we made about one of the localization method.

I cannot forget any of my friends that stood besides me in my Phd journey. I was lucky to have you all especially to encourage me for the pursuing my studies when it comes to hard situation each one of you in his special way. Believe me, all of you left a mark that i will not forget and especially some that played an important role in my journey. Because all my gratitude goes to you, I will preserve the privilege of not citing any of your names.

Last but not least, Lyne with all my love, here you go my Phd manuscript, you can read it from time to time hoping you will understand my scientific approaches in doing many things.

To Georges

*Nothing in life is to be feared, it is only to be understood.
Now is the time to understand more, so that we may fear
less.*

Marie Curie

1

Introduction

1.1 Context

The problem of source localization with sensors array consists in estimating the number, the direction of arrival and the power of sources transmitting signals in a given environment. This general problem has gained a growing interest among the researchers since the last four decades [21] due to the numerous applications such as radar, sonar, telecommunications, seismic and acoustic imaging. Among the work that has been published on this subject, relatively few of them deal with the so called distributed sources case taking into account the spatial extension of the source. Also, a very common hypothesis is that the sources are in the far-field of the sensor array. The aim of this thesis is to review the problem of source localization by taking into account both the spatial extension of the source and the near field context. Indeed the closer is the source to the antenna, the larger is its spatial extent.

Evolution of source localization methods started with spatial filtering methods [34] like Beamforming. In addition, adaptive methods like Capon technique were developed to improve the existing ones. After this stage, the introduction of subspace methods has marked a new era in the array processing field since such methods offer a high ability to distinguish two closely spaced sources. These methods are also called "high resolution methods". One of the well known high resolution method, named Multiple Signal Classification (MUSIC), will be considered in our study, Then, some extensions of MUSIC, will be proposed to localize near-field sources having a spatial extension.

Abundant applications address the problem of locating sources with spatial extension like radar sonar systems, communications, astrophysics, bio-medical research, seismology, and many highly active fields like acoustic imaging. This latter presents advanced techniques for acoustic source localization and power estimation from limited samples issued at a microphone array. Acoustic imaging is motivated by the needs of the vehicle and aviation industries to improve passenger comfort by reducing aero-acoustic noise [4, 5].

1.1.1 Applications

Array processing deals with data measured by an array of sensors located at different points in a wave-field. Due to phase difference among sensors, we can determine important features of the propagating waves such as Direction of Arrival (DOA), propagation velocities, range, polarization, etc. These quantities are of fundamental importance in radar, sonar, communications, geophysics, astronomy and acoustic imaging.

This thesis focus on the technology of acoustic imaging represents a sophisticated technique applied to a wide range of fields including non-destructive testing, medical imaging, underwater imaging, geophysical exploration, and many other relevant applications in automotive industry such as identifying aero-acoustic sources generated by the interaction of the flow with the car body. This experimentation consists of placing a vehicle (without the engine noise) in the center of a wind tunnel which simulates a wind flow of 160km/h in the front side of the car. The wind tunnel experiments carried out by Renault SAS [4, 5] is designed to simulate a fast traveling car on the high-way where it aims to localize the aero-acoustic sources on the car body and to measure their power. Once the sources are detected, decisions are taken to improve acoustical comfort of the vehicle passengers. In this thesis, we are going to apply the new proposed estimators on the real data issued from the Renault wind tunnel application.

1.1.2 Problem Statement and Motivation

The problem of locating sources using an array of passive sensors can be explained by the following. A source emits energy that may be acoustic, electromagnetic, etc. The receiving sensor may be any transducer that converts the received energy to electrical signals, like microphones, hydrophones, electromagnetic antennas and seismographers. This problem basically deals with how the energy is distributed over space (which may be air, water or earth), considering the source positions representing points with highly energy concentrations (also named by the spatial spectral estimation problem).

In array signal processing, most of the algorithms that estimate the DOA have been developed on the assumption of point emitting sources in far-field. This modeling assumption

is not suitable for several physical examples. Indeed in many applications such as the localization of acoustic sources, it can occur that the angular spread of the spatial extension cannot be ignored. One can cite as a motivating subject for this study, the relevance of considering this spatial extension in the near-field. Certainly, as the source gets closer to the array, the matter of considering its spatial extension becomes more important. Therefore, the point source assumption fails in this case.

Two models are classically used in the literature for spatial distributed sources. In telecommunications, the model considers independent local scatterers around the source [32]. In fact, the wave emitted by a mobile phone is reflected by several surrounding objects around the mobile. These reflections are generally independent. A second widely considered model [33] assumes that the source is continuously spatially extended around a nominal DOA with an angular spread distribution. This thesis is based on the second model.

Basically, when the point source assumption can not be respected, it is important to consider the distributed source aspect by introducing another parameter that characterizes the source extension. The source will be identified by its DOA and spatial extension named spread. Thus, we model the spread using a parametric function for a better description. The purpose is to estimate the DOA and spread of the source.

However, accounting the spread to characterize the distributed source reveals another important aspect to consider: the shape of the spread function. The shape presents an additional information on the source to be localized and plays an important role in improving the performance of the estimators based on the distributed assumption. Therefore, the thesis proposes methods for CD source localization that are also able to characterize the shape of this source.

The thesis presents two major challenges: i) the first one is to characterize the shape of the function that describes the source spread, indeed, as we are going to see later on, the shape appears to have an important impact on the source localization; ii) the second is to localize the aero-acoustic sources by accounting the distributed aspect.

The aero-acoustic source localization presents an interesting field of the acoustic imaging where the main idea consists in searching the noisy sources. Such application raises many challenges: i) improving the spatial resolution. The beamforming based methods are limited by their low spatial resolution and narrow dynamic range due to the high side-lobes and spatial aliasing effects, especially at low frequency. ii) Dealing with distributed sources. Methods used in the acoustic imaging generally rely on the point source assumption. Such an hypothesis fails in many practical situations as the source presents a spatial extension. iii) Providing reliable source power estimation. The challenge inhabits in detecting weak and powerful sources at once, in other words providing a wide dynamic range for power estimation. One can cite as a reason that may affect the power estimation is

considering the point source assumption. Other relevant challenges can be cited like the source interference problem and the important side-lobes effects due to the use of a non uniform array.

Upon giving this overview about the problem statement, we can define our motivations as follows:

1. As far as we know, the parametric high resolution estimators proposed in the literature do not take into consideration the aspect of spatial distributed sources in conjunction with the aspect of near-field propagation. However, for a given physical extension of the source, the angular spread becomes more relevant as the source gets closer to the array. As we are going to see later, the application of the wind tunnel experiment is a near-field experimentation where the array sensor plane is approximately at 4.5 meters from the sources. This is the reason that motivates us to explore distributed source location in this area.
2. The assumption of knowing the distribution function of the spatial extension is not realistic in practice. These reasons motivate us to propose an estimator of coherently distributed (CD) sources in near-field which is robust to the imperfect knowledge of the angular spread distribution. This limitation motivates us to propose a robust estimator to handle this lack of information.
3. Another motivation considering the studies in the aero-acoustic and source imaging field, is to introduce the CD source model to this field in order to allow a better description and characterization of the pattern and the structure of the aero-acoustic sources. The proposed estimator aims to better localize the source by providing its position, spread and shape.

1.2 Main Contributions

We first consider the CD source model [33] in conjunction with the aspect of near-field propagation where the physical extension of the source becomes more relevant as the source gets closer to the array. Next, by generalizing the Distributed Signal Parameter Estimator (DSPE) [33] to near-field we notice that this estimator presents a major drawback due to the need of an *a priori* information on the shape distribution function of the source. This reason motivates us to introduce a modification to this estimator that allows to describe the angular spread distribution. The proposed method called Joint Angle Distance Spread Shape Estimator (JADSSE) [3] presents the following features:

- It estimates a distribution shape parameter in addition to the other localization parameters (angle, distance and spread).
-

- It deals with an unknown angular spread distribution.
- It provides better robustness to several shapes of the angular distribution.
- It improves characterization of the source by providing an estimate of the spread and the shape of the distribution of the source.
- It presents a good angular resolution capacity in terms of DOA for overlapped sources.

Then, inspired by the Decoupled DSPE (DDSPE) method proposed in [37], we propose an hybrid localization approach named Decoupled Angle Distance Spread Shape Estimator (DADSSE). The DDSPE method consists in decoupling the estimation of the DOA from the estimation of the angular spread, meanwhile it only offers a robust estimation of the DOA with respect to an unknown angular shape distribution of the source. Therefore, we propose a generalized near-field approach of the DDSPE, the NF-DDSPE, which decouples the estimation of the DOA and range from the estimation of the angular spread. However, when the angular spread is required, the angular shape distribution must be known to use the NF-DDSPE. Afterwards, we present the hybrid approach that consists in combining the NF-DDSPE and the JADSSE estimators. This method improves the NF-DDSPE by:

- Eliminating the *a priori* knowledge on the source shape distribution to compute the spread estimation.
- Localizing sources with different shapes.
- Providing a shape reconstruction.

Finally, considering the CD model in the near-field introduced previously, we adapt this model for the aero-acoustic source localization application. After that, the earlier proposed methods are transposed to the Cartesian coordinate parametric form. We also provide source power estimator based on the CD model assumption. The last matter consists in running our approaches on real data of this application. We can list relevant contributions of the last point by:

- Proposing a suitable model for aero-acoustic source based on 2D-coherently distributed sources.
 - Proposing source power estimators based on the CD model.
 - Comparing the proposed methods with synthetic data scenario for source imaging. Simulations are done with the wind tunnel configuration experiment where performance analysis is also done.
 - Running the proposed approaches on the real data improves the aero-acoustic source localization using the distributed CD assumption compared to the point one.
-

1.3 Thesis Structure

In chapter 2, we introduce the localization principle by explaining the standard point source model, then, we explicit two different models of spatially distributed sources, the discrete and the continuous one. Next, concerning localization and power estimation methods, we recall the beamforming approach as well as the subspace-based MUSIC method for the point case. Then, we present generalization of this methods to deal with spatially distributed sources (for the continuous case). Finally, we briefly recall the extensions of standard methods and estimators to the near-field case.

The third chapter, considers the CD source model, explained in the previous chapter, in conjunction with the aspect of near-field propagation. The Distributed Signal Parameter Estimator (DSPE) [33] is generalized to near-field. Due to the need of knowing the shape distribution function of the source, this estimator presents a major disadvantage. More explicitly, an *a priori* information about the angular spread shape must be provided for good performance. Therefore, we propose a modification of the DSPE which consists in using a generic function family to describe the angular spread distribution. The Joint Angle Distance Spread Shape Estimator (JADSSE) method consists in the estimation of the distribution shape parameter in addition to other parameters. We run performance simulations to validate the proposed approach and compare it with other methods.

In chapter 4, we propose a decoupling version of JADSSE. The method is based on the Decoupled DSPE (DDSPE) proposed in [37] where the localization is done in a decoupled way as following: first the source DOA is estimated and then, using this estimated value, the angular spread can be estimated. This method provides a robust estimation only for DOA but it requires the knowledge of the angular spread shape distribution to estimate the angular spread parameter. Therefore, first, we review the DDSPE and we propose a generalization to the near-field case, the NF-DDSPE. Afterwards, we present the hybrid approach that consists in combining the NF-DDSPE and the JADSSE estimators called Decoupled ADSSE (DADSSE).

We propose in chapter 5 an aero-acoustic source model based on the CD source where the location and the spatial extension are assumed to be parameterized in Cartesian coordinates. Then, we recall standard methods (conventional and distributed Beamforming techniques along with the *a priori* shape based estimator (NF-DSPE) and JADSSE) in their Cartesian coordinates parametric form. Next, based on the CD modeling, we propose a least square source power estimator to overcome the challenge of estimating weak sources power. One of our main motivations in considering a distributed source model is to access a wide dynamic range of power estimation. Finally, our synthetic data simulated with the setup of the aero-acoustic wind tunnel application show that the proposed distributed estimators

NF-DSPE and JPSSE (JADSSE in the Cartesian coordinates parametrization) provide better localization, power estimation and shape distribution information (only for JPSSE) than standard approaches.

Chapter 6 presents the application for aero-acoustic source imaging of a RENAULT car in a wind tunnel. The previously proposed estimators are applied on real data. The classical beamforming, point source MUSIC and the NF-DSPE with various shape distributions are compared. Impact on the position and power estimation is discussed in the point source and distributed source cases.

The last chapter presents the essential conclusions in this thesis.

1.4 Author's Publications

- J. Abou Chaaya, J. Picheral and S. Marcos. Localization of spatially distributed near-field sources with unknown angular spread shape. **Signal Processing**, Vol. 106, pp 259-265, Jan. 2015, DOI 10.1016/j.sigpro.2014.07.007.
 - J. Abou Chaaya, J. Picheral and S. Marcos. Localisation des sources distribuées en champ proche. **GRETSI 2013**, Sep 2013, Brest, France. 4p. HAL Id: hal-00866981.
 - J. Abou Chaaya, J. Picheral and S. Marcos. Localization and power estimation of coherently distributed aero-acoustic sources with unidentified spread shape. To submit to **Journal of sound and Vibration**.
 - J. Abou Chaaya, J. Picheral and S. Marcos. Decoupled estimation for coherently distributed source localization in near-field with unknown spread shape. To submit to **Signal Processing**.
-

There is no need to be perfect and to inspire others, let others get inspired by how you deal with your imperfections.

Ziad K. Abdelnour

2

Modeling and Localizing Distributed Sources

We begin by introducing the basic point source model that reflects the relation between the unknown sources location and the signals received on the sensors. The discrete and the continuous models of spatially distributed sources are then described. They characterize how the reflectors in the vicinity of the sources are taken into account to explain the spatial extension of the sources.

Concerning the estimation strategies, for source localization and power estimation, we will recall how the spatial filtering-based methods, as beamforming and Capon, as well as the subspace-based methods, as MUSIC, have been generalized, in the case of the continuous model, to deal with spatially distributed sources. Finally, we will introduce the near-field model which will be considered in the other chapters of this thesis.

This chapter is organized as follows. In section 2.1, signal models are covered from the classical point one to the distributed one. Then, classical beam-forming based estimators for point and distributed sources are explained in section 2.2. Next, high resolution methods are developed for point and the Coherently Distributed (CD) case in section 2.3. Section 2.4 explains the particular near-field case. Finally, conclusions are introduced in the last section.

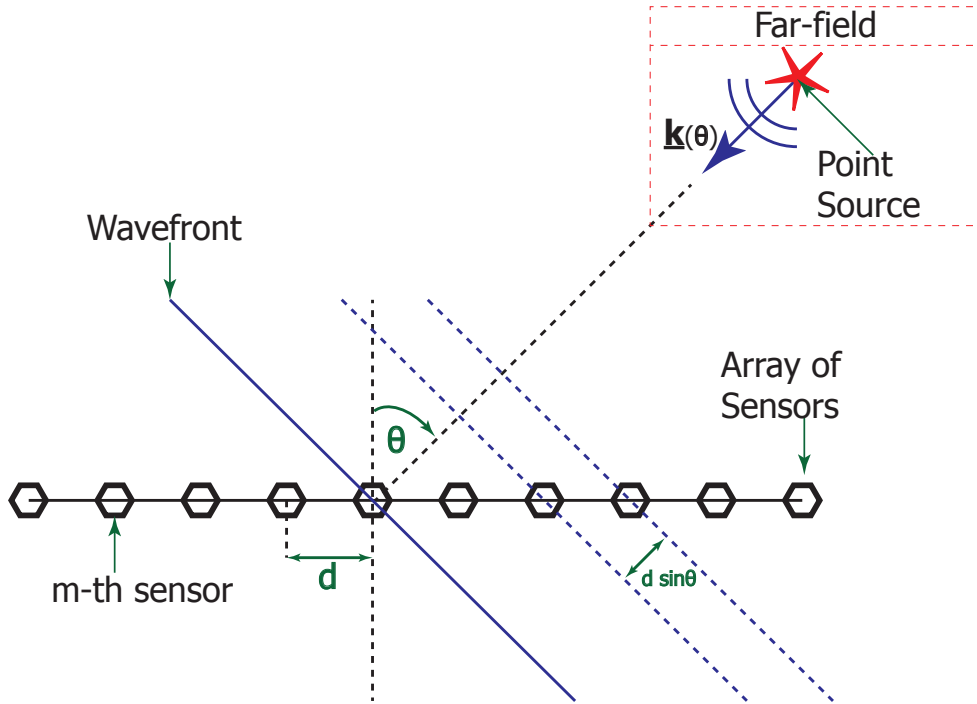


Figure 2.1: Localization principle of a point source in far-field with ULA.

2.1 Signal Models

This section highlights the difference between the point source model and the distributed source model. First, we introduce the classical point source modeling where the point emitting source is featured only by its Direction of Arrival θ . Next, we present a more thorough model for the discretely distributed source in subsection 2.1.2 and the continuously distributed source in subsection 2.1.3. The two previous approaches allow to model the spatial extension of the source. The discrete model explicits the components of the distributed source signal by taking into account a finite number of independent rays meanwhile the continuous model offers two types of source signal densities the Coherently Distributed (CD) components and the Incoherently Distributed (ID) components [19, 29, 33].

2.1.1 Point Source Model

According to Fig.2.1, a single waveform impinges upon an array of M sensors with a wave vector $\mathbf{k}(\theta)$ with θ the direction of arrival (DOA) measured relatively to a given coordinate

system of the array. Define $s(t)$ by the signal received on a reference sensor of the array, for example the first one. The signal received on sensor m can be written by:

$$x_m(t) = g_m s(t - \tau_m(\theta)) + n_m(t), \quad (2.1)$$

The delay of the wave-front to travel from the sensor m to the sensor of reference is denoted by $\tau_m(\theta) = \mathbf{k}(\theta)\mathbf{r}_m$, with \mathbf{r}_m is the coordinate vector of sensor m . $n_m(t)$ is the thermal noise or the background radiation impinging on the array. In the case of q sources, we have:

$$x_m(t) = \sum_{i=1}^q g_m s_i(t - \tau_{m,i}(\theta_i)) + n_m(t), \quad (2.2)$$

where $\tau_{m,i}(\theta_i) = \mathbf{k}(\theta_i)\mathbf{r}_m$. As the signals of the sources are assumed narrow-band¹, the signal delay can be expressed as the phase shift $s_i(t - \tau_{m,i}(\theta_i)) = \bar{s}_i(t)e^{-j2\pi f_0 \tau_{m,i}(\theta_i)}$ so (2.2) is written by:

$$x_m(t) = \sum_{i=1}^q g_m \bar{s}_i(t) e^{-j2\pi f_0 \tau_{m,i}(\theta_i)} + n_m(t), \quad (2.3)$$

with f_0 is the central frequency of the signals.

By introducing the M dimensional vector of the received signals:

$$\mathbf{x}(t) = [x_1(t), \dots, x_M(t)]^T, \quad (2.4)$$

we can write Eq. (2.3) in its vectorial expression:

$$\mathbf{x}(t) = \mathbf{A}(\theta)\mathbf{s}(t) + \mathbf{n}(t) = \sum_{i=1}^q \bar{s}_i(t)\mathbf{a}(\theta_i) + \mathbf{n}(t), \quad (2.5)$$

where $\mathbf{s}(t) = [\bar{s}_1(t), \bar{s}_2(t), \dots, \bar{s}_q(t)]^T$, $\mathbf{n}(t) = [n_1(t), \dots, n_M(t)]^T$ and

$\mathbf{A}(\theta) = [\mathbf{a}(\theta_1), \mathbf{a}(\theta_2), \dots, \mathbf{a}(\theta_q)]$ with:

$$\mathbf{a}(\theta_i) = \begin{bmatrix} 1 \\ g_2 e^{-j2\pi f_0 \tau_{2,i}(\theta_i)} \\ \vdots \\ g_M e^{-j2\pi f_0 \tau_{M,i}(\theta_i)} \end{bmatrix} \quad (2.6)$$

¹in the case of wide-band signals, this relation is also valid in the Fourier domain, in which f_0 would be replaced by f

It is worth noting that in the particular case of a Uniform Linear antenna Array (ULA) as shown in Fig. 2.1 with identical and omnidirectional sensor gain ($g_m = 1$), the wave-fronts are plane and the sensors are aligned and equidistant by d . Thus, the time delay $\tau_{m,i}(\theta_i)$ can be written as:

$$\tau_{m,i}(\theta_i) = (m - 1) \frac{d}{c} \sin(\theta_i), \quad (2.7)$$

with c the wave celerity.

The estimation methods to be studied in the thesis are based on the second order statistics of the signals. Therefore, let us introduce the $M \times M$ dimensional data correlation matrix \mathbf{R}_x , assuming that the signals are stationary and that the source signals and noise are independent :

$$\mathbf{R}_x = \mathbb{E}[\underline{\mathbf{x}}(t)\underline{\mathbf{x}}^H(t)] = \mathbf{A}(\theta)\mathbf{R}_s\mathbf{A}^H(\theta) + \mathbf{R}_n, \quad (2.8)$$

where \mathbf{R}_s is the source signals $q \times q$ dimensional correlation matrix and \mathbf{R}_n is the $M \times M$ -dimensional co-variance matrix of the noise. In what follows we will assume that the noise is spatially and temporally white so that $\mathbf{R}_n = \sigma^2\mathbf{I}_M$ and σ^2 is the variance of the noise. The data correlation matrix \mathbf{R}_x can be estimated from L snapshots $\underline{\mathbf{x}}(t_l)$ ($l = 1 \dots, L$), put together in the $M \times L$ data matrix:

$$\mathbf{X} = [\underline{\mathbf{x}}(t_1), \underline{\mathbf{x}}(t_2), \dots, \underline{\mathbf{x}}(t_L)], \quad (2.9)$$

so that:

$$\hat{\mathbf{R}}_x = \frac{1}{L}\mathbf{X}\mathbf{X}^H. \quad (2.10)$$

Note that from Eq. (2.5) \mathbf{X} can be expressed as:

$$\mathbf{X} = \mathbf{A}(\theta)\mathbf{S} + \mathbf{N}, \quad (2.11)$$

with $\mathbf{S} = [\underline{\mathbf{s}}(t_1), \dots, \underline{\mathbf{s}}(t_L)]$ and $\mathbf{N} = [\underline{\mathbf{n}}(t_1), \dots, \underline{\mathbf{n}}(t_L)]$ are of dimensions $q \times L$ and $M \times L$, respectively.

2.1.2 Discrete Distributed Model

The model that is going to be explained in this section will not be used in the sequel of the thesis, meanwhile it will be explained being one of the two most used distributed source models in the field. This modeling aspect was first developed to consider the communication scenario between a base station and a mobile terminal [6, 32]. It is based on the existence of independent scatterers around the source. Each scatterer is characterized by its complex gain $\gamma_n(t)$. The diffracted wave-fronts rays of the source are seen as an angular beam on each sensor, coming from a single source with an angular extension of width

σ_θ . To describe a distributed source, this model takes into account a finite number N of diffracted rays caused by the nearby reflectors in the vicinity of the source.

Let's assume q spatially distributed narrow-band far-field sources impinging on an array of M sensors. The $M \times 1$ baseband signal vector measured by the M sensors is given by $\underline{\mathbf{x}}(t) = [x_1(t), \dots, x_M(t)]^T$.

$$\underline{\mathbf{x}}(t) = \sum_{i=1}^q s_i(t) \sum_{n=1}^N \gamma_{n,i}(t) \underline{\mathbf{a}}(\theta_i + \tilde{\theta}_{n,i}(t)) + \underline{\mathbf{n}}(t). \quad (2.12)$$

- $s_i(t)$: emitted signal of the i -th source.
- $\gamma_{n,i}(t)$: complex random gain of the n -th ray for the i -th source.
 $\gamma_{n,i}(t) \sim \mathcal{N}(0, 1)$ with $\mathcal{N}(0, 1)$ is the Normal Probability Density Function (PDF) of zero-mean and unitary variance.
- $\tilde{\theta}_{n,i}(t)$: angular deviation (random) from the nominal DOA θ_i .
 $\tilde{\theta}_{n,i} \sim p_{\tilde{\theta}_{n,i}}(\theta_i, \sigma_{\theta_i}^2)$

$p_{\tilde{\theta}_{n,i}}(\theta_i, \sigma_{\theta_i}^2)$ denotes the PDF of mean θ_i and variance $\sigma_{\theta_i}^2$. We assume that the gain factor² $\gamma_{n,i}(t)$ is independent from ray to ray and from snapshot to snapshot.

For the mono-source scenario with a DOA θ , the (k, l) -th element of the array correlation \mathbf{R}_x is expressed by:

$$[\mathbf{R}_x]_{k,l} = \mathbb{E}[x_k(t)x_l^*(t)] \quad (2.13a)$$

$$= |s(t)|^2 \mathbb{E} \left[\sum_{n=1}^N \sum_{n'=1}^N \gamma_n(t)\gamma_{n'}^*(t) [\underline{\mathbf{a}}(\theta + \tilde{\theta}_n(t))]_k [\underline{\mathbf{a}}^*(\theta + \tilde{\theta}_{n'}(t))]_l \right] + \sigma_n^2 \delta_{kl}. \quad (2.13b)$$

The amplitude of the rays are assumed to be independent and temporally white rays with a unitary σ_γ^2 variance as explained above³. The ray DOAs $\tilde{\theta}_n$ are independent from the ray gains $\gamma_n(t)$ and modeled as independent and identically distributed (i.i.d) (all of the rays follow the same distribution and $p_{\tilde{\theta}_{n,i}}(\theta_i, \sigma_{\theta_i}^2)$ can be denoted by $p_{\tilde{\theta}_i}(\theta_i, \sigma_{\theta_i}^2)$). Thus,

²For a given source the gain factor can be expressed as $\gamma_n(t) = g_n(t)e^{j\alpha_n(t)}$ where $g_n(t)$ and $\alpha_n(t)$ represent the random amplitude and the random phase of the n -th ray, respectively

³ $\mathbb{E} [\gamma_n(t)\gamma_{n'}^*(t)] = \mathbb{E} [|\gamma_n(t)|^2] \delta_{nn'} = \delta_{nn'}$, (δ is the Kronecker delta)

expression (2.13) can be written as:

$$[\mathbf{R}_x]_{k,l} = |s(t)|^2 \sum_{n=1}^N \sum_{n'=1}^N \mathbb{E} \left[\gamma_n(t) \gamma_{n'}^*(t) \right] \delta_{nn'} \mathbb{E} \left[[\underline{\mathbf{a}}(\theta + \tilde{\theta}_n(t))]_k [\underline{\mathbf{a}}^*(\theta + \tilde{\theta}_{n'}(t))]_l \right] + \sigma_n^2 \delta_{kl}. \quad (2.14)$$

$$\begin{aligned} [\mathbf{R}_x]_{k,l} &= |s(t)|^2 \sum_{n=1}^N \mathbb{E} \left[|\gamma_n(t)|^2 \right] \mathbb{E} \left[g_k e^{-j2\pi f_0 \tau_k (\theta + \tilde{\theta}_n(t))} g_l^* e^{j2\pi f_0 \tau_l (\theta + \tilde{\theta}_n(t))} \right] + \sigma_n^2 \delta_{kl} \\ &= |s(t)|^2 \sum_{n=1}^N g_k g_l^* \mathbb{E} \left[e^{-j2\pi f_0 \mathbf{k} (\theta + \tilde{\theta}_n(t)) (\mathbf{r}_k - \mathbf{r}_l)} \right] + \sigma_n^2 \delta_{kl} \\ &= |s(t)|^2 \sum_{n=1}^N g_k g_l^* \int_{-\infty}^{+\infty} e^{-j2\pi f_0 \mathbf{k} (\theta + \tilde{\theta}_n(t)) (\mathbf{r}_k - \mathbf{r}_l)} p_{\tilde{\theta}}(\theta, \sigma_\theta) d\tilde{\theta} + \sigma_n^2 \delta_{kl}. \end{aligned} \quad (2.15a)$$

In a particular case of an Uniform Linear Array (ULA) and assuming that the angular spread σ_θ is small so that $\cos(\tilde{\theta})$ and $\sin(\tilde{\theta})$ can be approximated by the first term in the Taylor series expansion, Eq. (2.15) can be expressed by:

$$[\mathbf{R}_x]_{k,l} = |s(t)|^2 [\underline{\mathbf{a}}(\theta)]_{k-l} \int_{-\infty}^{+\infty} e^{-j2\pi \frac{f_0}{c} \cos(\theta) \tilde{\theta}(t) (k-l)} p_{\tilde{\theta}}(\theta, \sigma_\theta) d\tilde{\theta} + \sigma_n^2. \quad (2.16)$$

We can also rewrite equation (2.16) using the Fourier transform of the rays PDF $p_{\tilde{\theta}}(\theta, \sigma_\theta)$ also called the characteristic function corresponding to $p_{\tilde{\theta}}(\theta, \sigma_\theta)$ for the given spatial frequency $\frac{f_0}{c} \cos(\theta) (k-l)$:

$$[\mathbf{R}_x]_{k,l} = |s(t)|^2 [\underline{\mathbf{a}}(\theta)]_{k-l} \mathcal{F}\{p_{\tilde{\theta}}(\theta, \sigma_\theta)\} \left(\frac{f_0}{c} \cos(\theta) (k-l) \right) + \sigma_n^2. \quad (2.17)$$

2.1.3 Continuous Distributed Model

Here, a distributed source is no longer considered as the cluster of closely spaced point sources but as a continuum as shown in Fig.2.2. A spatial density function associated to an angle spread parameter is defined to characterize the angular distribution of the amplitude of the spatially distributed sources [19, 29, 33].

Authors in [19, 33] proposed the following model for the distributed sources in far-field:

$$\boxed{\underline{\mathbf{x}}(t) = \sum_{i=1}^q \int_{-\frac{\pi}{2}}^{\frac{\pi}{2}} \underline{\mathbf{a}}(\phi) v_i(\phi; \theta_i, \Delta_i, t) d\phi + \underline{\mathbf{n}}(t)}. \quad (2.18)$$

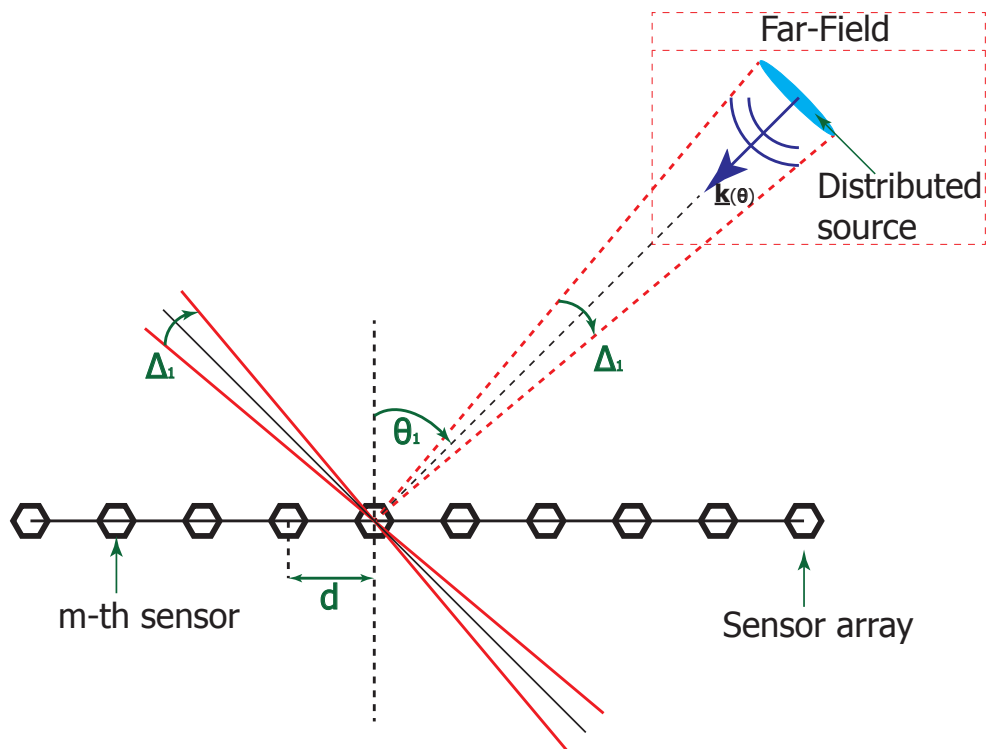


Figure 2.2: Localization of a distributed source in far-field

$\underline{\mathbf{a}}(\phi)$ is the $M \times 1$ steering vector of the far-field array response for a source of DOA ϕ defined in Eq. (2.6).

- $v_i(\phi, \theta_i, \Delta_i, t)$: signal angular distribution of the i -th source.
 θ_i : central DOA of the source.
 Δ_i : angular spread.

The source signal and noise time samples are modeled by random, complex Gaussian, centered and independent processes. Assume that the noise and the sources $v_i(\phi; \theta_i, \Delta_i, t)$ are uncorrelated from each other, considering the already mentioned assumptions, the correlation matrix of the array output is given by:

$$\begin{aligned} \mathbf{R}_x &= \mathbb{E}[\underline{\mathbf{x}} \underline{\mathbf{x}}^H] \\ &= \mathbf{R}_s + \sigma^2 \mathbf{I}. \end{aligned} \quad (2.19a)$$

\mathbf{R}_s is the noise free received signals component of the received signal correlation matrix:

$$\mathbf{R}_s(\theta, \Delta) = \sum_{i=1}^q \sum_{j=1}^q \int_{-\frac{\pi}{2}}^{\frac{\pi}{2}} \int_{-\frac{\pi}{2}}^{\frac{\pi}{2}} \underline{\mathbf{a}}(\phi) \mathbb{E}[v_i(\phi; \theta_i, \Delta_i, t) v_j^*(\phi'; \theta_j, \Delta_j, t)] \underline{\mathbf{a}}^H(\phi') d\phi d\phi'. \quad (2.20)$$

Let's define the angular cross-correlation kernel as:

$$\rho_{ij}(\phi, \phi'; \theta_i, \Delta_i, \theta_j, \Delta_j) = \mathbb{E}[v_i(\phi; \theta_i, \Delta_i, t) v_j^*(\phi'; \theta_j, \Delta_j, t)]. \quad (2.21)$$

The sources are assumed to be uncorrelated with each other. Thus, cross-correlation in Eq. (2.21) can be simplified to an auto-correlation kernel:

$$\rho_{ij}(\phi, \phi'; \theta_i, \Delta_i, \theta_j, \Delta_j) = \rho(\phi, \phi'; \theta_i, \Delta_i) \delta_{ij}. \quad (2.22)$$

We can rewrite Eq. (2.20) as:

$$\boxed{\mathbf{R}_s = \sum_{i=1}^q \int_{-\frac{\pi}{2}}^{\frac{\pi}{2}} \int_{-\frac{\pi}{2}}^{\frac{\pi}{2}} \underline{\mathbf{a}}(\phi) \rho(\phi, \phi'; \theta_i, \Delta_i) \underline{\mathbf{a}}^H(\phi') d\phi d\phi'} \quad (2.23)$$

In the upcoming, two cases of angular auto-correlation kernel are discussed: the separable one known as Coherently Distributed (CD) and the non separable one known as Incoherently Distributed (ID).

Coherently Distributed (CD)

From a physical point of view, the fully correlated components of a CD source received from different angles are the delayed and scaled duplicates of the same signal. Thus, a CD

source is described by a temporally invariant angular distribution and the components of the signal are fully correlated for the whole angular spread (see [33]). So, the signal angular distribution for the i -th CD source can be given by:

$$v_i(\phi; \theta_i, \Delta_i, t) = s_i(t)h_i(\phi; \theta_i, \Delta_i), \quad (2.24)$$

where $s_i(t)$ is a random complex signal emitted by the i -th source and $h_i(\phi; \theta_i, \Delta_i)$ represents a deterministic angular spread distribution. It is convenient to normalize the angular spread distribution $h_i(\phi; \theta_i, \Delta_i)$ as follows:

$$\int_{-\frac{\pi}{2}}^{\frac{\pi}{2}} h_i(\phi; \theta_i, \Delta_i) d\phi = 1. \quad (2.25)$$

The auto-correlation kernel in Eq. (2.22) can be expressed explicitly as:

$$\rho(\phi, \phi'; \theta_i, \Delta_i) = \mathbb{E}[|s_i(t)|^2]h_i(\phi; \theta_i, \Delta_i)h_i^*(\phi'; \theta_i, \Delta_i). \quad (2.26)$$

Note that $\mathbb{E}[|s_i(t)|^2]$ represents the i -th source signal power.

In the CD case, the equation model in Eq. (2.18) can also be written as:

$$\underline{\mathbf{x}}(t) = \sum_{i=1}^q s_i(t)\underline{\mathbf{c}}(\theta_i, \Delta_i) + \underline{\mathbf{n}}(t). \quad (2.27)$$

$\underline{\mathbf{c}}(\theta_i, \Delta_i)$ is the Generalized Steering Vector (GSV):

$$\underline{\mathbf{c}}(\theta_i, \Delta_i) = \int_{-\frac{\pi}{2}}^{\frac{\pi}{2}} \underline{\mathbf{a}}(\phi)h_i(\phi; \theta_i, \Delta_i) d\phi. \quad (2.28)$$

We can notice the similarity between the CD model in Eq. (2.27) and the point source model in Eq. (2.5). Indeed the CD model includes the GSV $\underline{\mathbf{c}}(\theta_i, \Delta_i)$ which integrates the the point source steering vector $\underline{\mathbf{a}}(\phi)$ (given in Eq. (2.6)) over an angular range $[-\pi/2, \pi/2]$. Each source is characterized by the GSV that depends on the DOA θ , spread Δ and the angular spread distribution h . Therefore the CD model presents a generalization of the point source model, consequently straightforward generalization can be made on the source and array correlation matrix. Indeed the rank of the noise-free correlation matrix is equal to the number of sources. Consequently, most classical direction-finding methods, which are based on the point source assumption, can be easily extended to the CD source case (see [2, 22, 33, 40]).

Starting from chapter 3 we will adopt the CD source model for the rest of the thesis. Also, the CD source model will be considered in the generalized near field context with

more details about the array correlation matrix given in Eq. (2.23).

Incoherently Distributed (ID)

A distributed source is said to be ID if its components arriving from different directions are independent. For example in the radio-waves transmission through troposphere scatter links or different sea bed layers, the reflected signal rays have uncorrelated phases. Similar effects are observed with signal rays reflections issued from different parts of a rough surface. When dealing with uncorrelated signal components the expression of the auto-correlation kernel in Eq. (2.22) is reduced to:

$$\rho(\phi, \phi'; \theta_i, \Delta_i) = \sigma_i^2 \rho(\phi; \theta_i, \Delta_i) \delta(\phi - \phi'). \quad (2.29)$$

$\delta(\phi - \phi')$ is the Dirac delta-function, σ_i^2 is the i -th source power and $\rho(\phi; \theta_i, \Delta_i)$ is the normalized angular power density. Therefore, we can express the noise free correlation matrix in Eq. (2.23) as:

$$\mathbf{R}_s = \sum_{i=1}^q \sigma_i^2 \int_{-\frac{\pi}{2}}^{\frac{\pi}{2}} \mathbf{a}(\phi) \rho(\phi; \theta_i, \Delta_i) \mathbf{a}^H(\phi) d\phi. \quad (2.30)$$

We can notice that the discrete model in Eq. (2.12) explained in section 2.1.2 tends to the ID model with a large number of rays N .

2.2 Classical Estimators

The localization problem is the estimation of the DOAs. First, we will consider the point model in Eq. (2.5) then we will present generalized methods for CD source model in Eq. (2.27). The methods to be described in this section are not based on any assumption related to the correlation structure of the data. Thus, they may be considered to be “non-parametric” (or non model-based). The main idea is based on defining a cost function $S(\theta)$ (also called criterion) that depends on the parameter of interest to estimate (like DOA θ). Then, the desired parameter estimation is obtained by $S(\theta)$ so that:

$$\hat{\theta} = \arg \max_{\theta} S(\theta). \quad (2.31)$$

2.2.1 Classical Beam Forming

Also known by *delay and sum*, the Classical Beam Forming (CBF) is the most standard method in source localization. The CBF can be interpreted as spatial filtering as explained in [13, 34] where the filter properties are defined in the following way:

- P1: it recovers the source signal $s(t)$ in a noise-free environment. In another words, it maximizes the filter power output for the source signal of DOA θ_f . Therefore, the constraint is: $\underline{\mathbf{w}}(\theta_f)^H \underline{\mathbf{a}}(\theta_f) = 1$;
- P2: it minimizes the filter power output for a spatially white noise input. It then involves: $\min_{\underline{\mathbf{w}}(\theta_f)} \underline{\mathbf{w}}(\theta_f)^H \underline{\mathbf{w}}(\theta_f)$.

The optimal weights $\underline{\mathbf{w}}(\theta_f)$ of the filter can be computed by the Lagrangian optimization method, it follows:

$$\underline{\mathbf{w}}(\theta_f) = \frac{\underline{\mathbf{a}}(\theta_f)}{\|\underline{\mathbf{a}}(\theta_f)\|^2}, \quad (2.32)$$

where $\underline{\mathbf{a}}(\theta_f)$ is the steering vector for a source coming form a DOA θ_f given in Eq. (2.6). The norm of this steering vector in the point source case (also in the near-field case) $\|\underline{\mathbf{a}}(\theta_f)\|^2 = M$. Localization of source using CBF filter consists in finding a DOA θ which maximizes the power of the output of the filter. It follows that the estimates is given by:

$$\hat{\theta} = \arg \max_{\theta} S_{\text{CBF}}(\theta), \quad (2.33)$$

with:

$$S_{\text{CBF}}(\theta) = \frac{\underline{\mathbf{a}}^H(\theta) \mathbf{R}_x \underline{\mathbf{a}}(\theta)}{M^2}. \quad (2.34)$$

From the above equations, one can see clearly that this method does not rely on any of the data model $\underline{\mathbf{x}}(t)$ as discussed in [23]. Meanwhile, the array measurements are collected to compute the estimated correlation matrix $\hat{\mathbf{R}}_x$ Eq. (2.10). Therefore, such method is known by the ease of its implementation.

Reviewing the CBF expression in Eq. (2.34), the above given filter properties (P1 and P2) can be verified. Considering the CBF weight in Eq. (2.32), the data correlation matrix given in Eq. (2.8) with $\mathbf{R}_n = \sigma^2 \mathbf{I}_M$ is inserted into Eq. (2.34):

$$\begin{aligned} S_{\text{CBF}}(\theta) &= \frac{1}{M^2} \left[\sum_{i=1}^q |s_i(t)|^2 |\underline{\mathbf{a}}^H(\theta) \underline{\mathbf{a}}(\theta_i)|^2 + \sigma^2 \mathbf{I}_M \underline{\mathbf{a}}^H(\theta) \underline{\mathbf{a}}(\theta) \right], \\ &= \frac{1}{M^2} \left[\sum_{i=1}^q |s_i(t)|^2 |\underline{\mathbf{a}}^H(\theta) \underline{\mathbf{a}}(\theta_i)|^2 + \sigma^2 M \mathbf{I}_M \right]. \end{aligned} \quad (2.35)$$

In a particular situation, of two point sources which are present in the view field of the array with DOAs θ_1 and θ_2 ($q = 2$), the criterion of the CBF in Eq. (2.35) for the first source is

denoted by:

$$\begin{aligned} S_{\text{CBF}}(\theta_1) &= \frac{1}{M^2} \left[\sum_{i=1}^2 |s_i(t)|^2 |\underline{\mathbf{a}}^H(\theta) \underline{\mathbf{a}}(\theta_i)|^2 + \sigma^2 M \mathbf{I}_M \right], \\ &= |s_1(t)|^2 + \frac{|s_2(t)|^2}{M^2} |\underline{\mathbf{a}}^H(\theta_1) \underline{\mathbf{a}}(\theta_2)|^2 + \frac{\sigma^2}{M} \mathbf{I}_M. \end{aligned} \quad (2.36)$$

We can see from Eq. (2.36) that CBF maintains the original source power and attenuates the background noise by the M factor. Whereas, for the second source, the attenuation is $\frac{|\underline{\mathbf{a}}^H(\theta_1) \underline{\mathbf{a}}(\theta_2)|^2}{M^2}$. Depending on the angular space between DOAs this interference term becomes significant. More precisely, the term $|\underline{\mathbf{a}}^H(\theta_1) \underline{\mathbf{a}}(\theta_2)|^2$ is lower bounded by M . Suppose θ_1 is too close to θ_2 ($\theta_1 \simeq \theta_2$) then the CBF peak will be affected by the second source power $|s_2(t)|^2$ and the desired beam will envelope the two estimated DOAs giving an error on the estimated $\hat{\theta}_1$. Whereas, the spatial resolution is an important characterization of the method performance.

In the literature, another beamformer method exists called Capon [11]. It is an adaptive method where the second filter property is exploited in a way to attenuate any other signal that actually impinges on the array from a different DOA ($\neq \theta$) of the original source signal. Thanks to the Minimum Variance Distortion-less Response (MVDR) criterion on the received signals, the Capon filter is also a direct method for source localization which has better spatial resolution than the CBF. Capon method is a less robust and a more complex method than the CBF, since it requires the inverse of the correlation matrix \mathbf{R}_x^{-1} .

2.2.2 Generalized Beam Forming

The distributed sources, especially the CD case, are characterized by their spread Δ and their spatial distribution h (see subsection 2.1.3) given in the Generalized Steering Vector (GSV) Eq. (2.54) of each source. In the conventional beam forming method, the maximizing weight vector $\underline{\mathbf{w}}(\theta_f)$ is given by the steering vector in Eq. (2.32). A straightforward generalization [38, 40] of the CBF can be applied to the case of CD source to give the Generalized Beam Forming (GBF) method. Noticing that the GSV is a function of the DOA θ and angular spread Δ of the source, the new beam former must account the two parameters. Therefore the new criterion of the GBF consists of a bi-dimensional search over θ and Δ space. It is expressed as:

$$(\hat{\theta}, \hat{\Delta}) = \arg \max_{\theta, \Delta} S_{\text{GBF}}(\theta, \Delta), \quad (2.37)$$

with:

$$S_{\text{GBF}}(\theta, \Delta) = \frac{\underline{\mathbf{c}}^H(\theta, \Delta) \mathbf{R}_x \underline{\mathbf{c}}(\theta, \Delta)}{\|\underline{\mathbf{c}}(\theta, \Delta)\|^2}, \quad (2.38)$$

and

$$\underline{\mathbf{c}}(\theta, \Delta) = \int_{-\frac{\pi}{2}}^{\frac{\pi}{2}} \underline{\mathbf{a}}(\phi) h(\phi; \theta, \Delta) d\phi \quad (2.39)$$

Unlike the CBF case, the norm of the GSV $\|\underline{\mathbf{c}}(\theta, \Delta)\|^2$ in Eq. (2.38), is a function of both the DOA and the source spread. Therefore, the GBF method suffers from a bi-dimensional optimization problem. The impact of the angular spread Δ has been studied in [26] via theoretical and simulations studies for the CD and ID sources.

We will discuss in chapter 5 how the CBF and the GBF will be used to localize the sources and estimate their powers. We also compare CBF and GBF to other methods. For the GBF, the expression of the GSV considers a two dimensional CD source that depends on the shape of the spatial spread distribution h .

Also a Generalized Capon (G-Capon) method can be developed for the CD source [19, 39]. Despite that, this method may improve the spatial resolution as discussed before meanwhile it still suffers from the same GBF optimization problem.

The common advantage of these two non parametric methods GBF and G-Capon is that they do not assume anything about the statistical properties of the data and, consequently, they can be used in situations where one lacks information about these properties. However, when dealing with closed multi-sources scenario; disadvantages of these methods appear in the resolution capacity, because the wide beam quickly deteriorates the method performance for a point or a CD sources. In the sequel we will present the concept of high resolution methods for point and distributed source.

2.3 High Resolution Estimators

These methods were developed in the 1980's. The high resolution term means theoretically: "Infinitely asymptotic resolution capacity". More precisely, we can theoretically resolve (detect) very closed sources for any SNR values when the snapshots number tends to infinity (to provide a better estimation of the array correlation matrix). Performance of such estimators approximately reaches the maximum likelihood performance with minor complexity burden [1].

Recalling the point source model in Eq. (2.5), we also assume that $\text{rank}(\mathbf{A}(\theta)) = q$ (full rank) which means that the steering vectors $\{\underline{\mathbf{a}}(\theta_i)\}_{i=1, \dots, q}$ are linearly independent. Since the sources are uncorrelated with each other, the matrix \mathbf{R}_s in equation (2.8) has a full rank ($\text{rank}(\mathbf{R}_s) = q$).

Given the above assumptions and considering that \mathbf{R}_x is semi-definite positive Hermitian ($\mathbf{R}_x = \mathbf{R}_x^H$) matrix Eq. (2.8), \mathbf{R}_x admits an Eigen Decomposition (ED). This ED results in orthonormal eigenvectors \mathbf{u}_i , ($i \in [1, \dots, M]$) and real positive eigenvalues λ_i satisfying $0 \leq \lambda_M \leq \lambda_{M-1} \leq \dots \leq \lambda_i \leq \dots \leq \lambda_1$; Thus we get:

$$\mathbf{R}_x = \mathbf{U}_x \mathbf{\Lambda}_x \mathbf{U}_x^H = \sum_{i=1}^M \lambda_i \mathbf{u}_i \mathbf{u}_i^H. \quad (2.40)$$

formed with $\mathbf{U}_x = [\mathbf{u}_1, \mathbf{u}_2, \dots, \mathbf{u}_M]$ is a unitary matrix ($\mathbf{U}_x \mathbf{U}_x^H = \mathbf{U}_x^H \mathbf{U}_x = \mathbf{I}_M$) the eigenvectors and $\mathbf{\Lambda}_x = \text{diag}(\lambda_1, \lambda_2, \dots, \lambda_M)$ is the diagonal matrix eigenvalues.

From Eq. (2.8) we notice that $\text{rank}(\mathbf{A}(\theta) \mathbf{R}_s \mathbf{A}^H(\theta)) = q$. Then accounting the ED of $\mathbf{A}(\theta) \mathbf{R}_s \mathbf{A}^H(\theta)$, define the matrix $\mathbf{\Lambda}_s \in \mathbb{R}^{*q}$ of the positive eigenvalues:

$$\mathbf{\Lambda}_s = \text{diag}(\tilde{\lambda}_1, \tilde{\lambda}_2, \dots, \tilde{\lambda}_q). \quad (2.41)$$

From Eq. (2.8), Eq. (2.40) and Eq. (2.41) we can understand the relationship between $\mathbf{\Lambda}_x$ (the eigenvalues of \mathbf{R}_x) and $\mathbf{\Lambda}_s$ as:

$$\begin{cases} \lambda_m = \tilde{\lambda}_m + \sigma^2 & \text{for } m = 1, 2, \dots, q, \\ \lambda_m = \sigma^2 & \text{for } m = q + 1, q + 2, \dots, M. \end{cases} \quad (2.42)$$

Then we can rewrite $\mathbf{\Lambda}_x$ from equation (2.40) as:

$$\mathbf{\Lambda}_x = \begin{bmatrix} \mathbf{\Lambda}_s + \sigma^2 \mathbf{I}_q & \mathbf{0} \\ \mathbf{0} & \sigma^2 \mathbf{I}_{M-q} \end{bmatrix}. \quad (2.43)$$

Given the relation in Eq. (2.43), the signal information $\mathbf{A}(\theta) \mathbf{R}_s \mathbf{A}^H(\theta)$ belongs to the q eigenvectors $[\mathbf{u}_1, \mathbf{u}_2, \dots, \mathbf{u}_q]$ associated to the q highest eigenvalues $[\lambda_1, \lambda_2, \dots, \lambda_q]$. Whereas, the noise information belongs to the $M - q$ eigenvectors associated to the smallest $M - q$ eigenvalues $[\lambda_{q+1}, \lambda_{q+2}, \dots, \lambda_M]$. We define the basis of the signal and noise subspaces as:

$$\begin{cases} \mathbf{E}_s = [\mathbf{u}_1, \mathbf{u}_2, \dots, \mathbf{u}_q] \\ \mathbf{E}_n = [\mathbf{u}_{q+1}, \mathbf{u}_{q+2}, \dots, \mathbf{u}_M]. \end{cases} \quad (2.44)$$

Some properties can be exploited with the previously defined subspaces.

$$\begin{aligned} \mathbf{R}_x \mathbf{E}_n &= \mathbf{E}_n \sigma^2 \mathbf{I}_{M-q} \\ \mathbf{A}(\theta) \mathbf{R}_s \mathbf{A}^H(\theta) \mathbf{E}_n &= \sigma^2 [\mathbf{E}_n \mathbf{I}_{M-q} - \mathbf{I}_M \mathbf{E}_n] = \mathbf{0} \\ \mathbf{A}^H(\theta) \mathbf{E}_n &= \mathbf{0}. \end{aligned} \quad (2.45)$$

From Eq. (2.45), the subspace spanned by \mathbf{E}_n (noise subspace) belongs to the null space of $\mathbf{A}^H(\theta)$ which is also called $\text{Ker}(\mathbf{A}^H(\theta))$.

2.3.1 Standard MUSIC

The Multiple Signal Classification (MUSIC) was proposed by Schmidt [28] and independently by Bienvenu and Kopp [8]. It is a generalization of Pisarenko work and relies on the orthogonality between the signal subspace \mathbf{E}_s and the noise subspace \mathbf{E}_n . Thus, one can write the following:

$$\mathbf{E}_n^H \underline{\mathbf{a}}(\theta_i) = 0 \text{ for } i = 1, \dots, q. \quad (2.46)$$

We define the following function:

$$g(\theta) = \underline{\mathbf{a}}^H(\theta) \mathbf{E}_n \mathbf{E}_n^H \underline{\mathbf{a}}(\theta). \quad (2.47)$$

The orthogonality property accounts that the q DOA θ_i for $i = 1, \dots, q$ are the roots of the function :

$$g(\theta_i) = 0 \text{ for } i = 1, \dots, q. \quad (2.48)$$

Practically, From the L measured snapshots, we estimate the correlation matrix \mathbf{R}_x according to Eq. (2.10), then we estimate the noise subspace $\hat{\mathbf{E}}_n$. For the estimation of the q DOAs of the source, we search for the q prominent peaks in the following MUSIC criterion:

$$\hat{\theta} = \arg \max_{\theta} S_{\text{MUSIC}}(\theta), \quad (2.49)$$

with:

$$S_{\text{MUSIC}}(\theta) = \frac{1}{\underline{\mathbf{a}}^H(\theta) \hat{\mathbf{E}}_n \hat{\mathbf{E}}_n^H \underline{\mathbf{a}}(\theta)}, \quad (2.50)$$

2.3.2 Generalized MUSIC for Distributed Sources

Following the approach of the point source based MUSIC method leading to equation (2.47), a generalization of the distributed source of this method (see [33] for more details on the generalization demonstration) consists in estimating both the DOA $\hat{\theta}$ and spread $\hat{\Delta}$ in the far-field case by the following expression:

$$(\hat{\theta}, \hat{\Delta}) = \arg \max_{\theta, \Delta} \frac{1}{\text{Tr}(\hat{\mathbf{E}}_n^H \mathbf{H}(\theta, \Delta) \hat{\mathbf{E}}_n)}, \quad (2.51)$$

where $Tr(\cdot)$ is the matrix trace and $\mathbf{H}(\theta, \Delta)$ is the matrix array manifold defined by:

$$\mathbf{H}(\theta, \Delta) = \int_{-\frac{\pi}{2}}^{\frac{\pi}{2}} \int_{-\frac{\pi}{2}}^{\frac{\pi}{2}} \underline{\mathbf{a}}(\phi) \rho^*(\phi, \phi'; \theta, \Delta) \underline{\mathbf{a}}^H(\phi') d\phi d\phi'. \quad (2.52)$$

In the CD source case, the DSPE can be expressed as follows:

$$(\hat{\theta}, \hat{\Delta}) = \arg \max_{\theta, \Delta} \frac{1}{\underline{\mathbf{c}}^H(\theta, \Delta) \hat{\mathbf{E}}_n \hat{\mathbf{E}}_n^H \underline{\mathbf{c}}(\theta, \Delta)}, \quad (2.53)$$

with $\underline{\mathbf{c}}(\theta, \Delta)$ represents the GSV in Eq. (2.54) as:

$$\underline{\mathbf{c}}(\theta, \Delta) = \int_{-\frac{\pi}{2}}^{\frac{\pi}{2}} \underline{\mathbf{a}}(\phi) h(\phi; \theta, \Delta) d\phi. \quad (2.54)$$

This method, known as Distributed Signal Parameter Estimator (DSPE) consists in searching q prominent peaks in a two dimensional grid. For the DSPE expression Eq. (2.53), a new parameter Δ is to be estimated compared to the MUSIC spectrum Eq. (2.50), whereas the DSPE requires a modest increase in computational load.

In the above expression, the angular spread distribution h and the angular power density $\rho(\phi; \theta_i, \Delta_i)$ (also given in Eq. (2.24) and Eq. (2.29)) must be *a priori* known for the CD and ID cases explained in subsection 2.1.3. However, the assumption of knowing the distribution function of the spatial extension is not realistic in practice. Since in our work we are only interested in the CD modeling case, we will introduce in the next chapter a new method to avoid the *a priori* knowledge of the angular distribution h .

Another subspace based method for distributed source exists namely Total Least Square - Estimation of Signal Parameters via Rotational Invariance Techniques (TLS-ESPRIT) [29] which is the ESPRIT [27] variant estimator for point source. The central angles are estimated using TLS-ESPRIT for both ID and CD sources. Once the DOA are estimated, for the CD source case, the spread estimation is obtained by re-injecting the DOA estimation into the DSPE and seeking for the value that maximizes the 1-D spectrum. This version demands less computational complexity than the DSPE. However, it requires a condition for the spacing between the sub-arrays and consists in considering an approximation of the steering vector.

2.4 Near Field (NFE)

The far-field assumption given in the signal modeling section is not valid in several applications [18, 20] especially in the aero-acoustic fields where the problem resides in localizing

sources in a near-field zone of the array. Usually when considering near-field situation, the source must be in the so-called Fresnel zone [18]. The source is characterized by an additional range r parameter that will also bring changes to the steering vector $\underline{\mathbf{a}}(\theta)$ described in section 2.1.

In the near-field context we should consider the spherical shape of the waves impinging on the sensors. Consequently, the time delay τ_{m+1} corresponding to the signal propagation time between the sensor m and a reference sensor (e.g the first one) can be approximated by (see [18] for details):

$$\tau_{m+1} = \frac{2\pi r}{\lambda} \left(\sqrt{1 + \frac{m^2 d^2}{r^2} - \frac{2md \sin(\theta)}{r}} - 1 \right). \quad (2.55)$$

Equation (2.55) can be further simplified assuming that the source is located in the Fresnel region. The Fresnel region is defined by the following inequality (see [36] for details):

$$0.62 \sqrt{d^3 (M-1)^3 / \lambda} < r < 2d^2 (M-1)^2 / \lambda. \quad (2.56)$$

Under this assumption the time delay Eq. (2.55) is given by:

$$\tau_{m+1} = -2\pi \frac{d}{\lambda} \sin(\theta) m + \pi \frac{d^2}{\lambda r} \cos^2(\theta) m^2 + \mathcal{O}\left(\frac{d^2}{r^2}\right), \quad (2.57)$$

where $\mathcal{O}(d^2/r^2)$ denotes the terms of the order or smaller than d^2/r^2 which are neglected. Thus, for $d = \lambda/2$, the $(m+1)$ th element of the steering vector $\underline{\mathbf{a}}(\theta, r)$ is denoted by:

$$a_{m+1}(\theta, r) = \exp\left(-j\pi \sin(\theta) m + j \frac{\pi \lambda}{4r} \cos^2(\theta) m^2\right). \quad (2.58)$$

2.4.1 Near Field Estimator

Assuming point sources, the standard DOA MUSIC estimator [28] can be generalized for near-field and it consists in searching the q peaks of the two-dimensional cost function $S_{\text{NFE}}(\theta, r)$ so that:

$$(\hat{\theta}, \hat{r}) = \arg \max_{\theta, r} S_{\text{NFE}}(\theta, r), \quad (2.59)$$

$$(\hat{\theta}, \hat{r}) = \arg \max_{\theta, r} \frac{1}{\underline{\mathbf{a}}^H(\theta, r) \hat{\mathbf{E}}_n \hat{\mathbf{E}}_n^H \underline{\mathbf{a}}(\theta, r)}. \quad (2.60)$$

Here, $\underline{\mathbf{a}}^H(\theta, r)$ is defined by equation (2.58) and $(\hat{\theta}, \hat{r})$ are the DOA and range estimates, respectively.

2.4.2 Near Field Side Works

Near-field sources localization has been an active field of research for many years. One can cite low complexity estimators by exploring periodic properties to approximate the array manifold in [35] or by generalizing the root-MUSIC [31] and then exploring parallelism techniques to compute the cost function. Another approach relies on the use of higher order ESPRIT-like algorithms where a performance analysis on the lower bound is investigated [36]. The maximum-likelihood estimator for wide-band near-field sources is given in [12] where DOA estimation is better over high frequencies than over lower ones. Also the range estimation can be obtained with unknown sensor location. To overcome complexity, pairing parameters and minimize the aperture loss, a joint DOA, range, frequency estimator is derived based on second order statistics [24]. All of the work given above can be used in the near-field. However, in our work, we will adopt the classical near field estimator explained in subsection 2.4.1.

2.5 Conclusion

First, we have introduced the source localization principle by explaining the classical model that relies on standard assumptions like point source situated in a far-field where the source is mainly described by its DOA. Then, two mainly distributed sources models (the discrete and continuous one) have been presented which rely on characterizing the spatial extension of the source by an additional spread parameter.

Next, For source localization we recalled the classical and the high resolution methods for point source assumption and their generalized distributed source case. The Beamforming techniques offer simple, direct and easy implementation. However, their poor spatial resolution presents serious disadvantages in a multi-source scenario and for closed CD sources especially with important spatial spreads. The reason that pushes us towards high resolution methods like MUSIC and DSPE because they offer a good spatial resolution.

Finally, We explain the property of the near-field that accounts the spherical wave propagation in the time delay expression Eq. (2.55). The main idea relies in considering the DOA and the range for characterizing the source. The conjunction of distributed source and near-field will be presented in the next chapter. We will explain the generalized CD model in near-field where the source will be characterized by three parameters: DOA, range and spread.

I have learned silence from the talkative, toleration from the intolerant, and kindness from the unkind; yet, strange, I am ungrateful to those teachers.

Gebran Khalil Gebran

3

Estimator with Unknown Angular Spread Shape

3.1 Introduction

In this chapter, we consider the (CD) source model in near-field explained in the subsection 2.1.3 of the previous chapter in order to propose a new estimator. The estimators proposed in the literature do not take into consideration the aspect of spatial distributed sources in conjunction with the aspect of near-field propagation.

The Distributed Signal Parameter Estimator (DSPE) [33], presented in subsection 2.3.2 of chapter 2, has a major drawback: it requires the knowledge of the distribution function of the angular spread distribution. Also, this method suffers from robustness issues with respect to the imperfect knowledge of this distribution. In other words, an *a priori* information about the angular spread shape must be provided for good performance. A solution based on decoupling the direction of arrival θ from the angular spread Δ estimation has been proposed in [7] using the correlation matching method. This method is developed in the case of ID sources but suffers from ambiguity problem. Zoubir and Wang proposed a decoupled estimation of the DOA and the angular spread for far-field sources [37]. This method provides a robust estimation only for DOA but it requires the knowledge of the angular spread shape distribution in order to estimate the angular spread parameter.

These reasons motivate us to propose an estimator of CD sources in near-field which is robust to the imperfect knowledge of the angular spread distribution. First, we extend the model [33] presented in subsection 2.1.3 in the near-field context with the aim of con-

sidering the angular spread when the sources are close to the array. Then, we discuss the limits of the DSPE algorithm with different angular distribution shapes for the near-field context. Finally, we propose a modification of the DSPE which consists in using a generic function family to describe the angular spread distribution. The method called Joint Angle, Distance, Spread, Shape Estimator (JADSSE) tends to estimate the distribution shape parameter in addition to the three other parameters.

The contributions of this chapter have been published in [3] and can be summarized by:

- Extending the CD source model [33] to near-field.
- Extending the DSPE [33] to near-field.
- Proposing the JADSSE to increase the robustness of the estimator without the knowledge of h in Eq. (2.24).

3.2 Signal Model of CD Source in Near-Field

Here, we extend the CD source model previously described in subsection 2.1.3 into the near-field context, considering an angular spread of DOA¹. Let us assume q spatially distributed narrow-band near-field sources impinging on M sensors (see Fig.3.1).

We also suppose that the sources and the sensors are in the same plane. The $M \times 1$ base-band signal vector measured by the M sensors is given by $\underline{\mathbf{x}}(t) = [x_1(t), \dots, x_M(t)]^T$. The far-field model in Eq. (2.27) can be generalized to the near-field using the steering vector in Eq. (2.58) explained in section 2.4 of the previous chapter. As explained in chapter 2, we recall that a CD source is described by a temporally invariant angular distribution where the signal components are fully correlated.

For multiple CD sources, the model of the received signal for q sources in near-field is given by:

$$\underline{\mathbf{x}}(t) = \sum_{i=1}^q s_i(t) \underline{\mathbf{c}}(\theta_i, \Delta_i, r_i) + \underline{\mathbf{n}}(t). \quad (3.1)$$

$s_i(t)$ is a random complex signal emitted by the i -th source and $h_i(\phi; \theta_i, \Delta_i)$ represents a deterministic angular spread distribution. $\underline{\mathbf{c}}(\theta_i, \Delta_i, r_i)$ is the vector obtained by integrating the steering vector $\underline{\mathbf{a}}(\phi, r_i)$ given in Eq. (2.58) with the angular distribution of the i -th

¹Similarly a range spread can be also considered. However, we only consider the angular spread in order to make this chapter more readable. Note that in chapter 5 the model is considered in its (x, y) coordinates system and the range spread will be implicitly considered in the modeling

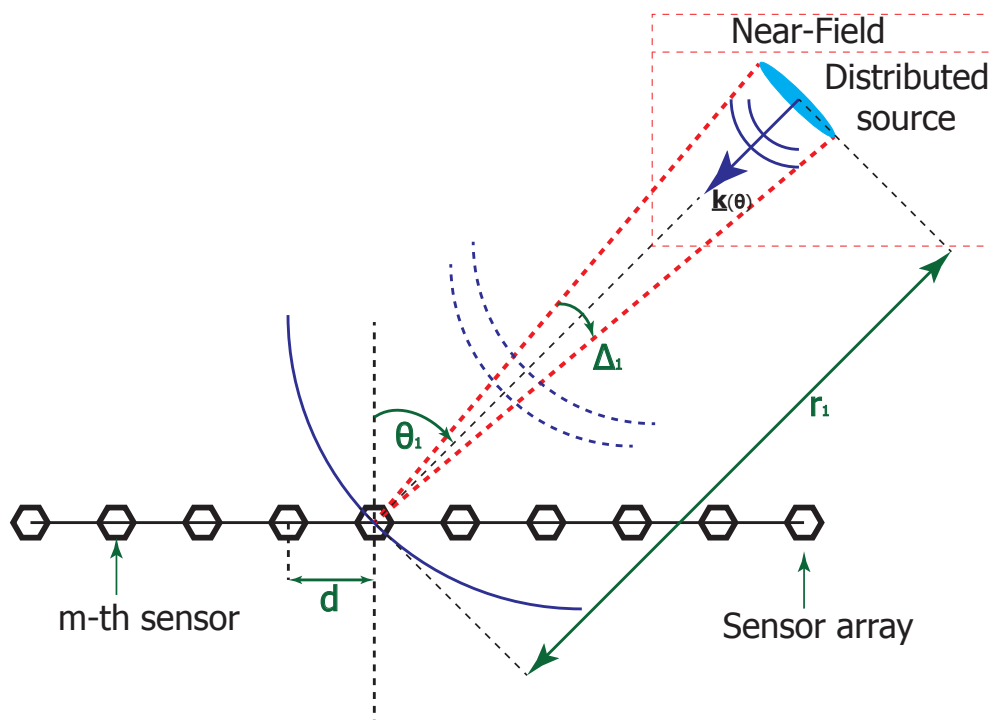


Figure 3.1: Localization of a distributed source in near-field

source $h_i(\phi; \theta_i, \Delta_i)$ as follows:

$$\underline{\mathbf{c}}(\theta_i, \Delta_i, r_i) = \int_{-\frac{\pi}{2}}^{\frac{\pi}{2}} \underline{\mathbf{a}}(\phi, r_i) h_i(\phi; \theta_i, \Delta_i) d\phi, \quad (3.2)$$

The source signal and noise time samples are modeled by random, complex, centered and independent processes. We assume that the noise and the sources $s_i(t)$ are uncorrelated.

3.3 Proposed Estimators

In this section, we present two methods for joint angle, spread and range estimation for the localization of CD sources in a near field. First, we introduce an extension of the MUSIC-like DSPE algorithm [33] (subsection 2.3.2 in chapter 2), called Near Field-DSPE (NF-DSPE). This method is highly dependent on the shape of $h(\phi; \theta, \Delta)$. Next, we present the Joint Angle, Distance, Spread and Shape Estimator (JADSSE). This algorithm consists of a robust estimation of all the above mentioned parameters to localize the distributed sources in a near field. Finally, for comparison between the distributed and point source models, we recall the Near Field Estimator (NFE) Eq. (2.60) from subsection 2.4.1 to localize the point sources [20].

3.3.1 Near Field-DSPE

In this subsection, we present the extension of the DSPE explained previously to the near-field case. It is a trivial extension, where we should consider the near-field range parameter r . Therefore, the NF-DSPE consists of a three dimensional optimization.

After an eigen analysis, the observation space of $\hat{\mathbf{R}}_x$ can be decomposed into a signal subspace and a noise subspace [28]. The estimated noise subspace basis $\hat{\mathbf{E}}_n$ is constructed with the $M - q$ eigenvectors $\hat{\mathbf{e}}_i$ associated with the lowest $M - q$ eigenvalues of $\hat{\mathbf{R}}_x$. Exploiting the properties of the eigenvectors gives us the following equality $\mathbf{C}^H \hat{\mathbf{E}}_n = 0$ [28].

The proposed estimator consists in minimizing the norm of the product between the estimated noise subspace $\hat{\mathbf{E}}_n$ and the analysis vector $\underline{\mathbf{c}}^H(\theta, \Delta, r)$. To obtain the estimated parameters $\hat{\theta}$, \hat{r} and $\hat{\Delta}$ for the q sources, the estimator consists in searching the q peaks of the three dimensional cost function $S_{\text{NF-DSPE}}(\theta, \Delta, r)$:

$$(\hat{\theta}, \hat{\Delta}, \hat{r}) = \arg \max_{\theta, \Delta, r} S_{\text{NF-DSPE}}(\theta, \Delta, r), \quad (3.3)$$

where:

$$S_{\text{NF-DSPE}}(\theta, \Delta, r) = \frac{1}{\underline{\mathbf{c}}^H(\theta, \Delta, r) \hat{\mathbf{E}}_n \hat{\mathbf{E}}_n^H \underline{\mathbf{c}}(\theta, \Delta, r)}, \quad (3.4)$$

$$\underline{\mathbf{c}}(\theta, \Delta, r) = \int_{-\frac{\pi}{2}}^{\frac{\pi}{2}} \underline{\mathbf{a}}(\phi, r) h(\phi, \theta, \Delta) d\phi. \quad (3.5)$$

and $\underline{\mathbf{a}}(\phi, r)$ is the near-field steering vector:

$$\underline{\mathbf{a}}(\phi, r) = \begin{bmatrix} 1 \\ e^{-j\pi \sin(\phi) + j\frac{\pi\lambda}{4r} \cos^2(\phi)} \\ \vdots \\ e^{-j\pi \sin(\phi)(M-1) + j\frac{\pi\lambda}{4r} \cos^2(\phi)(M-1)^2} \end{bmatrix} \quad (3.6)$$

Expression (3.4) is a MUSIC criterion with the analysis vector $\underline{\mathbf{c}}(\theta, \Delta, r)$ which depends on the angular distribution $h(\phi; \theta, \Delta)$. In the literature, the commonly used distributions are Gaussian and uniform. As explained in subsection 2.3.2, the main drawback of this approach is that the computation of $\underline{\mathbf{c}}(\theta, \Delta, r)$ in (3.5), requires *a priori* information about the angular spread distribution h .

3.3.2 Joint Angle Distance Spread Shape Estimator (JADSSE)

We aim here to localize and characterize CD sources in near-field with various angular spread shapes. Therefore, by adding a shape parameter we propose to use a parameterized functions family h which can adapt most of the well known angular distributions. For instance, we propose to represent $h(\phi; \theta, \Delta)$ by a Raised Cosine (RC) function. This function takes an additional positive parameter β into consideration to characterize the shape of the angular spread. The Raised Cosine is expressed by:

$$h(\phi; \theta, \Delta, \beta) = \begin{cases} 1/\Delta & \text{if } |\phi - \theta| \leq \frac{\Delta}{2}(1 - \beta), \\ 1/2\Delta \left[1 + \cos(\gamma) \right] & \text{if } \frac{\Delta}{2}(1 - \beta) < |\phi - \theta| \leq \frac{\Delta}{2}(1 + \beta), \\ 0 & \text{otherwise.} \end{cases} \quad (3.7)$$

with $\gamma = \frac{\pi}{\beta\Delta} \left[|\phi - \theta| - \frac{\Delta}{2}(1 - \beta) \right]$. This RC function can adapt various shapes of angular spread distributions: uniform distribution ($\beta = 0$) and bell shaped distribution ($\beta \neq 1$).

It follows that the proposed JADSSE consists in minimizing the norm of the product of $\hat{\mathbf{E}}_n$ and the vector $\underline{\mathbf{c}}(\theta, \Delta, r, \beta)$. The estimator relies on searching the q maxima of the

four-dimensional cost function:

$$(\hat{\theta}, \hat{\Delta}, \hat{r}, \hat{\beta}) = \arg \max_{\theta, \Delta, r, \beta} S_{\text{JADSSE}}(\theta, \Delta, r, \beta), \quad (3.8)$$

or equivalently:

$$(\hat{\theta}, \hat{\Delta}, \hat{r}, \hat{\beta}) = \arg \max_{\theta, \Delta, r, \beta} \frac{1}{\|\underline{\mathbf{c}}^H(\theta, \Delta, r, \beta) \hat{\mathbf{E}}_n\|^2}, \quad (3.9)$$

where:

$$\underline{\mathbf{c}}(\theta, \Delta, r, \beta) = \int_{-\frac{\Delta}{2}(1+\beta)}^{\frac{\Delta}{2}(1+\beta)} \underline{\mathbf{a}}(\phi, r) h(\phi; \theta, \Delta, \beta) d\phi. \quad (3.10)$$

The vector $\underline{\mathbf{c}}(\theta, \Delta, r, \beta)$ is a function of $h(\phi; \theta, \Delta, \beta)$. Choosing this parametric functions family ensures the ability to approximately fit functions like Gaussian for $\beta \geq 1$ and uniform for $\beta = 0$.

By introducing a general function family $h(\phi; \theta, \Delta, \beta)$ and by estimating the shape parameter β , the proposed JADSSE makes it possible to reconstruct the angular distribution without *a priori* information about its shape. This blind approach allows to increase the robustness of the estimation with respect to the shape of the angular spread distribution.

3.4 Numerical Results

Firstly, we compare the JADSSE and the NF-DSPE. Then, we show JADSSE asymptotic behavior in quadratic error versus SNR. Next, we compare the performance of the three methods (JADSSE, NF-DSPE and NFE) presented in section 3.3. The ULA consists of $M = 20$ sensors inter-spaced by $d = \lambda/2$ and the number of samples² is 1000 for estimating the correlation matrix in equation (2.10) using the model given in Eq. (3.1). For JADSSE, Raised Cosine angular spread distribution is used and the NF-DSPE performance is evaluated using three different angular spread distributions : Gaussian, uniform and Butterworth. To investigate the performance of the proposed estimators, the Root Mean Square Error (RMSE) of the estimates is evaluated with a Monte-Carlo simulation of 100 independent runs. The simplex based method is used to find the maximum of the cost function in equations (2.60), (3.3), and (3.9).

3.4.1 Criterion Analysis

This simulation consists of the following multi-sources scenario: two RCCD sources in near-field arrive from directions $\theta_1 = 0^\circ$ and $\theta_2 = 16^\circ$ with angular spreads of $\Delta_1 = 6^\circ$ and $\Delta_2 = 16^\circ$ and distances of $r_1 = 25\lambda$ and $r_2 = 25\lambda$, respectively, from the array and a

²Only in the first two simulations we take 100 snapshots

shape parameter $\beta_1 = \beta_2 = 0.5$. Both of the sources have an RC angular shape distribution (expression given in Eq. (3.7)). The SNR is fixed at 20 dB in this simulation.

In Fig.3.2 we plot the cost function (criterion) versus the DOA θ , spread Δ for fixed parameter r_1 : $S_{NF-DSPE}(\Delta, \theta; r_1)$ for the NF-DSPE Eq. (3.3) and for $S_{JADSSE}(\Delta, \theta; r_1, \beta_1)$ for the JADSSE Eq. (3.9) with fixed parameters $r = r_1, \beta = \beta_1$. These criteria are computed for NF-DSPE using Gaussian(Fig.3.2b), uniform(Fig.3.2c) and Butterworth [33] (Fig.3.2d) angular shape distribution. The plotted cost functions are normalized by the maximum value of $S(\Delta, \theta; r_1, \beta_1)$.

For the two Raised Cosine CD (RCCD) sources, JADSSE criterion S_{JADSSE} plotted in Fig.3.2a presents narrow peaks at the correct DOAs and spreads values. This property allows to easily localize the sources by finding the estimated values of DOAs $\hat{\theta}_1, \hat{\theta}_2$ and angular spreads $\hat{\Delta}_1, \hat{\Delta}_2$. Consequently, JADSSE offers a selective cost function to accurately estimate the same parameters.

Fig.3.2b depicts the NF-DSPE using Gaussian angular distribution. It presents two peaks at the correct DOAs values but spreads can not be estimated. It is the consequence of the mismatch between the angular distribution used to compute the criteria and the real distribution of the source. In addition, one can notice that the peaks are wide and of small amplitude especially for the second source which has a wide spread. Thus, the DOA estimation is expected to be less accurate compared to JADSSE. In Fig.3.2c, for the NF-DSPE with uniform angular distribution, the plot of the cost function presents two peaks approximately at the right position but with a small value and a wider peak extension for the second source (θ_2, Δ_2). Concerning the NF-DSPE with the Butterworth angular distribution in Fig.3.2d, the cost function presents a fuzzy image with two extremely small peaks relatively to Fig.3.2a that mismatch the initial source parameters. Therefore, this latter method suffers from poor performance.

The plots illustrate the fact that the criterion is strongly imputed by the choice of the shape of the source dispersion. Consequently, the estimation performance is expected to deteriorate when the shape of the spatial extension of the source mismatches with the actual shape. For the three above estimators, the difference in shape selection influences the cost function of the NF-DSPE that affects the maximum peaks search and subsequently deteriorates the estimator performance.

3.4.2 JADSSE Performance

In order to evaluate the estimation performance of JADSSE, we consider the following scenario. Herein, the simulation considers two mixed RCCD sources with the following

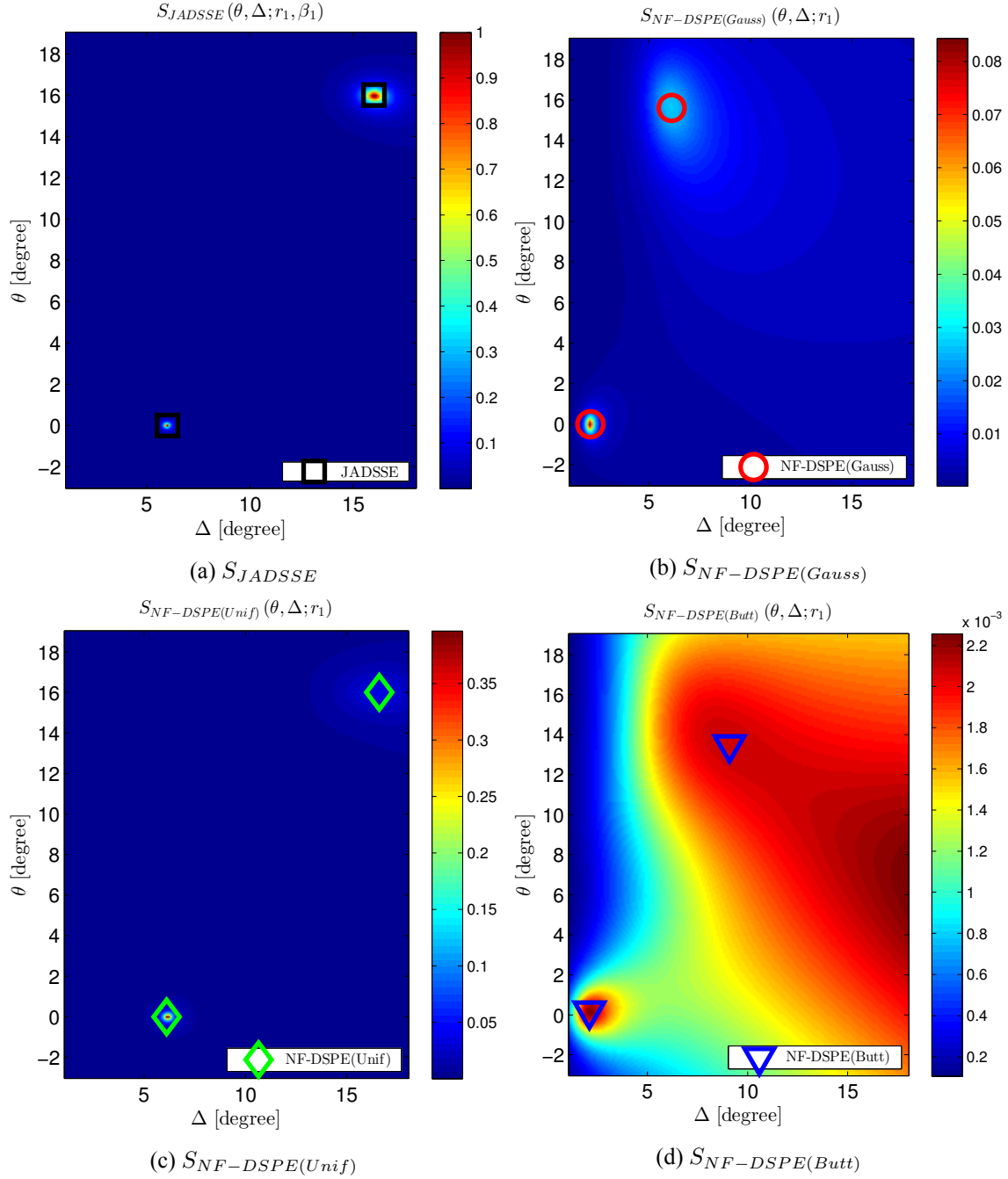


Figure 3.2: Plot of the cost function S for the Multi RCCD sources scenario at SNR=20dB. For each estimator S is plotted versus the DOA θ , spread Δ and for fixed parameters r_1, β_1 : $S(\Delta, \theta; r_1, \beta_1)$. True parameters for the first RCCD source: $\theta_1 = 0^\circ$, $\Delta_1 = 6^\circ$, $r_1 = 25\lambda$ and $\beta_1 = 0.5$, for the second RCCD source: $\theta_2 = 16^\circ$, $\Delta_2 = 16^\circ$, $r_2 = 25\lambda$ and $\beta_2 = 0.5$. Markers represent the maximum positions in the above criteria for the couple $(\hat{\Delta}, \hat{\theta})$. (\square : JADSSE, \diamond : NF-DSPE using uniform shape, \circ : NF-DSPE using Gaussian shape, ∇ : NF-DSPE using Butterworth shape).

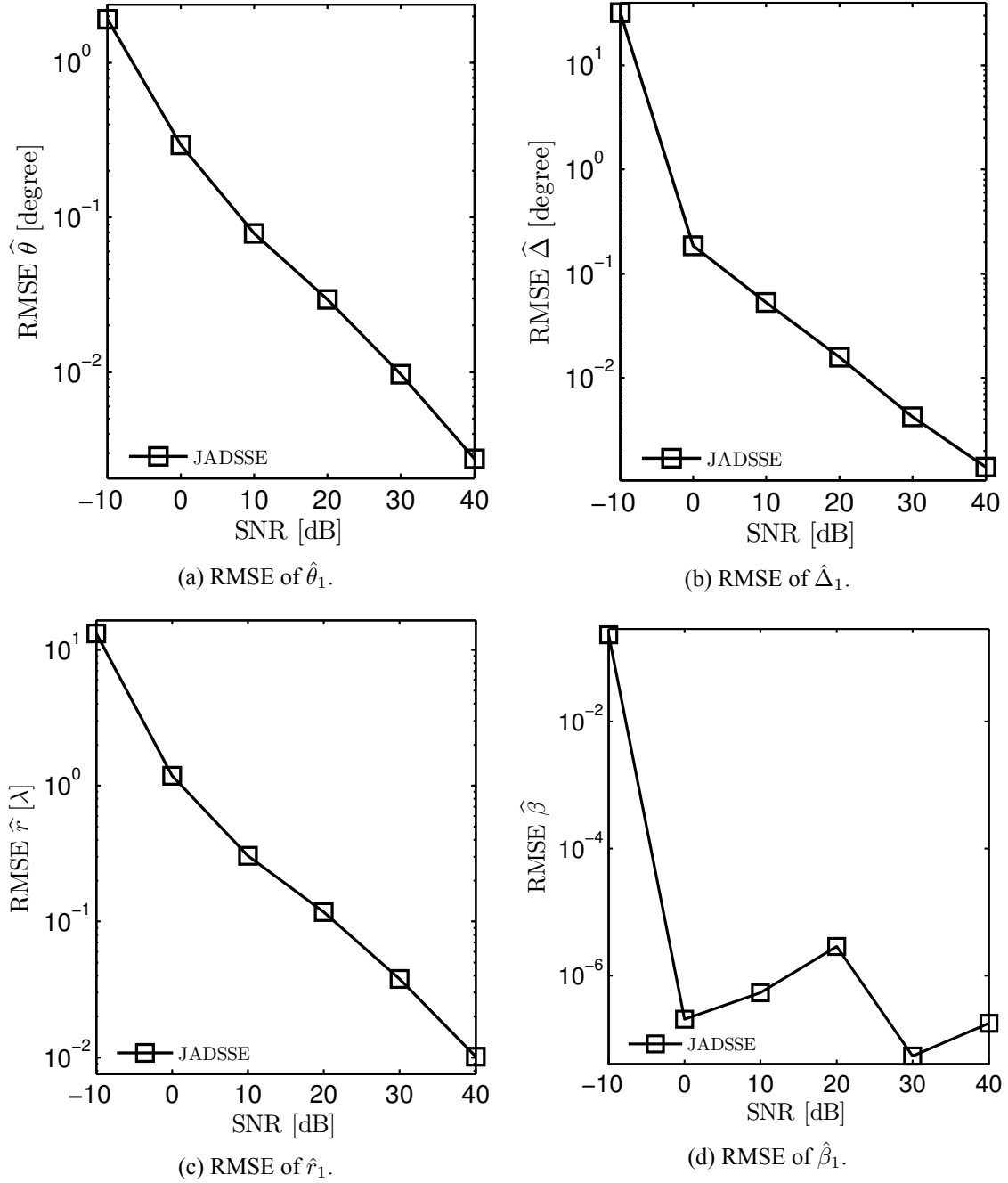


Figure 3.3: Root Mean Square Error of the estimated parameters $\hat{\theta}$, $\hat{\Delta}$, \hat{r} and $\hat{\beta}$ versus SNR for the first RCCD source in the mixed RCCD scenario. True parameters $\theta_1 = 0^\circ$, $\Delta_1 = 8^\circ$, $r_1 = 30\lambda$ and $\beta_1 = 0$.

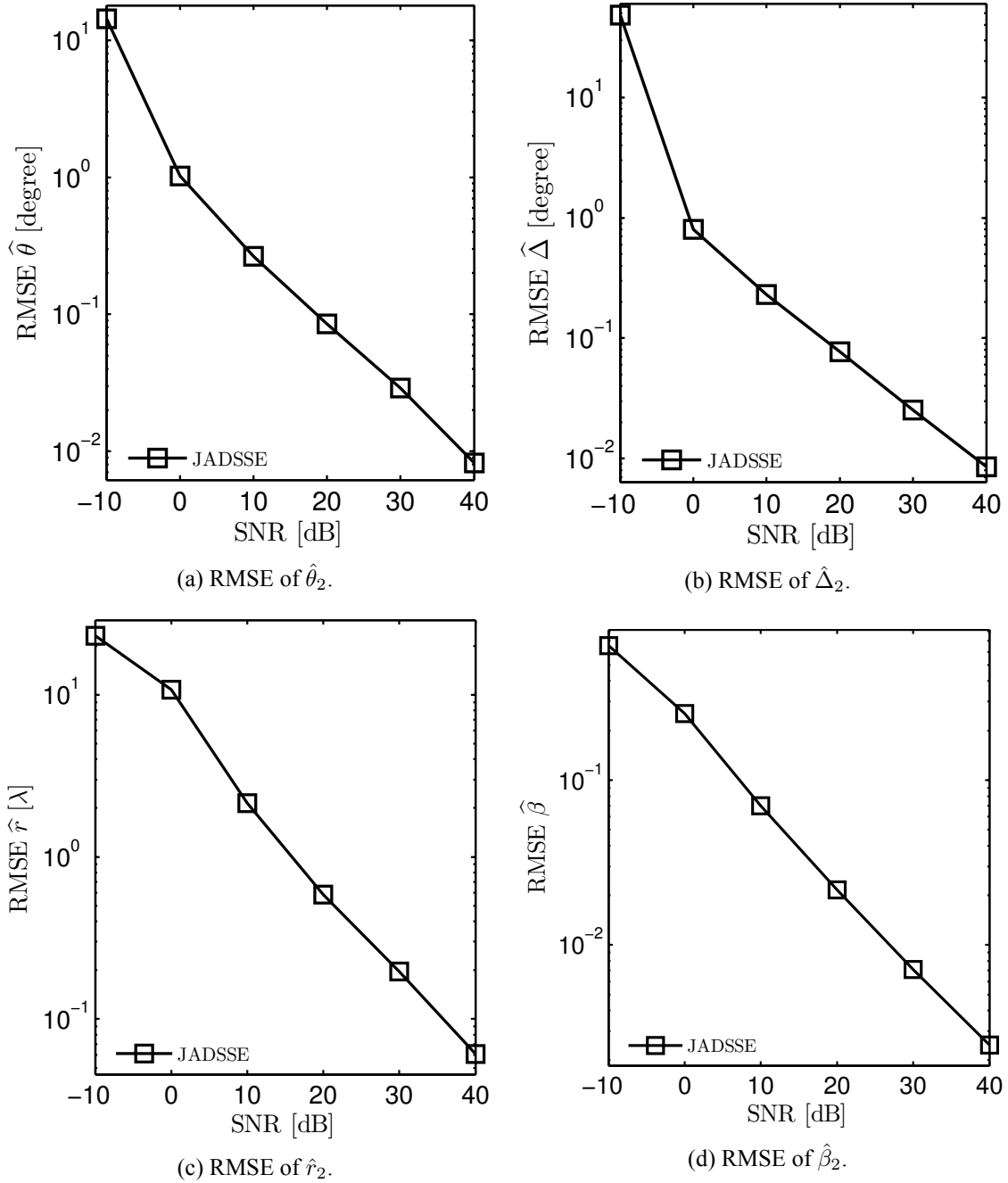


Figure 3.4: Root Mean Square Error of the estimated parameters $\hat{\theta}$, $\hat{\Delta}$, \hat{r} and $\hat{\beta}$ versus SNR for the second RCCD source in the mixed RCCD scenario. True parameters $\theta_2 = 30^\circ$, $\Delta_2 = 10^\circ$, $r_2 = 25\lambda$ and $\beta_2 = 1$.

parameters $\theta_1 = 0^\circ$, $\Delta_1 = 8^\circ$, $r_1 = 30\lambda$ and $\beta_1 = 0$ for the first source and $\theta_2 = 30^\circ$, $\Delta_2 = 10^\circ$, $r_2 = 25\lambda$ and $\beta_2 = 1$ for the second source. Fig.3.3 and Fig.3.4 depict the performance versus the SNR for all of the estimated parameters. For both sources, the RMSEs are plotted for the DOA $\hat{\theta}$ in Fig.3.3a and 3.4a, for the angular spread $\hat{\Delta}$ in Fig.3.3b and 3.4b, for the distance \hat{r} in Fig.3.3c and 3.4c and for the shape parameter $\hat{\beta}$ in Fig.3.3d and 3.4d. For all of the above parameters we can clearly see the asymptotic decrease of the RMSE for JADSSE. As expected, an asymptotical behavior for the JADSSE estimator appears in the simulations except for the case of $\hat{\beta}_1$. However, we must clarify that JADSSE operates well in this region and reaches relatively low RMSE values (10^{-6}).

3.4.3 Performance versus SNR

In the upcoming simulation, we consider the following multi-sources scenario: two CD sources and one point source in near-field that arrive from directions $\theta_1 = 0^\circ$, $\theta_2 = 30^\circ$ and $\theta_3 = 60^\circ$ with angular spreads $\Delta_1 = 5^\circ$, $\Delta_2 = 8^\circ$ and $\Delta_3 = 0^\circ$ with distances $r_1 = 30\lambda$, $r_2 = 25\lambda$ and $r_3 = 30\lambda$, respectively, from the array.

The source of $\theta_3 = 60^\circ$ is a point source whereas, the source of $\theta_1 = 0^\circ$ is Gaussian CD (GCD) with the angular spread distribution :

$$h(\phi, \theta_1, \Delta_1) = \frac{1}{\Delta_1 \sqrt{2\pi}} \exp \left[-0.5 \left(\frac{\phi - \theta_1}{\Delta_1} \right)^2 \right]. \quad (3.11)$$

The source of $\theta_2 = 30^\circ$ is Uniformly CD (UCD), that is

$$h(\phi, \theta_2, \Delta_2) = \begin{cases} \frac{1}{\Delta_2} & \text{if } |\phi - \theta_2| \leq \frac{\Delta_2}{2}, \\ 0 & \text{Otherwise.} \end{cases} \quad (3.12)$$

Note that the definition of the parameter Δ depends on the shape of the angular spread distribution. For the Raised Cosine function, Δ is the width of the function at half amplitude whereas for the Gaussian function, it is the standard deviation. Finally, for the bell function with a Butterworth correlation kernel (used in [33]) Δ is the -3dB extension width.

The RMSE of the DOA θ and distance r estimates is plotted in Fig. 3.5a-3.6a for the GCD source, in Fig. 3.5b-3.6b for the UCD source and in Fig. 3.5c-3.6c for the point source.

Comparing the different estimators, as expected, the point source estimator (NFE) presents poor performance for locating distributed sources. Four conclusions can be drawn from these results:

Firstly, NF-DSPE performance is highly sensitive to the angular spread distribution. NF-

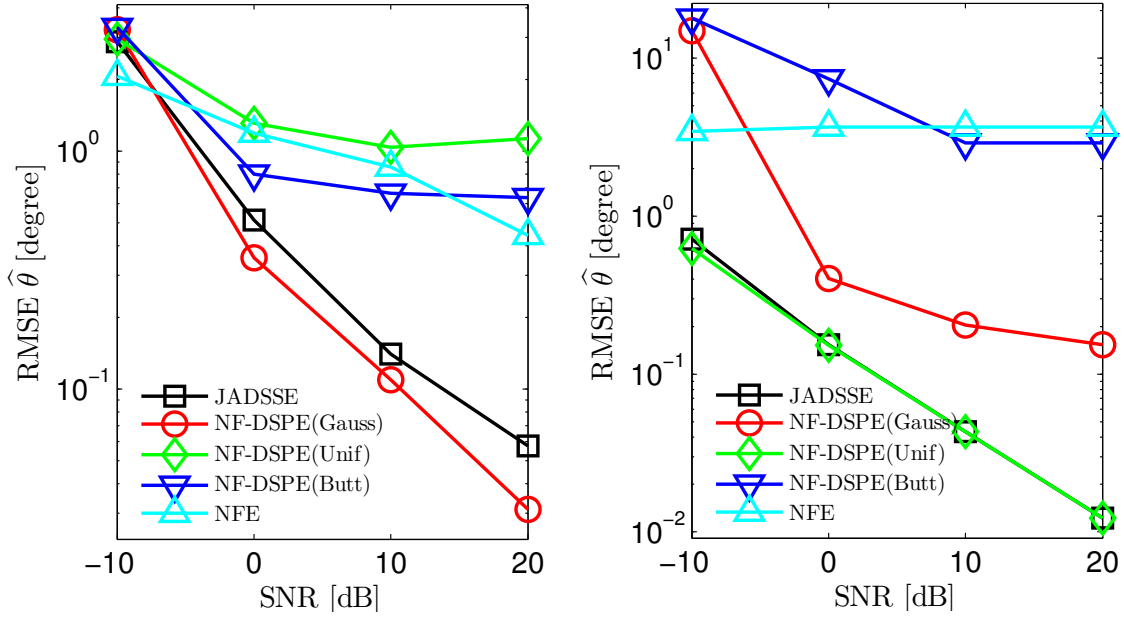
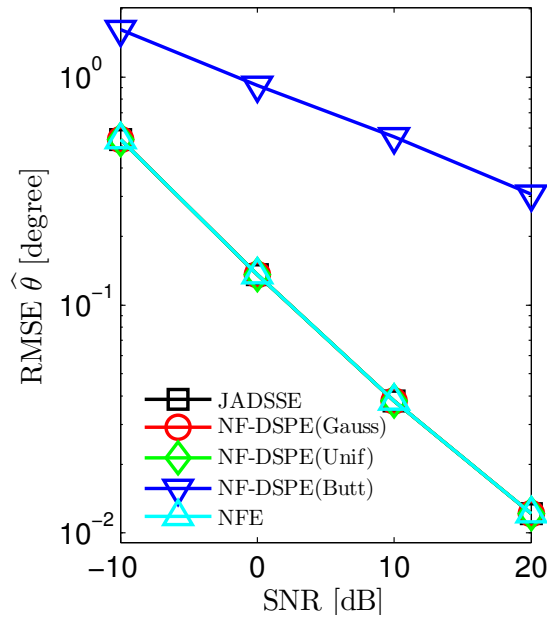
(a) RMSE of $\hat{\theta}_1$ for GCD source.(b) RMSE of $\hat{\theta}_2$ for UCD source.(c) RMSE of $\hat{\theta}_3$ for the point source.

Figure 3.5: Root Mean Square Error of the DOA parameter $\hat{\theta}$ versus SNR for the 3 sources. True DOAs $\theta_1 = 0^\circ$, $\theta_2 = 30^\circ$ and $\theta_3 = 60^\circ$.

DSPE has the best performance when the distribution used by the estimator is the same as the distribution of the source, but when the distributions are different, the performance degrades.

Secondly, when the distribution of the source belongs to the RC family, the JADSSE performance reaches that of NF-DSPE using the true distribution (see UCD source in Fig. 3.5b and Fig. 3.6b). This means that estimating the fourth parameter (the shape parameter β) does not penalize the proposed estimator.

Thirdly, JADSSE provides reliable estimation even when the distribution of the source does not belong to the RC family (see GCD source in Fig. 3.5a and Fig. 3.6a). This result shows that JADSSE using an RC family is quite robust to the shape of the angular spread distribution of the source.

Fourthly, NF-DSPE (except with Butterworth) and JADSSE performance perfectly fit those of NFE when dealing with a point source (see Fig. 3.5c and Fig. 3.6c).

It follows that JADSSE becomes particularly more interesting in multi-source scenarios where the point and distributed sources with unknown shape distributions are mixed. Therefore, these results clearly illustrate the important use of the proposed JADSSE estimator.

3.4.4 Reconstruction of Angular Shape Distribution

The same three sources scenario like that of subsection 3.4.3 is considered here. The true angular spread distribution $h(\phi)$ is plotted (dashed magenta thick line) in Fig.3.7 for both CD sources³. The estimated distributions $\hat{h}(\phi)$ are also plotted where $\hat{h}(\phi)$ is constructed using the $\hat{\theta}$, $\hat{\Delta}$ (and $\hat{\beta}$ for JADSSE) estimates at SNR=10dB.

The obtained results show that NF-DSPE provides good reconstruction when the used distribution $h(\phi)$ is the same as the actual distribution of the source. In the other cases the estimated distribution is poorly approximated due to the mismodeling error on h . On the contrary, JADSSE provides an accurate estimation of the angular spread distribution even for the GCD source (which is not included in the RC function family).

To illustrate the separation behavior of the proposed method, we simulate two overlapped UCD and GCD sources. The CD sources parameters are the same as the previous scenario except for the DOA of the UCD source $\theta_2 = 7^\circ$. Figure 3.8 depicts the true and the estimated angular spread distribution $h(\phi)$. Even with overlapped sources, JADSSE provides good localization for both sources and good shape approximation for UCD and GCD sources. Meanwhile, NF-DSPE with Gaussian or Butterworth angular distribution,

³The third point source of $\theta_3 = 60^\circ$ is not plotted since the true angular distribution is a Dirac with infinite value

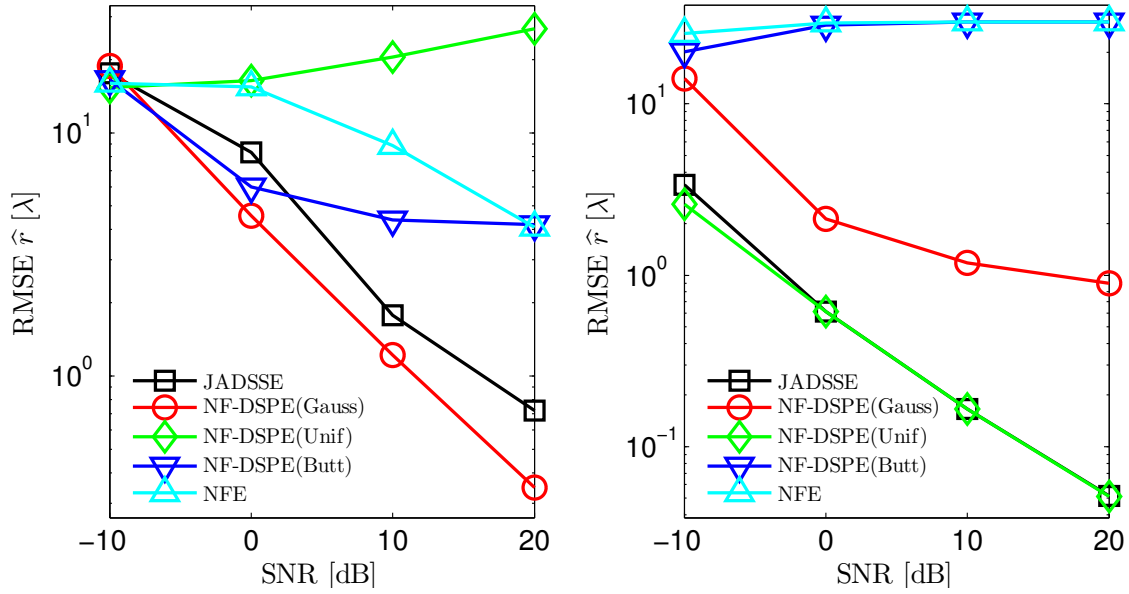
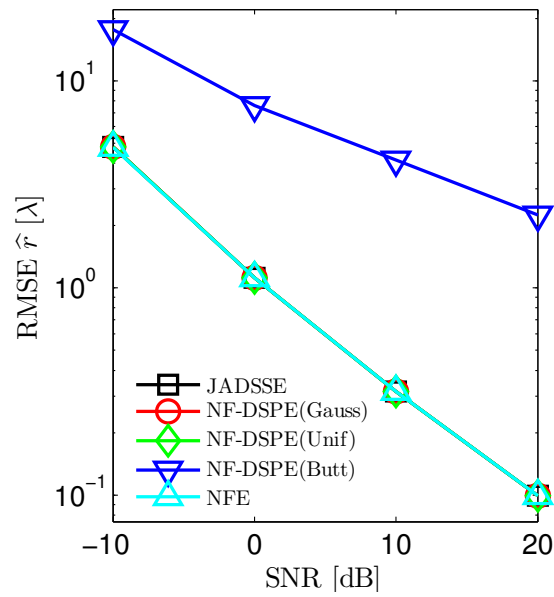
(a) RMSE of \hat{r}_1 for GCD source.(b) RMSE of \hat{r}_2 for UCD source.(c) RMSE of \hat{r}_3 for point source.

Figure 3.6: Root Mean Square Error of the distance parameter \hat{r} versus SNR for the 3 sources. True distances $r_1 = 30\lambda$, $r_2 = 25\lambda$ and $r_3 = 30\lambda$.

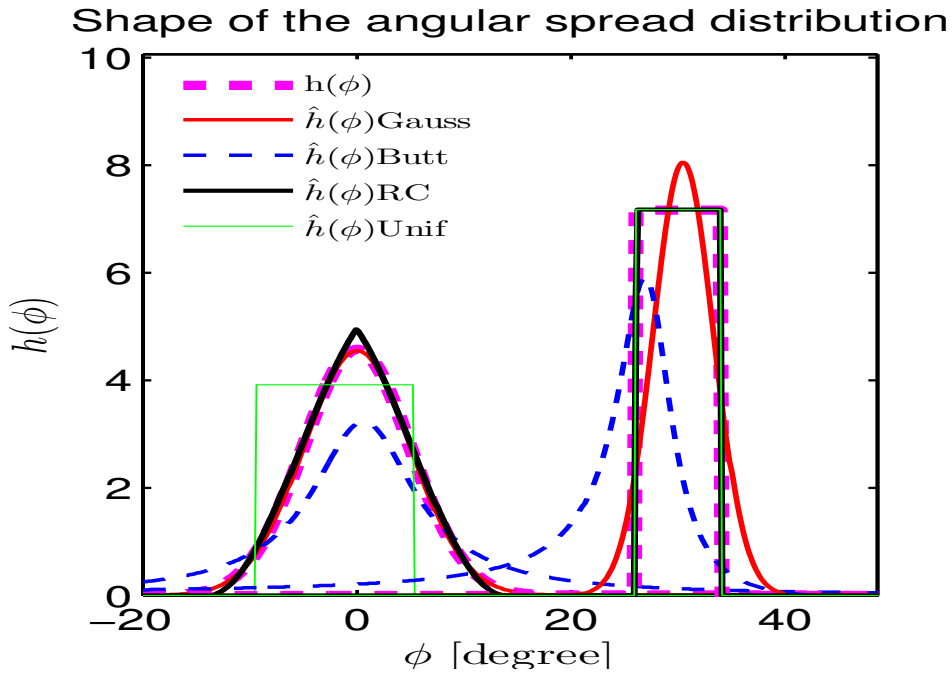


Figure 3.7: Reconstruction of the angular spread distribution $\hat{h}(\phi)$.

fails to detect the Uniform source. On the other side, NF-DSPE, using the Uniform angular distribution, resolve the DOA for both sources (the DOA estimation of the GCD source is biased) but it can not correctly reconstruct the angular distribution $h(\phi)$ for the GCD source.

3.4.5 Performance Versus the Angular Spread and Shape Parameters

In this simulation, one source with a Raised Cosine distribution is considered with $\theta_1 = 10^\circ$, $r_1 = 25\lambda$ and $\text{SNR}=20\text{dB}$. Firstly, the performances is plotted in Fig. 3.9a versus the shape parameter β with an angular spread fixed at $\Delta = 8^\circ$. JADSSE keeps almost stable performance as a function of β . Whereas, NF-DSPE presents higher RMSE values when a mismatched $h(\phi)$ is used by the estimator. For instance, NF-DSPE with Uniform distribution approaches JADSSE performance for source with small β but when β increases (corresponding to a source with a bell shape) the NF-DSPE (Unif) performances decreases. Conversely, the behavior of NF-DSPE with a Gaussian distribution is better when β increases in the RC source.

Secondly, performance is also plotted in Fig. 3.9b versus dispersion (Δ) of the source for a fixed shape parameter ($\beta = 0.5$). JADSSE exhibits good performance with only a slight increase in RMSE versus the angular spread. Meanwhile, above $\Delta > 5^\circ$, ignoring the shape of the angular spread distribution degrades dramatically the performance of NFE and NF-

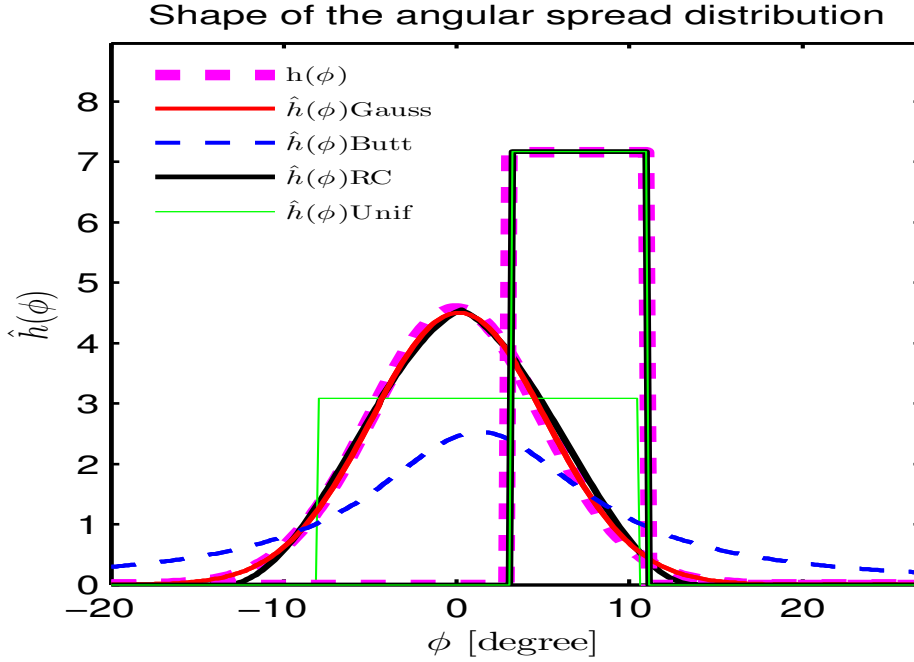


Figure 3.8: Reconstruction of the angular spread distribution $\hat{h}(\phi)$. True DOAs $[\theta_1 = 0^\circ, \theta_2 = 7^\circ]$

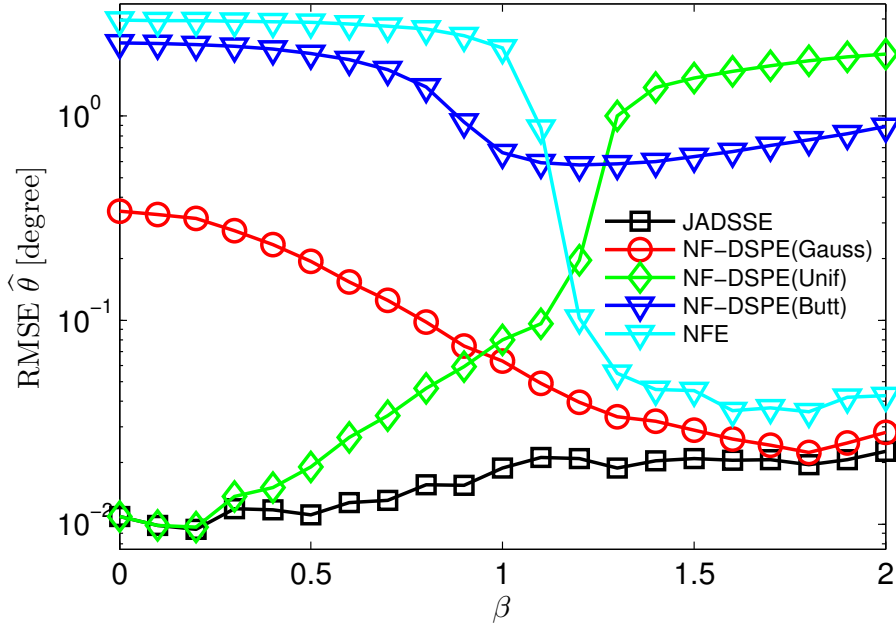
DSPE (with mismatch in distribution shapes). More generally, above a given dispersion, the knowledge or an accurate estimation of the distribution shape is essential to obtain good DOA and range estimates. This motivates the use of JADSSE.

3.4.6 Performance Versus DOA Separation

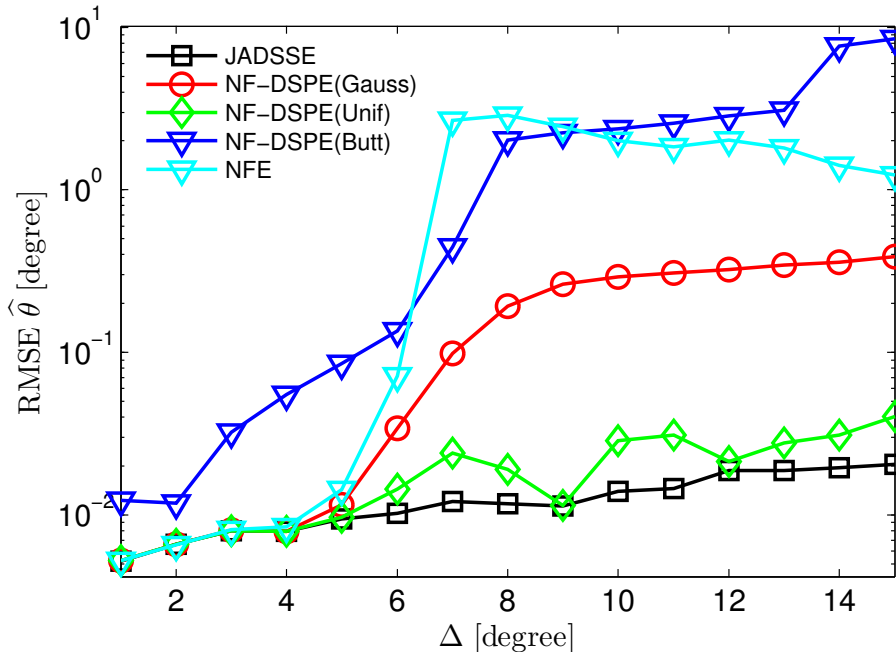
For this simulation, two uniform coherently distributed sources are considered at $r_1 = r_2 = 25\lambda$ with $\Delta_1 = 5^\circ$, $\Delta_2 = 8^\circ$; $\theta_1 = 0^\circ$ and $\theta_2 = \theta_1 + \delta_\theta$ where δ_θ is the DOA source separation. The SNR is fixed at 20dB . The RMSE of the DOA θ is plotted as a function of the DOA separation δ_θ in Fig. 3.10a for the first source and in Fig. 3.10b for the second source.

The results show that even for a large overlap of both sources for $\delta_\theta < 10^\circ$, the DOAs are accurately estimated by JADSSE, while the NF-DSPE with mismodeling error suffers from low resolution.

On one hand, for the first source ($\Delta_1 = 5^\circ$) in Fig. 3.10a and for small DOA separation, only JADSSE (and of course NF-DSPE(U)) provides accurate estimates. Referring to the mono-source case (Fig. 3.9b), one can notice that for this dispersion ($\Delta_1 = 5^\circ$), NF-DSPE performance was roughly the same as that of JADSSE. On the other hand, for the second source ($\Delta_2 = 8^\circ$), NF-DSPE (except with the uniform distribution) fails to accurately estimate the DOA, even for large separation of the DOAs due to the large dispersion of the



(a) RMSE versus β for a fixed $\Delta = 8^\circ$.



(b) RMSE versus Δ for a fixed $\beta = 0.5$.

Figure 3.9: Root Mean Square Error of DOA $\hat{\theta}$ for Raised Cosine source at SNR=20dB. True parameters $\theta = 10^\circ$ and $r = 25\lambda$.

source (as seen in the previous mono-source experiment (Fig. 3.9b)).

3.5 Conclusion

In this chapter, we proposed the JADSSE algorithm for the localization of coherently distributed (CD) sources in near-field. It jointly estimates the angle, the distance and the angular spread with an additional shape parameter. Simulation results have shown that NF-DSPE is limited to the case where the angular spread distribution is known. However, JADSSE accurately localizes sources even when h imperfectly fits the Raised Cosine family. The proposed estimator JADSSE also shows good asymptotic performance when the angular function h belongs to the Raised Cosine family. The practical interest of JADSSE can be summarized by:

- i) its ability to deal with an unknown angular spread distribution ;
- ii) its robustness to various shapes of the angular distribution (RC, Gaussian, uniform and point);
- iii) its improved characterization of the source by providing an estimate of the angular spread distribution and the shape of the source;
- iv) its angular resolution capability in terms of DOA for overlapped sources.

Further study in the next chapter will focus on the investigation of an approach that provides a decoupled estimation of the DOA and the angular spread under particular conditions. Also this approach requires the knowledge of the angular spread shape distribution to estimate the angular spread parameter[37].

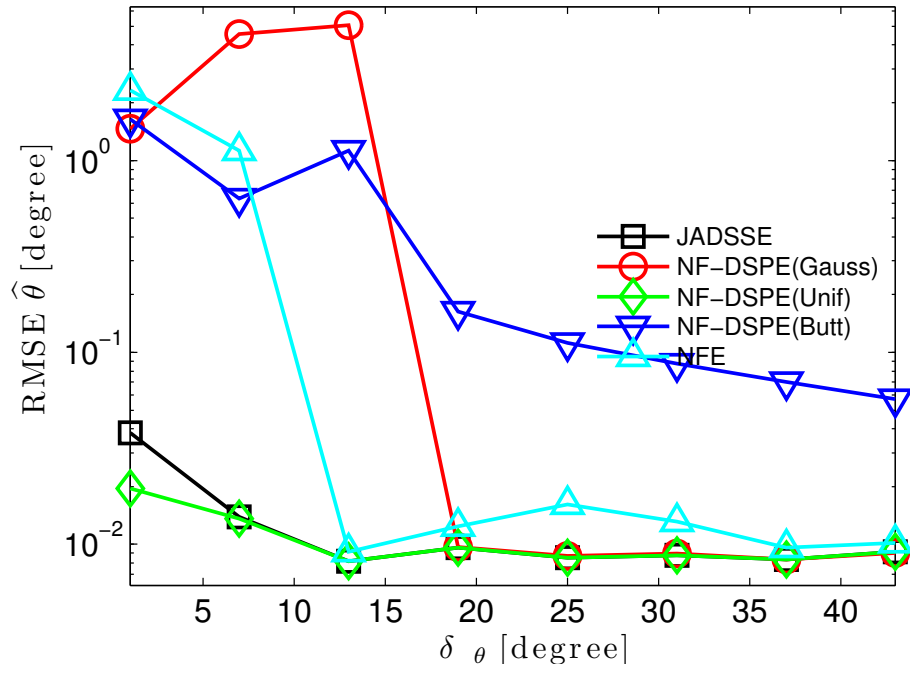
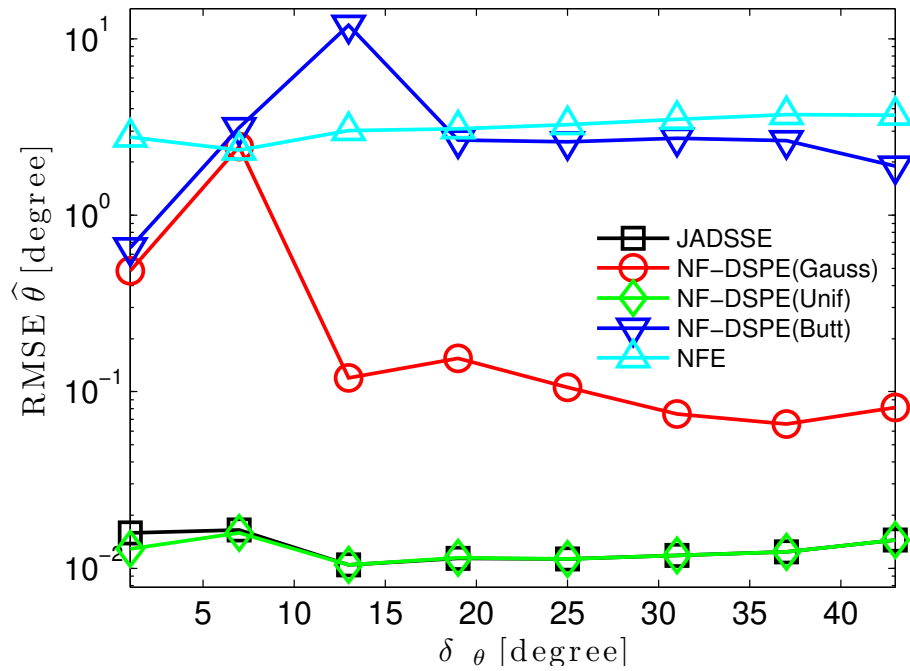
(a) RMSE for UCD source with $\Delta_1 = 5^\circ$.(b) RMSE for UCD source with $\Delta_2 = 8^\circ$.

Figure 3.10: Root Mean Square Error of DOA $\hat{\theta}$ versus δ_{θ} for both UCD sources at SNR=20dB. True parameters $\theta_1 = 0^\circ$, $\theta_2 = \theta_1 + \delta_{\theta}$, $\Delta_1 = 5^\circ$, $\Delta_2 = 8^\circ$ and $r_1 = r_2 = 25\lambda$.

4

Decoupled Estimation of the DOA and Angular Spread of CD Sources

We have proposed in the previous chapter a method for localizing CD sources with unknown angular shape distribution. This method called JADSSE provides good localization performance, angular spread and shape estimation. In this chapter we propose a decoupled version of JADSSE based on the Decoupled DSPE (DDSPE) method proposed in [37]. First we review the DDSPE proposed by Zoubir et al. in [37] and we propose an extension of DDSPE in the near-field case, the NF-DDSPE. Afterwards, we present a hybrid approach that consists in combining the NF-DDSPE and the JADSSE estimators.

The contributions of this chapter are:

- Generalizing the DDSPE approach to the near-field case.
- Presenting the hybrid approach that consists in combining the NF-DDSPE and the JADSSE estimators. This method called Decoupled Angle Distance Spread Shape Estimator (DADSSE) improves the NF-DDSPE by:
 - Eliminating the *a priori* knowledge on the source shape distribution to compute the spread estimation.
 - Localizing sources with different shapes.
 - Providing a shape reconstruction.

4.1 The DDSPE Method in Far-Field

4.1.1 Decoupling the Generalized Steering Vector in Far-Field

The DDSPE method proposed in the far-field by Zoubir [37], relies on a first order approximation of the generalized steering vector $\underline{\mathbf{c}}(\theta_0, \Delta_0)$ when the angular spread Δ_0 is supposed to be relatively small. Let us recall that:

$$\underline{\mathbf{c}}(\theta_0, \Delta_0) = \int_{-\infty}^{+\infty} \underline{\mathbf{a}}(\phi)h(\phi; \theta_0, \Delta_0)d\phi, \quad (4.1)$$

where $\underline{\mathbf{a}}(\phi)$ is the steering vector of a point source arriving from a DOA ϕ and impinging on an antenna of M sensors arranged in any geometry. $h(\phi; \theta_0, \Delta_0)$ is the angular spread distribution of the source and is assumed to be non-vanishing only around $\phi = \theta_0$, so that:

$$h(\phi; \theta_0, \Delta_0) = 0, \text{ for } |\phi - \theta_0| > \epsilon_{\Delta_0}, \quad (4.2)$$

with ϵ_{Δ_0} depends on Δ_0 . For example, if h is the uniform function of support Δ_0 , $\epsilon_{\Delta_0} = \Delta_0/2$. If h is the Gaussian function, we can suppose that $\epsilon_{\Delta_0} = \zeta\Delta_0$ with Δ_0 is the variance σ^2 and ζ is a real non-negative parameter.

Based on Eq. (4.1), with a change of variables, $\underline{\mathbf{c}}(\theta_0, \Delta_0)$ can be rewritten as:

$$\underline{\mathbf{c}}(\theta_0, \Delta_0) = \int_{-\epsilon_{\Delta_0}}^{+\epsilon_{\Delta_0}} \underline{\mathbf{a}}(\theta_0 + \phi)h(\theta_0 + \phi, \Delta_0)d\phi. \quad (4.3)$$

Note that in the case of an arbitrary array geometry, $\underline{\mathbf{a}}(\theta) = [e^{j\varphi_1(\theta)}, e^{j\varphi_2(\theta)}, \dots, e^{j\varphi_M(\theta)}]^T$, where $\varphi_m(\theta)$ depends on the sensor position. Assuming that Δ_0 is small, that is to say ϵ_{Δ_0} and, consequently, ϕ are small compared to θ_0 , we can introduce a first order approximation of $\varphi_m(\theta_0 + \phi)$ as follows:

$$\varphi_m(\theta_0 + \phi) = \varphi_m(\theta_0) + \phi\dot{\varphi}_m(\theta_0) + \mathcal{O}(\phi), \quad (4.4)$$

where $\dot{\varphi}_m(\theta_0) = \left. \frac{\partial \varphi_m(\theta)}{\partial \theta} \right|_{\theta_0}$ and $\mathcal{O}(\phi)$ is a negligible value compared to ϕ . Substituting Eq. (4.4) in Eq. (4.3), the m -th component of $\underline{\mathbf{c}}(\theta_0, \Delta_0)$ reduces to:

$$[\underline{\mathbf{c}}(\theta_0, \Delta_0)]_m \simeq \int_{-\epsilon_{\Delta_0}}^{+\epsilon_{\Delta_0}} e^{j\varphi_m(\theta_0)} e^{j\phi\dot{\varphi}_m(\theta_0)} h(\theta_0 + \phi; \Delta_0)d\phi, \quad (4.5a)$$

$$\simeq [\underline{\mathbf{a}}(\theta_0)]_m \alpha_m. \quad (4.5b)$$

$[\underline{\mathbf{a}}(\theta_0)]_m$ is the m -th component of $\underline{\mathbf{a}}(\theta_0)$ and α_m is given by:

$$\alpha_m = \int_{-\epsilon_{\Delta_0}}^{+\epsilon_{\Delta_0}} e^{j\phi\varphi_m(\theta_0)} h(\theta_0 + \phi; \Delta_0) d\phi. \quad (4.6)$$

Finally, we can write:

$$\underline{\mathbf{c}}(\theta_0, \Delta_0) \simeq \text{diag}\{\underline{\mathbf{a}}(\theta_0)\} \underline{\boldsymbol{\alpha}}(\theta_0, \Delta_0), \quad (4.7)$$

with $\underline{\boldsymbol{\alpha}}(\theta_0, \Delta_0) = [\alpha_1(\theta_0, \Delta_0), \dots, \alpha_M(\theta_0, \Delta_0)]^T$ and $\text{diag}\{\underline{\mathbf{a}}(\theta_0)\}$ is a diagonal matrix in which the diagonal terms are the components of $\underline{\mathbf{a}}(\theta_0)$. Note that $\underline{\mathbf{a}}(\theta_0)$ depends only on θ_0 and the array geometry whereas $\underline{\boldsymbol{\alpha}}(\theta_0, \Delta_0)$ depends on θ_0 , the array geometry, the angular spread and the shape distribution.

4.1.2 The ULA Particular Case

In the particular case of an ULA, we have:

$$\varphi_m(\theta) = -\frac{2\pi d}{\lambda}(m-1)\sin\theta,$$

and

$$\dot{\varphi}_m(\theta) = -\frac{2\pi d}{\lambda}(m-1)\cos\theta.$$

Let us introduce $\nu_0 = \frac{d \cos(\theta_0)}{\lambda}$. Thus we can express Eq. (4.6) as:

$$\begin{aligned} \alpha_m &= \int_{-\epsilon_{\Delta_0}}^{+\epsilon_{\Delta_0}} e^{-j2\pi\nu_0(m-1)\phi} h(\theta_0 + \phi; \Delta_0) d\phi \\ &\simeq \int_{-\infty}^{+\infty} e^{-j2\pi\nu_0(m-1)\phi} h(\theta_0 + \phi; \Delta_0) d\phi. \end{aligned} \quad (4.8a)$$

Here we recognize that α_m represents the Fourier transform \mathcal{F} of $h(\theta_0 + \phi; \Delta_0)$:

$$\alpha_m = \mathcal{F}\{h(\theta_0 + \phi; \Delta_0)\}(\nu_0(m-1)) \triangleq \tilde{h}_{\Delta_0}(\nu_0(m-1)). \quad (4.9)$$

Finally, we get:

$$[\underline{\mathbf{c}}(\theta_0, \Delta_0)]_m \simeq [\underline{\mathbf{a}}(\theta_0)]_m \tilde{h}_{\Delta_0}(\nu_0(m-1)), \quad (4.10)$$

or also in a vector notation:

$$\boxed{\underline{\mathbf{c}}(\theta_0, \Delta_0) \simeq \underline{\mathbf{a}}(\theta_0) \odot \tilde{\mathbf{h}}_{\Delta_0}(\nu_0)}. \quad (4.11)$$

\odot is the element wise product, $\underline{\tilde{\mathbf{h}}}_{\Delta_0}(\nu_0)$ is the M -dimensional vector containing $\tilde{h}_{\Delta_0}(\nu_0(m-1))$ and $\tilde{h}_{\Delta_0}(\nu)$ is the Fourier transform of the shape distribution $h(\theta_0 + \phi; \Delta_0)$. Note that Eq. (4.11) can also be written in the more general form of Eq. (4.7) in which :

$$\underline{\alpha}(\theta_0, \Delta_0) = \underline{\tilde{\mathbf{h}}}_{\Delta_0}(\nu_0). \quad (4.12)$$

Particular Case of a Gaussian Angular Distribution

In the case of a Gaussian angular distribution of standard deviation Δ_0 , $h(\phi; \theta_0, \Delta_0) = \frac{1}{\Delta_0 \sqrt{2\pi}} e^{-\frac{1}{2} \left(\frac{\phi - \theta_0}{\Delta_0} \right)^2}$. The corresponding Fourier transform is:

$$\tilde{h}_{\Delta_0}(\nu_0(m-1)) = \exp \left[-\frac{1}{2} \left(2\pi \Delta_0 \nu_0(m-1) \right)^2 \right]. \quad (4.13)$$

Particular Case of a Uniform Angular Distribution

In the case of a Uniform (rectangular) angular distribution of support Δ_0 :

$$h(\phi; \theta_0, \Delta_0) = \begin{cases} \frac{1}{\Delta_0} & \text{if } |\phi - \theta_0| \leq \frac{\Delta_0}{2} \\ 0 & \text{Otherwise.} \end{cases}$$

The corresponding Fourier transform is then:

$$\tilde{h}_{\Delta_0}(\nu_0(m-1)) = \text{sinc} \left[\frac{\pi d}{\lambda} (m-1) \Delta_0 \cos \theta_0 \right], \quad (4.14)$$

where sinc is the sinus cardinal function.

4.1.3 Decoupled DSPE

Let us recall that the DSPE method consists in searching both the DOA θ and the angular spread Δ as the arguments of an extended MUSIC pseudo-spectrum using a generalized steering vector, so that:

$$(\hat{\theta}_0, \hat{\Delta}_0) = \arg \max_{\theta, \Delta} \frac{\underline{\mathbf{c}}^H(\theta, \Delta) \underline{\mathbf{c}}(\theta, \Delta)}{\underline{\mathbf{c}}^H(\theta, \Delta) \mathbf{E}_n \mathbf{E}_n^H \underline{\mathbf{c}}(\theta, \Delta)}. \quad (4.15)$$

In Eq. (4.15), \mathbf{E}_n refers to the $M \times (M - q)$ matrix containing the eigenvectors of the data correlation matrix, associated to the smallest eigenvalue. Using the approximation Eq. (4.11) which can also be written:

$$\underline{\mathbf{c}}(\theta, \Delta) \simeq \mathbf{D}(\theta) \underline{\tilde{\mathbf{h}}}(\theta, \Delta), \quad (4.16)$$

where $\mathbf{D}(\theta) = \text{diag}\{\underline{\mathbf{a}}(\theta)\}$, we obtain:

$$(\hat{\theta}_0, \hat{\Delta}_0) = \arg \max_{\theta, \Delta} \frac{\tilde{\underline{\mathbf{h}}}^H(\theta, \Delta) \mathbf{D}^H(\theta) \mathbf{D}(\theta) \tilde{\underline{\mathbf{h}}}(\theta, \Delta)}{\tilde{\underline{\mathbf{h}}}^H(\theta, \Delta) \mathbf{D}^H(\theta) \mathbf{E}_n \mathbf{E}_n^H \mathbf{D}(\theta) \tilde{\underline{\mathbf{h}}}(\theta, \Delta)}. \quad (4.17)$$

Knowing that $\mathbf{D}^H(\theta) \mathbf{E}_n \mathbf{E}_n^H \mathbf{D}(\theta)$ is an Hermitian matrix, $\tilde{\underline{\mathbf{h}}}^H(\theta, \Delta) \mathbf{D}^H(\theta) \mathbf{E}_n \mathbf{E}_n^H \mathbf{D}(\theta) \tilde{\underline{\mathbf{h}}}(\theta, \Delta)$ turns into a real number. Moreover, $|\underline{\mathbf{a}}(\theta)_m| = 1$ where $|\cdot|$ is the modulus operator, so that $\tilde{\underline{\mathbf{h}}}^H(\theta, \Delta) \mathbf{D}^H(\theta) \mathbf{D}(\theta) \tilde{\underline{\mathbf{h}}}(\theta, \Delta)$ reduces to $\|\tilde{\underline{\mathbf{h}}}(\theta, \Delta)\|^2$ which is a real scalar. Also note from Eq. (4.6) that α_m is real¹ when $h(\theta_0 + \phi, \Delta_0)$ is symmetric in ϕ . Consequently, Eq. (4.17) can also be written as:

$$(\hat{\theta}_0, \hat{\Delta}_0) = \arg \max_{\theta, \Delta} \frac{\|\tilde{\underline{\mathbf{h}}}(\theta, \Delta)\|^2}{\tilde{\underline{\mathbf{h}}}^H(\theta, \Delta) \Re\{\mathbf{D}^H(\theta) \mathbf{E}_n \mathbf{E}_n^H \mathbf{D}(\theta)\} \tilde{\underline{\mathbf{h}}}(\theta, \Delta)}. \quad (4.18)$$

If $\tilde{\underline{\mathbf{h}}}(\theta, \Delta)$ is known, this maximization problem can be solved in a different way by taking into account the particular form of the components of $\tilde{\underline{\mathbf{h}}}(\theta, \Delta)$. Indeed, in the case of a Gaussian angular distribution, (see Eq. (4.13)), the components of $\tilde{\underline{\mathbf{h}}}(\theta, \Delta)$ are positive smaller than 1 and in decreasing values, so that:

$$1 = \tilde{h}_{\Delta_0}(0) \geq \tilde{h}_{\Delta_0}(\nu_0) \geq \dots \geq \tilde{h}_{\Delta_0}(\nu_0(m-1)) \geq \dots \tilde{h}_{\Delta_0}(\nu_0(M-1)) \geq 0. \quad (4.19)$$

In the case of a uniform angular distribution (see Eq. (4.14)), property Eq. (4.19) is valid when the argument of sinc is in the main lobe, such as $\frac{\pi d}{\lambda}(M-1)\Delta_0 \cos \theta_0 \leq \pi$ which means approximately:

$$\Delta_0 \leq \frac{2}{M-1} \quad (4.20)$$

The maximization of Eq. (4.18) can then be expressed in the following form:

$$\hat{\theta}_0 = \arg \max_{\theta} \left\{ \max_{\underline{\mathbf{x}}} \frac{\underline{\mathbf{x}}^T \underline{\mathbf{x}}}{\underline{\mathbf{x}}^T \Re\{\mathbf{D}^H(\theta) \mathbf{E}_n \mathbf{E}_n^H \mathbf{D}(\theta)\} \underline{\mathbf{x}}} \right\} \quad (4.21)$$

s.t. $x_1 \geq x_2 \geq x_3 \geq \dots \geq x_M \geq 0$ and $x_1 = 1$,

where $\underline{\mathbf{x}} = [x_1, x_2, \dots, x_M]^T$. This maximization to obtain $\hat{\theta}_0$ can be reduced to:

$$\hat{\theta}_0 = \arg \max_{\theta} \left\{ \max_{\tilde{\underline{\mathbf{x}}}} \frac{\tilde{\underline{\mathbf{x}}}^T \tilde{\underline{\mathbf{x}}} + 1}{[1, \tilde{\underline{\mathbf{x}}}^T] \Re\{\mathbf{D}^H(\theta) \mathbf{E}_n \mathbf{E}_n^H \mathbf{D}(\theta)\} [1, \tilde{\underline{\mathbf{x}}}^T]^T} \right\} \quad (4.22)$$

s.t. $\mathbf{J} \tilde{\underline{\mathbf{x}}} \leq \mathbf{e}$.

¹The imaginary part of $e^{j\phi\phi_m(\theta_0)}$ being an odd function of ϕ , its contribution in Eq. (4.6) is zero.

Here, $\tilde{\mathbf{x}} = [x_2, x_3, \dots, x_M]^T$, $\mathbf{e} = [1, 0, \dots, 0]^T$ and \mathbf{J} is the $M \times (M-1)$ matrix defined as follows:

$$\mathbf{J}_{M,M-1} = \begin{pmatrix} 1 & 0 & \cdots & 0 & 0 \\ -1 & 1 & \ddots & \vdots & \vdots \\ 0 & -1 & \ddots & 0 & 0 \\ \vdots & \ddots & \ddots & 1 & 0 \\ 0 & \cdots & 0 & -1 & 1 \end{pmatrix}.$$

The maximization problem in Eq. (4.22) can be solved using a sequential quadratic programming (SQP) method. The Matlab function *fmincon*, based on the SQP method, will be used in the simulation section. Note that in this way only $\hat{\theta}$ is retrieved without requiring the knowledge of the angular shape distribution. If the estimation of the angular spread is required, the classical DSPE Eq. (4.18) can be used taking into account the DOA estimated by Eq. (4.22) and assuming the shape of h is known beforehand, it is to say:

$$\hat{\Delta}_0 = \arg \max_{\Delta} \frac{\tilde{\mathbf{h}}^H(\hat{\theta}_0, \Delta) \tilde{\mathbf{h}}(\hat{\theta}_0, \Delta)}{\tilde{\mathbf{h}}^H(\hat{\theta}_0, \Delta) \Re\{\mathbf{D}^H(\hat{\theta}_0) \mathbf{E}_n \mathbf{E}_n^H \mathbf{D}(\hat{\theta}_0)\} \tilde{\mathbf{h}}(\hat{\theta}_0, \Delta)}. \quad (4.23)$$

Let us note that for the estimation of Δ_0 , the angular shape distribution h must be known. Let us resume that the advantage of the DDSPE is twofold: i) the estimation of the DOA does not require the knowledge of the angular shape distribution ii) the estimation of multiple DOAs does not require that the sources have the same angular shape distribution. The drawbacks of DDSPE are that, the knowledge of h is required to estimate the angular spread. In the following section, we will show that the DDSPE can be extended to the case of near-field sources.

4.2 DDSPE Generalized to the Near-Field Case

4.2.1 Decoupling the Generalized Steering Vector in Near-Field

We generalize the approximation of the far-field GSV for a CD source to the near field case where it is given by:

$$\underline{\mathbf{c}}(\theta_0, \Delta_0, r_0) = \int_{-\infty}^{+\infty} \underline{\mathbf{a}}(\phi, r_0) h(\phi; \theta_0, \Delta_0) d\phi, \quad (4.24)$$

with $\underline{\mathbf{a}}(\phi, r_0)$ is the $M \times 1$ near-field steering vector (for an ULA²) given in equation Eq. (3.6) and its m -th element is given by $[\underline{\mathbf{a}}(\phi, r_0)]_m e^{(-j\pi \sin(\phi)(m-1) + j\frac{\pi\lambda}{4r_0} \cos^2(\phi)(m-1)^2)}$. We intro-

²the approach can be easily adopted for other antenna geometries

duce the variable $\vartheta = \phi - \theta_0$ then the m -th element of the vector $\underline{\mathbf{c}}(\theta_0, \Delta_0, r_0)$ is expressed by:

$$[\underline{\mathbf{c}}(\theta_0, \Delta_0, r_0)]_m = \int_{-\infty}^{+\infty} e^{(-j\pi \sin(\vartheta+\theta_0)(m-1) + j\frac{\pi\lambda}{4r_0} \cos^2(\vartheta+\theta_0)(m-1)^2)} h(\vartheta + \theta_0; \Delta_0) d\vartheta. \quad (4.25)$$

Using the trigonometric identities, we get:

$$\begin{aligned} [\underline{\mathbf{c}}(\theta_0, \Delta_0, r_0)]_m &= \int_{-\infty}^{+\infty} e^{-j\pi (\sin(\vartheta) \cos(\theta_0) + \sin(\theta_0) \cos(\vartheta)) (m-1)} \\ &e^{+j\frac{\pi\lambda}{4r_0} \frac{1}{2} (1 + \cos(2\theta_0) \cos(2\vartheta) - \sin(2\theta_0) \sin(2\vartheta)) (m-1)^2} h(\vartheta + \theta_0; \Delta_0) d\vartheta. \end{aligned} \quad (4.26)$$

We can use the first order terms of the Taylor approximation of $\sin(\vartheta) \simeq \vartheta$, $\sin(2\vartheta) \simeq 2\vartheta$ and $\cos(\vartheta) \simeq \cos(2\vartheta) \simeq 1$ in Eq. (4.26) to write:

$$\begin{aligned} [\underline{\mathbf{c}}(\theta_0, \Delta_0, r_0)]_m &\simeq \int_{-\epsilon_{\Delta_0}}^{+\epsilon_{\Delta_0}} e^{-j\pi (\vartheta \cos(\theta_0) + \sin(\theta_0)) (m-1)} \\ &e^{+j\frac{\pi\lambda}{4r_0} \frac{1}{2} (1 + \cos(2\theta_0) - \sin(2\theta_0) 2\vartheta) (m-1)^2} h(\vartheta + \theta_0; \Delta_0) d\vartheta, \\ &\simeq e^{-j\pi \sin(\theta_0)(m-1) + j\frac{\pi\lambda}{4r_0} \cos^2(\theta_0)(m-1)^2} \\ &\int_{-\epsilon_{\Delta_0}}^{+\epsilon_{\Delta_0}} e^{[-j2\pi\vartheta (\frac{\cos(\theta_0)}{2}(m-1) + \frac{\lambda}{8r_0} \sin(2\theta_0)(m-1)^2)]} h(\vartheta + \theta_0; \Delta_0) d\vartheta, \\ &\simeq [\underline{\mathbf{a}}(\theta_0, r_0)]_m \int_{-\epsilon_{\Delta_0}}^{+\epsilon_{\Delta_0}} e^{[-j2\pi\vartheta (\frac{\cos(\theta_0)}{2}(m-1) + \frac{\lambda}{8r_0} \sin(2\theta_0)(m-1)^2)]} \\ &h(\vartheta + \theta_0; \Delta_0) d\vartheta. \end{aligned} \quad (4.27)$$

Let us introduce $\nu'_{0,m} = (\frac{\cos(\theta_0)}{2}(m-1) + \frac{\lambda}{8r_0} \sin(2\theta_0)(m-1)^2)$ similarly to Eq. (4.9), we can express the integral in Eq. (4.27) as the Fourier transform of the angular distribution $h(\vartheta + \theta_0; \Delta_0)$ in $\nu'_{0,m}$:

$$\mathcal{F}\{h(\vartheta + \theta_0; \Delta_0)\}(\nu'_{0,m}) = \tilde{h}(\nu'_{0,m}) = \int_{-\epsilon_{\Delta_0}}^{+\epsilon_{\Delta_0}} e^{-j2\pi\vartheta\nu'_{0,m}} h(\vartheta + \theta_0; \Delta_0) d\vartheta. \quad (4.28)$$

We can rewrite Eq. (4.27) as:

$$[\underline{\mathbf{c}}(\theta_0, \Delta_0, r_0)]_m \simeq [\underline{\mathbf{a}}(\theta_0, r_0)]_m [\tilde{\underline{\mathbf{h}}}(\theta_0, r_0)]_m, \quad (4.29)$$

where $[\tilde{\mathbf{h}}(\theta_0, r_0)]_m = \tilde{h}(\nu'_{0,m})$, or with the vector notation:

$$\boxed{\underline{\mathbf{c}}(\theta_0, \Delta_0, r_0) \simeq \underline{\mathbf{a}}(\theta_0, r_0) \odot \tilde{\mathbf{h}}(\theta_0, r_0)}. \quad (4.30)$$

Here, $\tilde{\mathbf{h}}(\theta_0, r_0)$ is the $M \times 1$ real valued vector that represents the Fourier transform of the angular distribution $h(\vartheta + \theta_0; \Delta_0)$. The expression for the Gaussian case is given by:

$$[\tilde{\mathbf{h}}(\nu'_0)]_m = \exp \left[-\frac{1}{2} \left(2\pi\Delta_0 \left(\frac{\cos(\theta_0)}{2} (m-1) + \frac{\lambda}{8r_0} \sin(2\theta_0) (m-1)^2 \right) \right)^2 \right], \quad (4.31)$$

and for the uniform case is denoted by:

$$\begin{aligned} [\tilde{\mathbf{h}}(\nu'_0)]_m &= \text{sinc}[\pi\nu'_0(m-1)\Delta_0] \\ &= \text{sinc} \left[\pi \left(\frac{\cos(\theta_0)}{2} (m-1) + \frac{\lambda}{8r_0} \sin(2\theta_0) (m-1)^2 \right) \Delta_0 \right]. \end{aligned} \quad (4.32)$$

We can also show that equations (4.31) and (4.32) satisfy the inequality Eq. (4.19).

4.2.2 The Near-field DDSPE (NF-DDSPE)

According to Eq. (4.30) and as Eq. (4.16), we can write:

$$\underline{\mathbf{c}}(\theta, \Delta, r) \simeq \mathbf{D}(\theta, r) \tilde{\mathbf{h}}(\theta, \Delta, r), \quad (4.33)$$

with $\mathbf{D} = \text{diag}\{\underline{\mathbf{a}}(\theta, r)\}$. It follows that, as in the far-field case Eq. (4.15), the extended MUSIC pseudo spectrum-based estimation is given by:

$$(\hat{\theta}_0, \hat{\Delta}_0, \hat{r}_0) = \arg \max_{\theta, \Delta, r} \frac{\tilde{\mathbf{h}}^H(\theta, \Delta, r) \mathbf{D}^H(\theta, r) \mathbf{D}(\theta, r) \tilde{\mathbf{h}}(\theta, \Delta, r)}{\tilde{\mathbf{h}}^H(\theta, \Delta, r) \mathbf{D}^H(\theta, r) \mathbf{E}_n \mathbf{E}_n^H \mathbf{D}(\theta, r) \tilde{\mathbf{h}}(\theta, \Delta, r)}. \quad (4.34)$$

Following the same concept as in subsection 4.1.3, and noticing that the condition Eq. (4.19) can be applied in the particular cases of the Gaussian and uniform angular shape distributions (assuming a small angular spread in the uniform case), the maximization Eq. (4.34) can be efficiently solved for the DOA and range estimation by:

$$\boxed{(\hat{\theta}_0, \hat{r}_0) = \arg \max_{\theta, r} \left\{ \max_{\tilde{\mathbf{x}}} \frac{\tilde{\mathbf{x}}^T \tilde{\mathbf{x}} + 1}{[1, \tilde{\mathbf{x}}^T] \Re\{\mathbf{D}^H(\theta, r) \mathbf{E}_n \mathbf{E}_n^H \mathbf{D}(\theta, r)\} [1, \tilde{\mathbf{x}}^T]^T} \right\}} \quad (4.35)$$

s.t. $\mathbf{J}\tilde{\mathbf{x}} \leq \mathbf{e}$.

$\tilde{\mathbf{x}}$, \mathbf{e} and \mathbf{J} have been defined in subsection 4.1.3. In the near-field case, the DOA and range estimation are still decoupled of the angular spread estimation and does not require the knowledge of the angular shape distribution. However, if the angular spread is needed, the angular shape distribution is to be known.

In the following, we are proposing a Decoupled Angle, Distance, Spread and Shape estimator (DADSSE) which does not require the knowledge of the angular shape distribution and provides an estimation of this distribution.

4.2.3 Decoupled Angle Distance Spread and Shape Estimator (DADSSE)

Herein, we present the DADSSE approach that consists in combining NF-DDSPE with JADSSE. It consists in estimating the DOA $\hat{\theta}$ and the distance \hat{r} of the source by NF-DDSPE approach and then re-injecting them into the JADSSE estimator to estimate the spread and shape parameters without *a priori* assumptions on the shape of the angular distribution. The DADSSE estimator can be summarized by:

- Estimate the DOA $\hat{\theta}$ and the distance \hat{r} using Eq. (4.35).
- Estimate the spread $\hat{\Delta}$ and the shape parameter $\hat{\beta}$ using the JADSSE method in equation (3.9) in chapter 3 and using the estimated $\hat{\theta}$ and \hat{r} from the first step.

$$(\hat{\Delta}, \hat{\beta}) = \arg \max_{\Delta, \beta} \frac{1}{\|\underline{\mathbf{c}}^H(\hat{\theta}, \Delta, \hat{r}, \beta) \hat{\mathbf{E}}_n\|^2}, \quad (4.36)$$

where β in the GSV $\underline{\mathbf{c}}^H(\hat{\theta}, \Delta, \hat{r}, \beta)$ is given by equation (3.7) in chapter 3.

4.3 Simulations Results

In this section we aim to investigate the performance of the NF-DDSPE estimator and compare it to the NF-DSPE with different angular distribution shapes, to the JADSSE and DADSSE methods. The performance evaluation consists in computing the Root Mean Square Error (RMSE) of the parameters to be estimated ($\hat{\theta}$ and \hat{r}) versus the performance parameters, the Signal to Noise Ratio (SNR) and the DOA source separation δ_θ .

The framework consists in considering two CD sources coming from different DOAs θ , having different angular spreads Δ and angular shape distributions $h(\phi; \theta, \Delta)$. The simulations were done considering an ULA of M sensors where the spacing between adjacent sensors is d expressed in wavelength λ unit. Performance is evaluated by a Monte-carlo simulation of N independent executions each with L snapshots.

4.3.1 Mixture of Uniform Coherently Distributed (UCD) Sources

Framework									
Sources						Array		Simulations	
N.	θ	Δ	r	β	Shape	M	d	L	N
1	0°	5°	30λ	-	UCD	20 sensors	$\lambda/2$	300 snapshots	10 realizations
2	30°	15°	25λ	-	UCD				

Table 4.1: Summarizing Parameter values of the framework with two UCD sources.

In this first scenario, we consider two UCD sources in a near-field, the parameters are given in Tab.4.1. The RMSE of the estimated DOA $\hat{\theta}$ and range \hat{r} are plotted in Fig.4.1a-Fig.4.1b and Fig.4.1c-Fig.4.1d, for the two sources, respectively.

First, for the UCD sources, considering the simulation parameters in table 4.1), the condition in Eq. (4.19) is satisfied in the near-field case (given in Eq. (4.32)) for and angular spread of $\Delta_1 \simeq \Delta_2 \leq 5.7$ degree for the two sources.

It follows that whereas Eq. (4.19) is true for source 1, it is not true for source 2. As seen in Fig.4.1a-Fig.4.1d, the RMSEs of $\hat{\theta}$ and \hat{r} for the two sources, asymptotically decrease as function of SNR for JADSSE, which does not require the knowledge on the sources angular distributions and for NF-DSPE when these latter are known.

One can see on Fig.4.1a-Fig.4.1b, that NFE, which supposes the sources as points, gives larger RMSEs than JADSSE but it is however not a bad solution because of the relatively small angular spread $\Delta_1 = 5$ degree of the first source. The NF-DDSPE gives better results than the NFE and nearly the same results as JADSSE until SNR=20dB. Note that NF-DDSPE can be used for source 1 since $\Delta_1 = 5$ degree corresponds to the conditions of Eq. (4.19). At SNR values higher than 20 dB, the modeling error which consists in assuming a small angular spread to obtain the decoupling Eq. (4.33) is more visible and prevents the RMSEs to decrease anymore.

In the case of the second source, the angular spread $\Delta_2 = 15$ degree is large enough so the decoupling is no longer valid, also conditions Eq. (4.19) are no longer valid. Indeed we can see in Fig.4.1c-Fig.4.1d that NF-DDSPE does not really work whatever the value of the SNR. Also note that the NFE which assumes point sources does no longer work.

Table 4.2 gives the mean values of the estimated $\hat{\theta}$ and \hat{r} for the two sources. We can see that for the low-spread source 1, the errors compared to the true values, even for NFE, are very small whereas for the large-spread source 2, these errors are large except for JADSSE which behaves like NF-DSPE with the known angular shape distribution. Note that JADSSE also allows to estimate the distribution of the angular shape through parameters Δ and β .

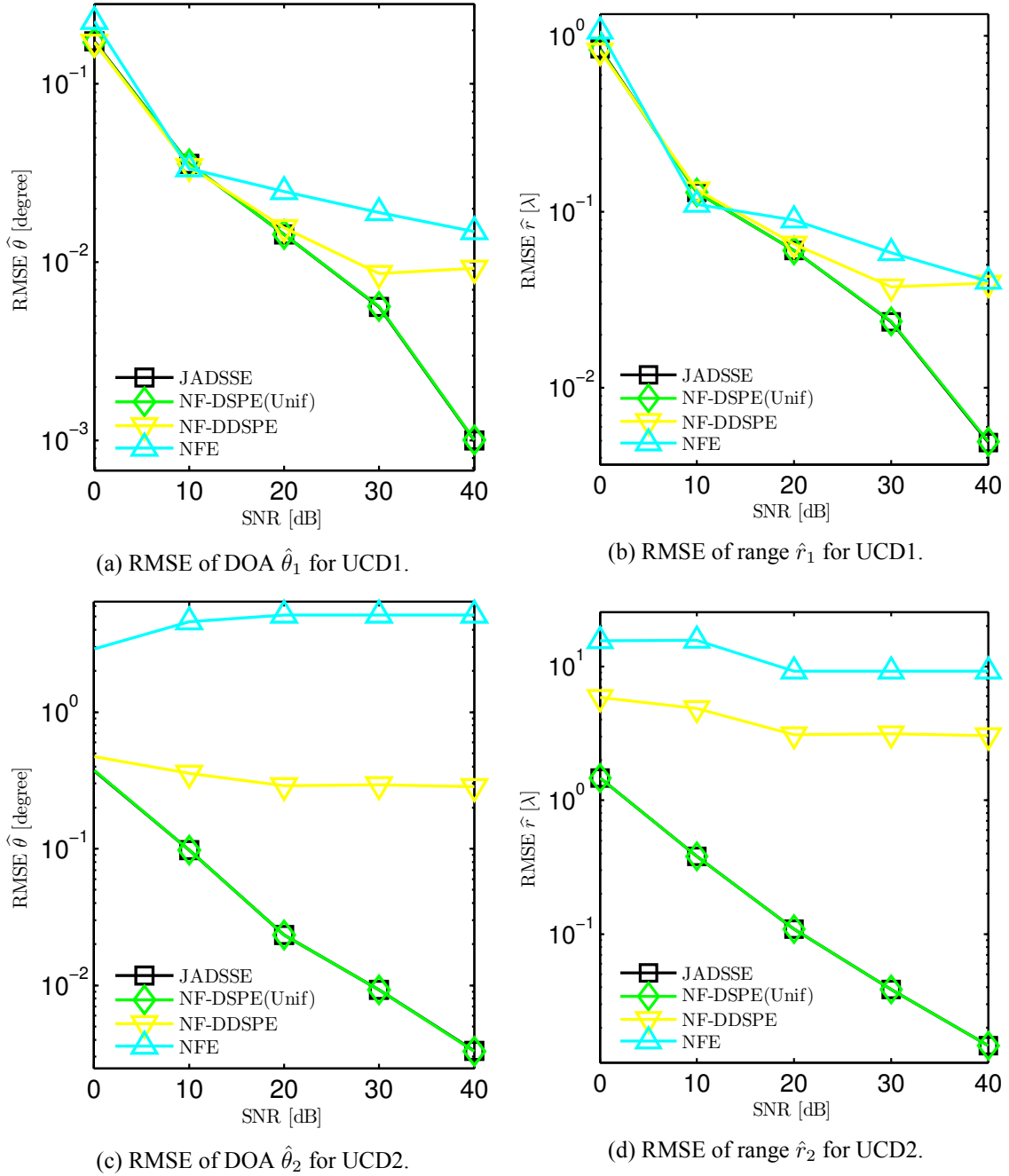


Figure 4.1: Root Mean Square Error versus SNR for two UCD sources. True parameters $\theta_1 = 0^\circ$, $\theta_2 = 30^\circ$, $\Delta_1 = 5^\circ$, $\Delta_2 = 15^\circ$ and $r_1 = 30\lambda$, $r_2 = 25\lambda$. (Note that for NF-DSPE the angular shape distribution is known).

True Values								
	θ_1	Δ_1	r_1	Shape	θ_2	Δ_2	r_2	Shape
	0°	5°	30λ	UCD	30°	15°	25λ	UCD
Estimated parameters								
	$\hat{\theta}_1$	$\hat{\Delta}_1$	\hat{r}_1	$\hat{\beta}_1$	$\hat{\theta}_2$	$\hat{\Delta}_2$	\hat{r}_2	$\hat{\beta}_2$
NFE	0	-	30.03	-	35.1	-	15.7	-
NF-DSPE(Unif)	0	5	29.9	-	30	15	24.9	-
NF-DDSPE	0	-	29.9	-	29.7	-	28.01	-
JADSSE	0	5	29.9	0.02	30	15	24.9	0.01

Table 4.2: True and estimated parameters of the Multi - UCD sources scenario at SNR=40 dB.

Fig.4.2 represents the reconstruction of the angular distribution $\hat{h}(\phi)$ with the estimated parameters given in Tab.4.2. For the JADSSE and NF-DSPE it is plotted in the continuous black (-) and green lines (-) compared with the true angular distribution $h(\phi)$ plotted in thick magenta (- -). NF-DSPE and JADSSE perfectly plot the shape of the distribution where NF-DDSPE needs *a priori* the shape information of h meanwhile JADSSE does not need this information due to its adaptation capacity for shapes fitting. Concerning the NF-DDSPE, after obtaining the DOA estimation, we need to choose an angular distribution h so we can re-inject the estimated DOA $\hat{\theta}$ and distance \hat{r} in the expression Eq. (4.34). Once we find $\hat{\Delta}$ we can plot the angular distribution $\hat{h}(\phi)$.

4.3.2 Mixture of Overlapping UCD and GCD Sources

Framework									
Sources						Array		Simulations	
N.	θ	Δ	r	β	Shape	M	d	L	N
1	0°	5°	30λ	-	GCD	20 sensors	$\lambda/2$	300 snapshots	10 realizations
2	7°	8°	25λ	-	UCD				

Table 4.3: Summarizing Parameters values of the framework with two UCD & GCD sources.

In the second scenario, we suppose two mixed UCD and GCD near-field sources where the detailed parameters are presented in Tab.4.3. The RMSE of the estimated DOA $\hat{\theta}$ and range \hat{r} is potted in Fig.4.3a-Fig.4.3b for the GCD source and in Fig.4.3c-Fig.4.3d for the UCD source.

For the GCD source, one can see in Fig.4.3a and Fig.4.3b that the RMSEs on $\hat{\theta}_1$ and \hat{r}_1 decrease asymptotically with SNR for NF-DDSPE and NF-DSPE. For this latter, note

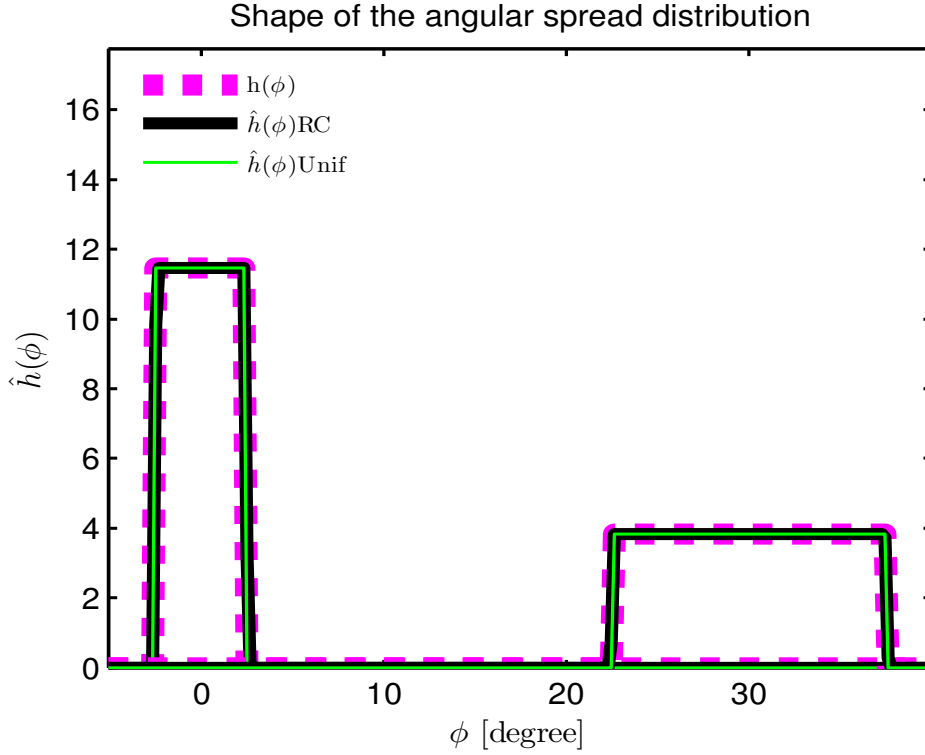


Figure 4.2: Reconstruction of the true $h(\phi)$ and estimated angular spread distribution $\hat{h}(\phi)$ for JADSSE and NF-DSPE(Unif) at SNR=40dB

that the angular shape distribution has to be known. This means that the approximation necessary for the decoupling Eq. (4.33) and the constraints in Eq. (4.19) are valid in the case of GCD with $\Delta_1 = 5$ degree. Concerning JADSSE, the threshold appearing on the RMSEs for SNRs larger than 20 dB corresponds to the mismodeling of a Gaussian shape distribution with a raised-cosine function. However JADSSE exhibits better performance than NF-DSPE when the angular shape is supposed to be uniformly distributed whereas it is Gaussian. The bad performance of NFE means that the sources can no longer be supposed as points in the case of close sources, even if the angular spread is not so large.

In the case of the UCD, Fig.4.3c and Fig.4.3d show that JADSSE performs as NF-DSPE for which the angular shape distribution is known to be uniform. On the other hand, NF-DDSPE exhibits poor performance as NF-DSPE in which the angular shape distribution is supposed Gaussian instead of uniform, and even worse than NFE which assumes point sources. This is because the decoupling approximation and the DDSPE constraints are no longer valid in the case of UCD with a large $\Delta_2 = 8$ degrees.

We can summarize the results as follows :

- NF-DDSPE performs well when the approximation Eq. (4.33) and constraints Eq. (4.19)

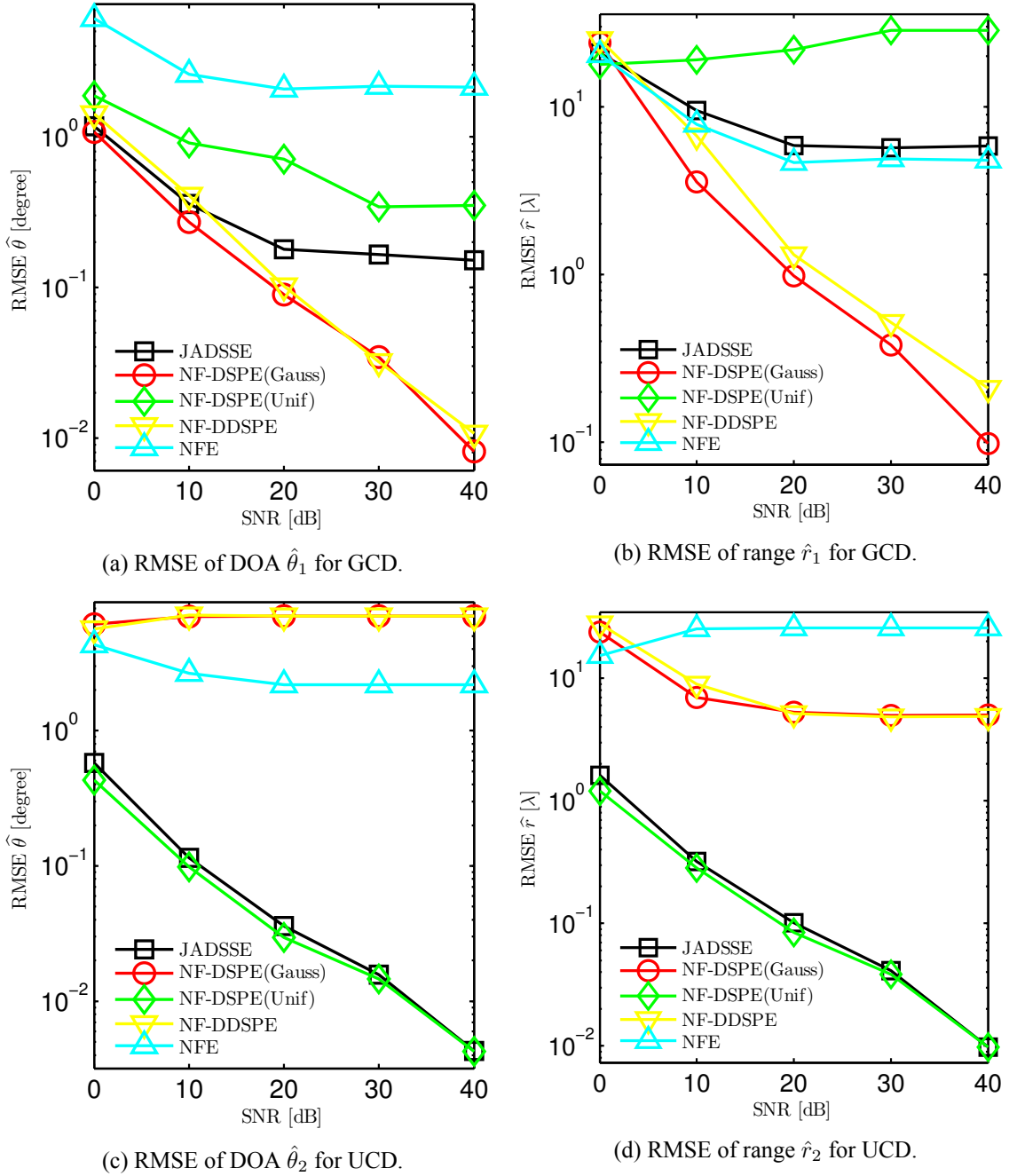


Figure 4.3: Root Mean Square Error versus SNR for two UCD sources. True parameters $\theta_1 = 0^\circ$, $\theta_2 = 7^\circ$, $\Delta_1 = 5^\circ$, $\Delta_2 = 8^\circ$ and $r_1 = 30\lambda$, $r_2 = 25\lambda$.

True Values								
	θ_1	Δ_1	r_1	Shape	θ_2	Δ_2	r_2	Shape
	0°	5°	30λ	GCD	7°	8°	25λ	UCD
Estimated parameters								
	$\hat{\theta}_1$	$\hat{\Delta}_1$	\hat{r}_1	$\hat{\beta}_1$	$\hat{\theta}_2$	$\hat{\Delta}_2$	\hat{r}_2	$\hat{\beta}_2$
NFE	2.1	-	34.8	-	4.8	-	50.8	-
NF-DSPE(Unif)	0.2	20.4	86.09	-	7	8	24.9	-
NF-DSPE(Gauss)	0	5	29.9	-	0	5	29.9	-
NF-DDSPE	0	-	29.76	-	0	-	29.76	-
JADSSE	0.2	12	35.7	1.26	7	8	24.9	0.01

Table 4.4: True and estimated parameters of the mixed GCD & UCD sources scenario at SNR=40 dB. Recalling that the estimated $\hat{\Delta}_1$ models a different extension given the distribution used by the estimator. For example, the spread for JADSSE represents the extension given at the mid-height of the distribution whereas for NF-DSPE(Gauss) it depicts the standard deviation.

are valid. This can be a severe limitation in practical situations where angular spreads may be large and source angular distributions may overlap. Besides, if an angular spread estimation is needed, the angular shape distribution must be known.

- JADSSE exhibits very good performance for UCD sources. It achieves limited performance at high SNR in the case of GCD but with acceptable RMSEs compared to NF-DSPE in which there would be a wrong angular shape distribution and to NFE which assumes point sources. The advantage of JADSSE is to jointly estimate the angular spread and shape distribution

The reconstruction of the angular distribution $\hat{h}(\phi)$ using the estimated parameters (DOA $\hat{\theta}$ and angular spread $\hat{\Delta}$) are plotted in Fig.4.4 where thick magenta (- -) represents the true angular distribution, the continuous red line (-) represents the NF-DSPE with Gaussian distribution, the green line (-) shows the NF-DSPE with the uniform distribution and the black line (-) depicts the JADSSE method. We can clearly see that the NF-DSPE with Gaussian angular distribution only reconstruct the GCD source (where it fails in the first place to localize the UCD one). Concerning the NF-DSPE with the uniform angular distribution, it provides a good reconstruction for the UCD source and fails in providing a good shape for the GCD source. However, the JADSSE succeeds in reconstructing the angular shape distribution of the two GCD and UCD sources (for detailed estimation values see Tab.4.4).

These results led us to test the resolution ability of the NF-DDSPE in such overlapped source scenario. For these reasons we run simulations test to compute the RMSE of the estimated DOA $\hat{\theta}$ versus the DOA separation δ_θ for the same above given framework.

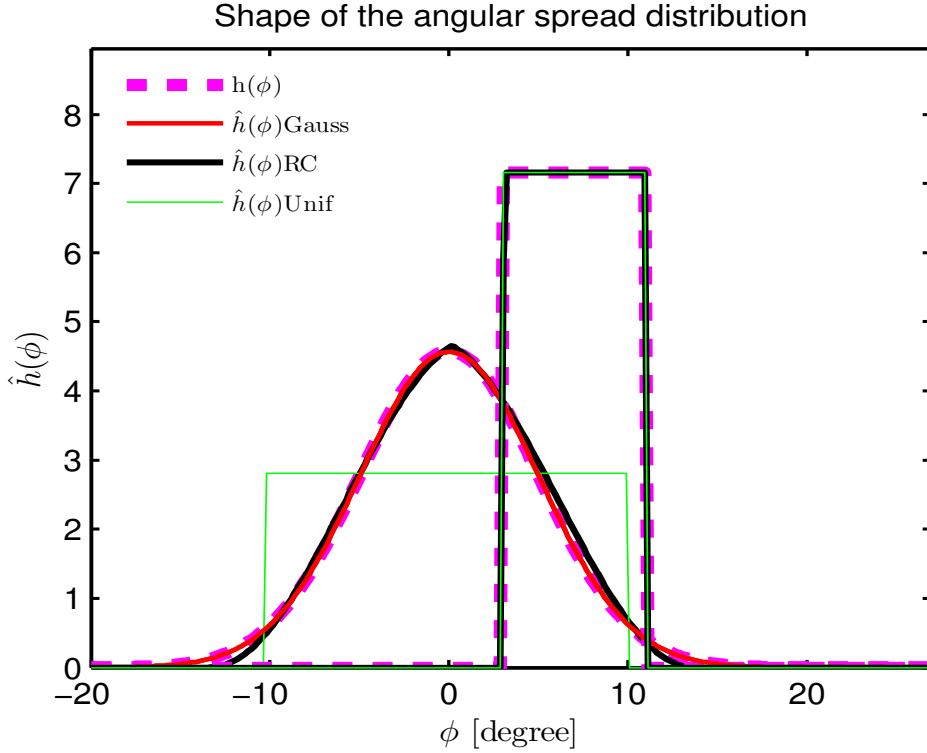


Figure 4.4: Reconstruction of the angular spread distribution $\hat{h}(\phi)$.

4.3.3 Resolution of Mixed CD Sources

In the aim to investigate the resolution capability of the NF-DDSPE, we consider the two GCD and UCD sources taken in subsection 4.3.2. We compute the RMSE versus the DOA source separation δ_θ for a fixed SNR= 20dB.

The RMSE of the estimated DOA $\hat{\theta}$ for the GCD source is plotted in Fig.4.5a and for the UCD source in Fig.4.5b. As we can observe, firstly, NF-DDSPE follows approximately the behavior of NF-DSPE with the Gaussian angular distribution for the first GCD source. The RMSE of JADSSE decreases as the DOA separation δ_θ increases. Secondly, for the UCD source, JADSSE follows NF-DSPE with the uniform angular distribution and allows accurate localization with good separation capabilities. However, the NF-DDSPE method presents poor separation strength for $\delta_\theta < 15^\circ$ so that it presents a failure in the resolution of the two overlapped GCD and UCD sources. This confirms the previous discussed results. It is important to note that the inequality Eq. (4.19) seriously impacts the NF-DDSPE DOA separation capabilities.

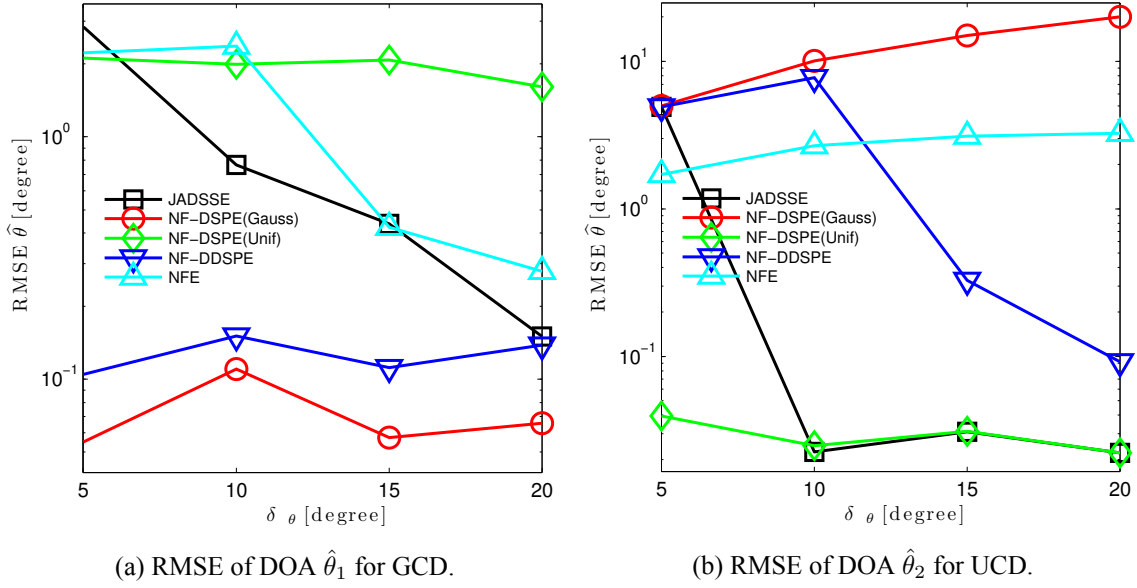


Figure 4.5: Root Mean Square Error of DOA $\hat{\theta}$ versus δ_θ for both UCD sources at SNR=20dB. True parameters $\theta_1 = 0^\circ$, $\theta_2 = \theta_1 + \delta_\theta$, $\Delta_1 = 5^\circ$, $\Delta_2 = 8^\circ$ and $r_1 = 30\lambda$, $r_2 = 25\lambda$.

Framework									
Sources						Array		Simulations	
N.	θ	Δ	r	β	Shape	M	d	L	N
1	0°	7°	30λ	1	RCCD	20	$\lambda/2$	300	20
2	30°	8°	25λ	-	UCD	sensors			

Table 4.5: Summarizing parameters values of the framework with two UCD & RCCD sources.

4.3.4 A Mixture of Raised-Cosine and Uniform CD Sources

In real physical applications, sources may present various angular shape distributions. In the literature, these distributions are generally assumed to be Gaussian or uniform functions. The proposed raised-cosine function already proposed for the generalized steering vector used in JADSSE, allows to model a family of possible angular shape distributions parametrized by β . In this subsection, we consider a mixture of two raised-cosine based CD sources with two different parameters β .

For the first source $\beta = 1$ (bell shaped angular distribution) and for the second source $\beta = 0$ corresponding to a UCD. Fig.4.6a and Fig.4.6b exhibit the RMSEs of the DOA $\hat{\theta}_1$ and range \hat{r}_1 versus SNR for the RCCD source. As JADSSE is based on this CD sources modeling, it performs very well and better than all the other methods. Indeed, the angular spread is too large to make NF-DDSPE performs very well at high SNR, NF-DSPE uses models of angular shape distribution which are not the good one and NFE assumes point sources. Fig.4.6c and Fig.4.6d exhibit the RMSEs for the second source which is UCD. As

the uniform angular shape distribution enters the family of RCCD functions (for $\beta = 0$) which are used by JADSSE, this latter performs as well as NF-DSPE which directly uses the knowledge of a uniform distribution. They exhibit much better results than the other methods for the same reasons mentioned for source 1.

In Fig.4.7, we compare the estimation performance of the angular spread $\hat{\Delta}$ with JADSSE and its decoupled version DADSSE proposed in subsection 4.2.3. One can see that DADSSE which uses successively NF-DDSPE and JADSSE has approximately the same source performance as JADSSE for the RCCD source with $\beta = 1$. However its performance at high SNR is limited in the case of UCD. It is certainly because of the approximation Eq. (4.33) or constraints Eq. (4.19) that are no longer valid.

4.4 Conclusions

In this chapter we proposed a generalized near-field approach of the DDSPE [37] method, the NF-DDSPE, for localizing CD sources in near-field when their angular shape distributions are unknown. This method is based on the decoupling of the estimation of the DOA θ and range r from the estimation of the angular spread Δ . As stated in [37], two assumptions are required. The first one concerns a small angular spread around the DOA so that the GSV $\underline{c}(\theta_0, \Delta_0, r_0)$ can be written as the element-wise product of the steering vector $\underline{a}(\theta_0, r_0)$ of the point source case and the Fourier transform vector $\tilde{\underline{h}}(\theta_0, \Delta_0, r_0)$ of the angular shape distribution $h(\phi + \theta_0, \Delta_0)$. The second assumption requires that the components of $\tilde{\underline{h}}(\theta_0, \Delta_0, r_0)$ are such that the first one is equal to one and the others are in decreasing order and positive.

Under these assumptions, the NF-DDSPE method allows to estimate the DOAs and the ranges of CD sources without knowing their angular shape distribution. However when the angular spread is required, the angular shape distribution must be known to use the NF-DDSPE. Also, we proposed in this chapter to use JADSSE in conjunction with NF-DDSPE to successively estimate the DOA and the range and then the spread and the shape of the source. This method is called DADSSE. As expected, the performance, in terms of parameters estimation and source resolution, of these decoupling-based NF-DDSPE and DADSSE degrades when the assumptions are not verified.

Finally, it appears that JADSSE outperforms NFE, NF-DDSPE, DADSSE and NF-DSPE when the assumed angular shape distribution is not the good one, and behaves nearly as NF-DSPE with the known angular shape distribution (exactly for RCCD and UCD and slightly poorer than NF-DSPE for GCD).

At this stage, it is a point of interest to explore the previously proposed estimators in

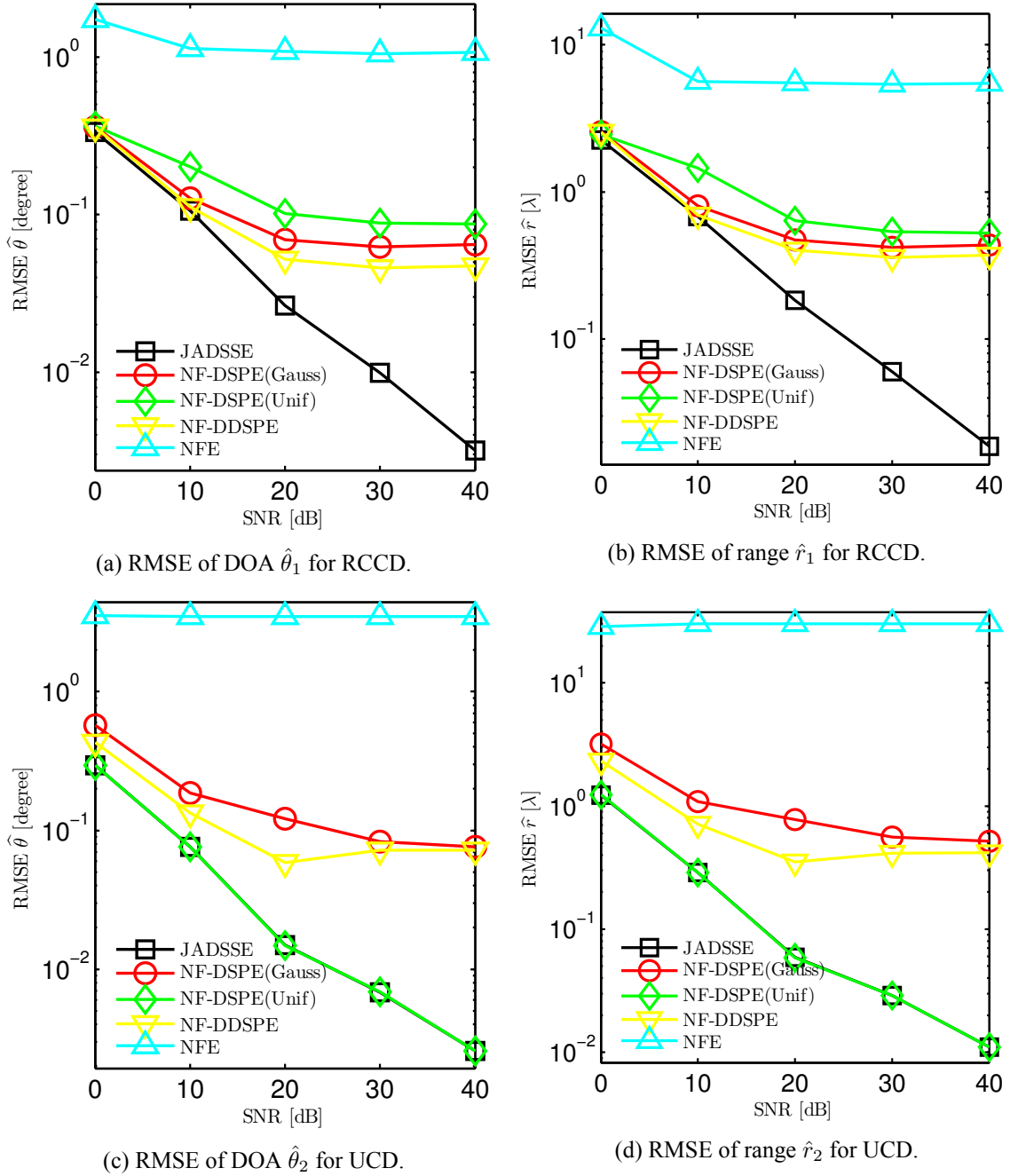


Figure 4.6: Root Mean Square Error versus SNR for RCCD(with $\beta = 1$) & UCD sources. True parameters $\theta_1 = 0^\circ$ $\theta_2 = 30^\circ$, $\Delta_1 = 7^\circ$, $\Delta_2 = 8^\circ$ and $r_1 = 30\lambda$, $r_2 = 25\lambda$.

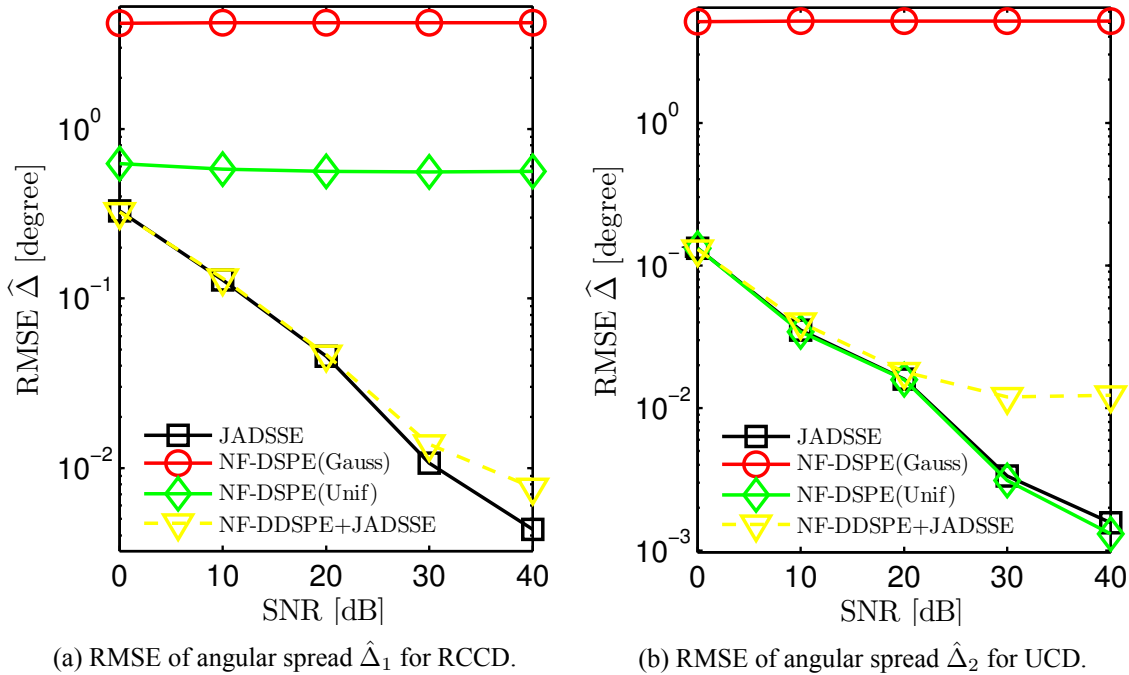


Figure 4.7: Root Mean Square Error versus SNR for RCCD(with $\beta = 1$) & UCD sources. True parameters $\theta_1 = 0^\circ$, $\theta_2 = 30^\circ$, $\Delta_1 = 7^\circ$, $\Delta_2 = 8^\circ$ and $r_1 = 30\lambda$, $r_2 = 25\lambda$.

an application framework to see their advantages in practical situations. Therefore, in the upcoming chapters, we will introduce the CD model parametrized in the Cartesian coordinates system instead of its angular system in the aero-acoustic imaging framework. The goal is to transpose the previously proposed CD model and methods to the aero-acoustic application for synthetic sources in chapter 5 and then for real data in chapter 6.

You have to learn the rules of the game. And then you have to play better than anyone else.

Albert Einstein

5

Localization Estimators for Two Dimensional CD Sources

Acoustic imaging represents a dynamic field of research that allows, in particular, the vehicle and aviation industries to improve passenger comfort by reducing aerodynamic noise. The approach consists of methods that have been developed for acoustic source localization and power reconstruction of an object.

Among the methods that have been developed in the literature, in the field of acoustic imaging, beamforming and spatial filtering techniques are known for their simple implementation but suffer from a wide beam and significant side-lobes that induce poor spatial resolution. Therefore, the development of methods like: deconvolution method DAMAS [10], iterative deconvolution method CLEAN [30] and inverse problems with a sparsity constraint to improve the resolution [15] have become important for aero-acoustic source localization in wind tunnel experiments. The drawbacks of these methods are sensitivity to background noise and possible elimination of weak sources. In [16], high resolution is achieved using a MUSIC-like method for the aero-acoustic sources localization in the transportation industry [4, 5].

However, considering this context, the configuration of the aero-acoustic experimentation satisfies the point source assumption [9]. The deconvolution methods identifies the Point Spread Functions (PSF) [30] which also supports the point source assumption. The reason why coherent distributed sources in the acoustic imaging is a relevant subject to

study. Unfortunately, the monopole point source assumption fails when the sources to be localized present a spatial extent rather than being gathered in a point. For this reason, in [30] the author proposed some deconvolution techniques to explore this source extension. Papamoschou [25] also considered the coherence noisy source on a jet surface by using a uni-dimensional linear distribution in the modeling aspect. Nevertheless, these methods do not offer a suitable description of the source extension like considering the two dimensional spread in a plane to better describe the source.

In this chapter, we firstly extend the aero-acoustic source model based on the CD source to the 2D case. Location and spatial extension are parameterized in the Cartesian coordinates. This model aims to characterize the two dimensional spatial coherence around the source for the wind tunnel application [4, 5]. Then, conventional, distributed Beamforming and NF-DSPE are formulated with the Cartesian coordinates parametrization. Next, to overcome the unknown or imperfectly known source shape distributions and based on the JADSSE presented in chapter 3, we propose the Joint Position Spread and Shape Estimator (JPSSE) method based on a generic function family (that takes into account an additional shape parameter) to provide good source shape approximation. In addition and based on the distributed source modeling, we propose a least square source power estimator to overcome the challenge of reconstructing weak source power. As mentioned in chapter 2, one of our important motivations of considering a distributed source model consists in accessing a wide dynamic range of power estimation. Finally, synthetic data are simulated and show that the proposed distributed estimators NF-DSPE and JPSSE provide better localization, power reconstruction and shape distribution information (only for JPSSE) of these sources.

The contributions of this chapter are:

- Proposing a suitable aero-acoustic source model with a two dimensional (2D) spatial extension in a plane with the Cartesian coordinates based on the CD model.
- Proposing source power estimators based on the distributed CD model.

5.1 Problem Formulation

The goal of the experiment in Fig.5.1 is to localize the aero-acoustic sources on the body of a car and to estimate their powers. Figure 5.1a depicts the vehicle in the wind tunnel and the microphones (sensors) plane location outside the wind tunnel. The microphones array consists of a 2D plane and a Non Uniform Array (NUA). The orientation axis x , y and z are shown in Figure 5.1c, where the x axis is in the opposite direction of the wind, the y axis is directed upwards and the z axis is oriented from the vehicle towards the array. The

origin center $O(0, 0, 0)$ is located at the ground level in the middle of the car. We consider that the aero-acoustic sources are present in the plane $z = z_0$ parallel to the array plane z_c . The sources that are not present in the vertical plane are assumed to be masked by the body of the car, for this reason we ignore their contribution.

5.2 Modeling of Aero-acoustic Signal Source Propagation

In this subsection, we first give the modeling of a two-dimensional coherently distributed (2D-CD) source. Next, we develop the 2D-CD model for an accurate source description.

5.2.1 Two Dimensional CD Source

Here, we generalize the model explained in section 3.2 to consider the spread over a two dimensional shape distribution. We also consider the source parametrization in the (x, y, z) Cartesian coordinates system. The signal spatial distribution v_i for the i -th CD source can be expressed by:

$$v_i(x, y, t; \underline{\mathbf{p}}_i, \Delta_i) = s_i(t)h_i(x - x_{si}, y - y_{si}; \Delta_i), \quad (5.1)$$

where $s_i(t)$ is a random complex signal emitted by the i -th source and $h_i(x - x_{si}, y - y_{si}; \Delta_i)$ represents a deterministic 2D spatial spread distribution over x and y . h reflects the shape of the CD source supposed to be temporally invariant. $\underline{\mathbf{p}}_i = [x_{si}, y_{si}, z_{si}]$ represents the Cartesian coordinates of the center of the source and Δ_i is the spatial spread. In this chapter we assume that the spread over x (Δ_{ix}) is equal to the spread over y (Δ_{iy}). In the next chapter we consider the case of $\Delta_{ix} \neq \Delta_{iy}$ to explore different source shapes.

The received signal components from a 2D-CD source at different positions around the spread are fully correlated, the reason we call it coherently. For uncorrelated signals from different 2D-CD sources, the cross-correlation kernel can be expressed as:

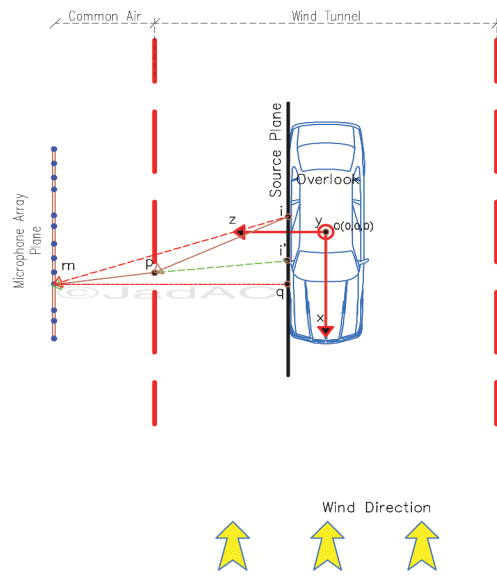
$$\begin{aligned} \rho_{iiv'}(x, x', y, y'; \underline{\mathbf{p}}_i, \Delta_i, \underline{\mathbf{p}}_{i'}, \Delta_{i'}) &= \rho(x, x', y, y'; \underline{\mathbf{p}}_i, \Delta_i) \delta_{ii'}, \\ &= \mathbb{E}[v_i(x, y, t; \underline{\mathbf{p}}_i, \Delta_i) v_i^*(x', y', t; \underline{\mathbf{p}}_i, \Delta_i)]. \end{aligned} \quad (5.2a)$$

$\mathbb{E}[\cdot]$ stands for the statistical expectation and $\delta_{ii'}$ refers to the Kronecker delta. We can express the auto-correlation of the i -th CD source by:

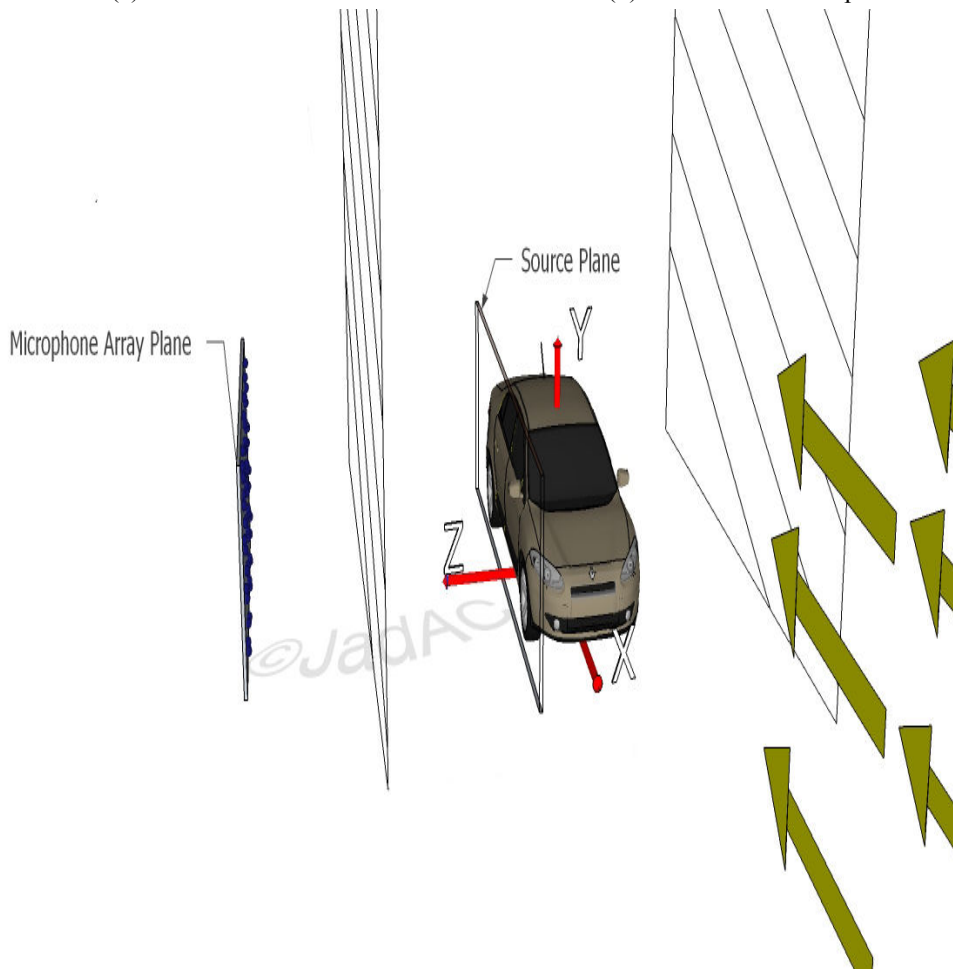
$$\rho(x, x', y, y'; \underline{\mathbf{p}}_i, \Delta_i) = \mathbb{E}[|s_i(t)|^2] h_i(x - x_{si}, y - y_{si}; \Delta_i) h_i^*(x' - x_{si}, y' - y_{si}; \Delta_i). \quad (5.3)$$



(a) Wind tunnel S2A



(b) Overlook of the experimentation



(c) 3D schematic view of the experimentation

Figure 5.1: Configurations of Wind Tunnel Platform.

In the sequel of our study, it is convenient to normalize h :

$$\int_{-\infty}^{\infty} \int_{-\infty}^{\infty} h_i(x - x_{si}, y - y_{si}; \Delta_i) dx dy = 1. \quad (5.4)$$

Considering this normalization, the source signal power is given by $\sigma_{s_i}^2 = \mathbb{E}[|s_i(t)|^2]$ from Eq. (5.3).

5.2.2 2D Spatial Distributions

In this subsection, we give some examples of the two dimensional spatial distribution $h(x - x_s, y - y_s; \Delta)$.

Gaussian

In the following, the two dimensional Gaussian function is considered for modeling the distribution of a CD source. A two dimensional elliptical Gaussian function is given by:

$$h(x, y) = A \exp \left[- \left(a(x - x_s)^2 + 2b(x - x_s)(y - y_s) + c(y - y_s)^2 \right) \right], \quad (5.5)$$

where A is the amplitude and x_s, y_s are the coordinates of the center of the source. One particular form will be used in the sequel using $A = \frac{1}{2\pi\Delta_x\Delta_y}$, $a = c = \frac{1}{2}$ and $b = 0$. The 2D Gaussian function is then given by:

$$h(x, y; \Delta_x, \Delta_y) = A \exp \left(- \frac{1}{2} \left[\left(\frac{x - x_s}{\Delta_x} \right)^2 + \left(\frac{y - y_s}{\Delta_y} \right)^2 \right] \right), \quad (5.6)$$

with Δ_x, Δ_y are the x and y standard deviations¹. Fig.5.2 shows a 2D Gaussian CD source for $x_s = 0, y_s = 0$ and $\Delta = 10cm$.

2D Raised Cosine

Similarly to the one dimensional case discussed in chapter 3, and for more general shapes and extension widths, we generalize the function family RC into the 2D case. We present two types of this generalization: the first with a separable Kernel and the second with a symmetrical distribution. The aim of these two representations is to take into account different shapes of the source.

¹We recall that in this chapter the spatial extension over the dimensions x and y are supposed to be equal, therefore we use a unique Δ .

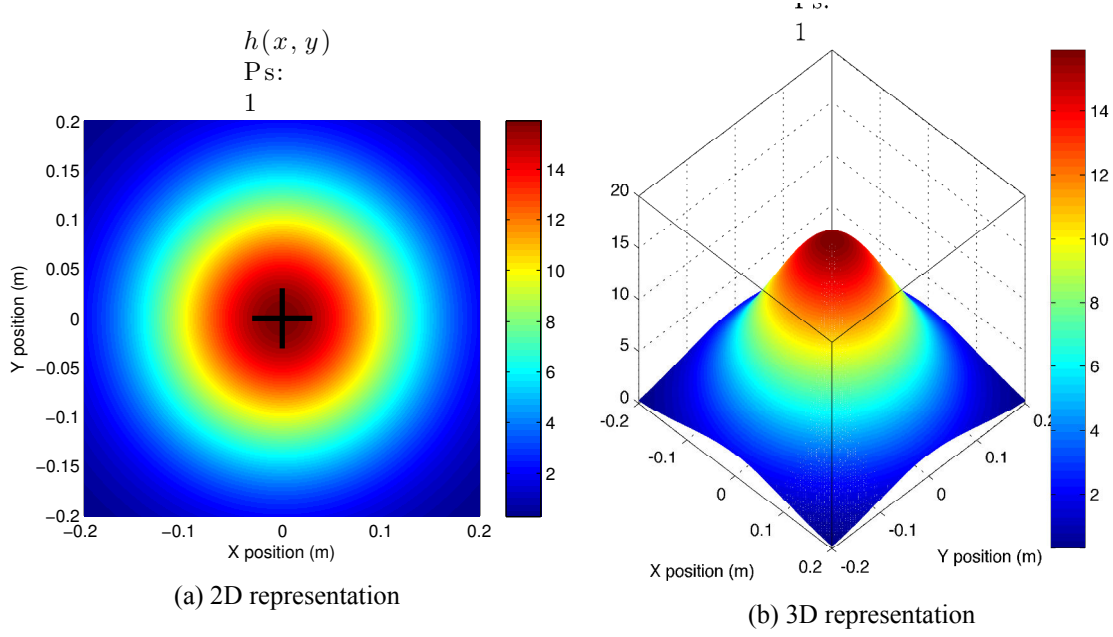


Figure 5.2: The two dimensional Gaussian spatial distribution with a spatial extension $\Delta = 10cm$.

Separable 2D Kernel This 2D distribution is obtained by multiplying two separate 1D RC functions $h(x; \Delta_x, \beta)$ and $h(y; \Delta_y, \beta)$ (similarly to the 1D angular distribution in 3.3.2):

$$h(x, y; \Delta, \beta) = h(x; \Delta_x, \beta) \cdot h(y; \Delta_y, \beta), \quad (5.7)$$

with the same shape parameter β for the distribution over x and y . $h(x; \Delta, \beta)$ has the following expression:

$$h(x; \Delta, \beta) = \begin{cases} 1/\Delta & \text{if } |x - x_s| \leq \frac{\Delta}{2}(1 - \beta), \\ 1/2\Delta [1 + \cos(\gamma_x)] & \text{if } \frac{\Delta}{2}(1 - \beta) < |x - x_s| \leq \frac{\Delta}{2}(1 + \beta), \\ 0 & \text{otherwise,} \end{cases} \quad (5.8)$$

with $\gamma_x = \frac{\pi}{\beta\Delta} [|x - x_s| - \frac{\Delta}{2}(1 - \beta)]$.

For $0 \leq \beta < 1$ the 1D function ($h(x; \Delta_x, \beta)$ or $h(y; \Delta_y, \beta)$) is normalized following $\int_{-\infty}^{\infty} h(x, \Delta, \beta) dx = 1$. Therefore :

$$\int_{-\infty}^{\infty} \int_{-\infty}^{\infty} h(x, y, \Delta, \beta) dx dy = \int_{-\infty}^{\infty} h(x, \Delta_x, \beta) dx \int_{-\infty}^{\infty} h(y, \Delta_y, \beta) dy = 1. \quad (5.9)$$

We show in Fig.5.3 and Fig.5.4 the two dimensional RC with separable Kernel for different β values. We can clearly see the square-core of the function for $\beta = 0$ and the smoothie edge effect on the distribution for $\beta = 0.5$. This 2D parameterized functions family h can

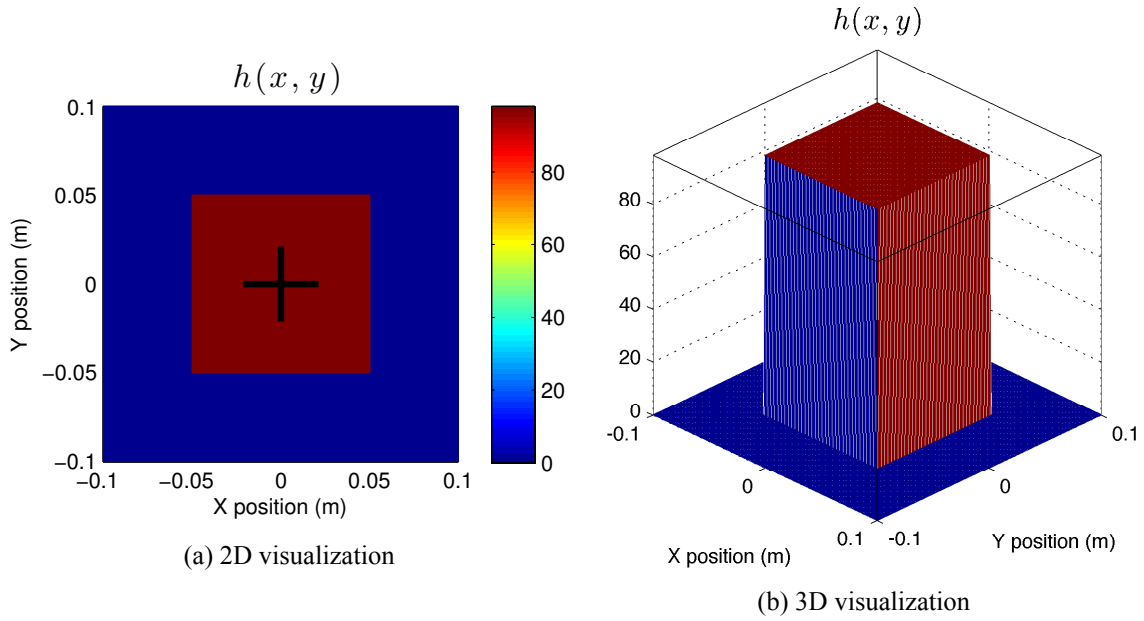


Figure 5.3: The 2D Separable Kernel RC given for shape value $\beta = 0$.

adapt most of the well known distributions like the 2D Gaussian distribution and the 2D uniform distribution.

Symmetrical distribution It consists in a circular symmetric function. The 2D symmetrical Raised Cosine is expressed by:

$$h(x - x_s, y - y_s; \Delta, \beta) = \begin{cases} 1/A & \text{if } r_s \leq \frac{\Delta}{2}(1 - \beta), \\ 1/2A \left[1 + \cos(\gamma) \right] & \text{if } \frac{\Delta}{2}(1 - \beta) < r_s \leq \frac{\Delta}{2}(1 + \beta), \\ 0 & \text{otherwise,} \end{cases}$$

where:

$$A = \left[\pi \frac{\Delta}{2} (1 - \beta) \right]^2, \quad (5.10a)$$

$$r_s = \sqrt{(x - x_s)^2 + (y - y_s)^2}, \quad (5.10b)$$

$$\gamma = \frac{\pi}{\beta \Delta} \left[r_s - \frac{\Delta}{2} (1 - \beta) \right]. \quad (5.10c)$$

The shape parameter β determines the shape of the distribution and the spatial extension

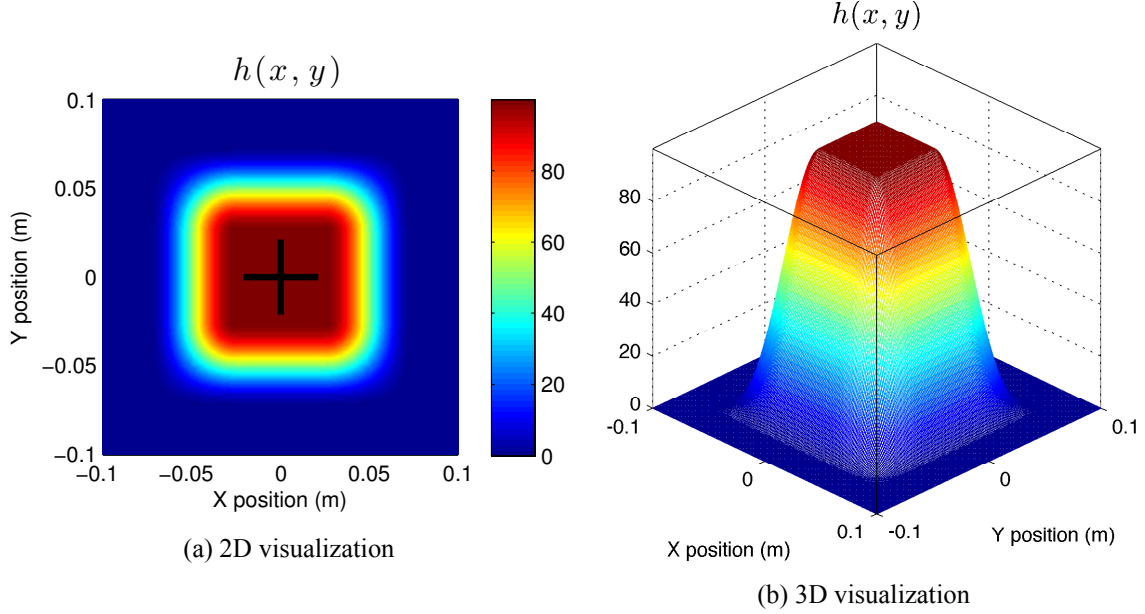


Figure 5.4: The 2D Separable Kernel RC given for shape value $\beta = 0.5$.

is Δ . The source center is determined by x_s and y_s . Fig. 5.5 and Fig.5.6 represents one 2D raised cosine distribution with two different β values.

Uniform

Another distribution to consider is the uniform one which is expressed as:

$$h(x, y; \Delta) = \begin{cases} \frac{1}{\Delta} & \text{if } |x - x_s| \leq \frac{\Delta}{2} \text{ and } |y - y_s| \leq \frac{\Delta}{2} \\ 0 & \text{Otherwise} \end{cases} \quad (5.11)$$

We notice that this distribution is a special case of the RC, so the distribution also exists under two different ways: the separable kernel and the symmetrical distribution (see the RC case for $\beta = 0$ in Fig.5.5 and Fig. 5.3).

5.2.3 2D Signal Modeling for CD Sources

Suppose q two dimensional CD sources illuminating an array of M sensors. The near-field sources are at position $\mathbf{P} = [\mathbf{p}_1, \dots, \mathbf{p}_q]^\top$ with $\mathbf{p}_i = [x_{si}, y_{si}, z_{si}]$ being the coordinates of the i -th source. The wide-band acoustic signals emitted by the i -th source, is denoted by $s_i(t)$. The received signal is sampled on each microphone sensor. These samples are then divided into J segments with each one consisting of L snapshots. The total sampling

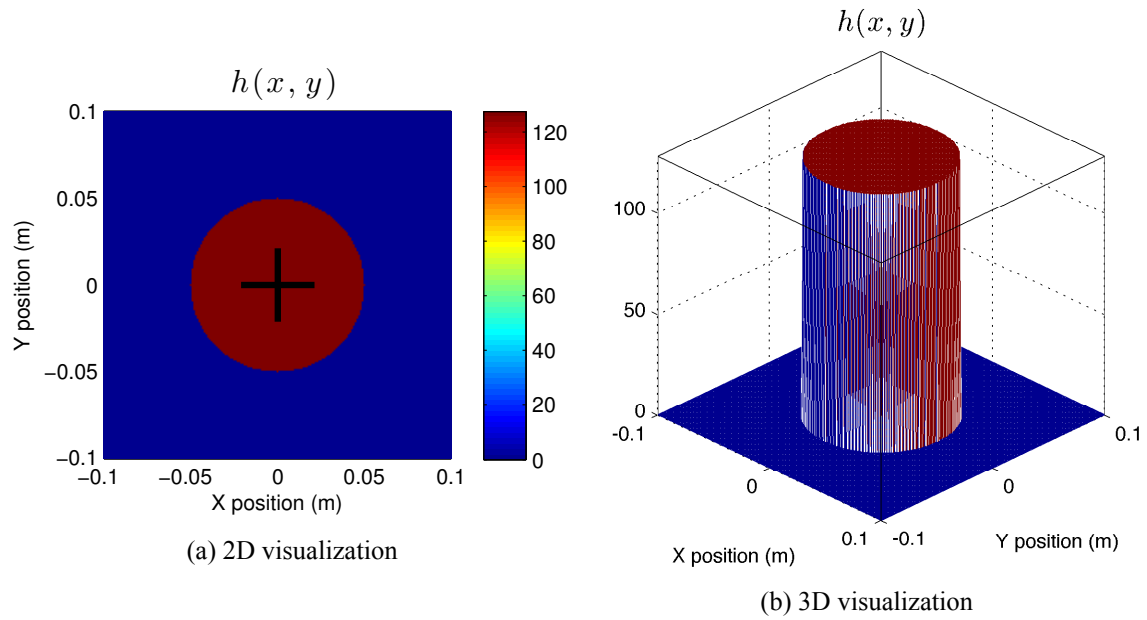


Figure 5.5: The 2D symmetrical RC given for shape value $\beta = 0$.

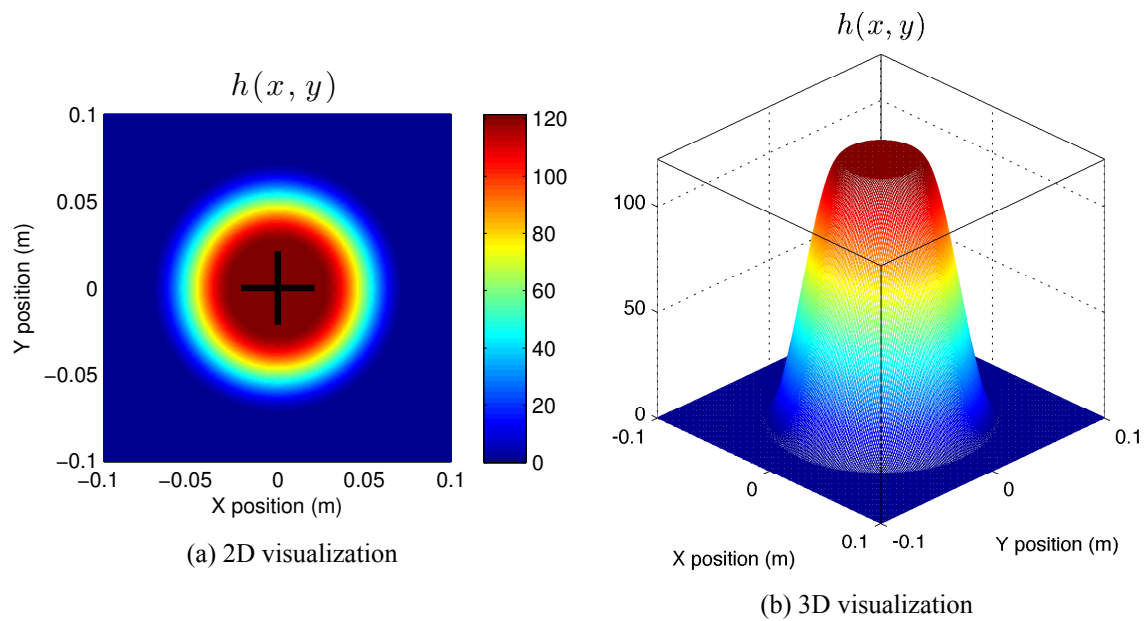


Figure 5.6: The 2D symmetrical RC given for shape value $\beta = 0.5$.

number is given by $T = JL$. Afterwards, we apply a Discrete Fourier Transform (DFT) in the time domain for each segment to get L narrow-band frequencies. Therefore, the measured signals for the j -th segment can be written in the frequency domain as:

$$\underline{\mathbf{x}}_j(f_l) = \mathbf{C}(\mathbf{P}, f_l)\underline{\mathbf{s}}_j(f_l) + \underline{\mathbf{n}}_j(f_l). \quad (5.12)$$

The $M \times 1$ vector $\underline{\mathbf{x}}_j(f_l) = [x_{j,1}(f_l), x_{j,2}(f_l), \dots, x_{j,M}(f_l)]^\top$ models the sensors output for the given frequency f_l ($l \in [1, L]$) in the sampled segment j ($j \in [1, J]$). $\mathbf{C}(\mathbf{P}, f_l) = [\underline{\mathbf{c}}(\underline{\mathbf{p}}_1, \Delta_1, f_l), \dots, \underline{\mathbf{c}}(\underline{\mathbf{p}}_q, \Delta_q, f_l)]$ is the $M \times q$ near-field Generalized Steering (GS) matrix containing the column vectors $\underline{\mathbf{c}}(\underline{\mathbf{p}}_i, \Delta_i, f_l)$ for $i = 1, \dots, q$, where $\underline{\mathbf{c}}(\underline{\mathbf{p}}_i, \Delta_i, f_l)$ is the GS vector given by:

$$\underline{\mathbf{c}}(\underline{\mathbf{p}}_i, \Delta_i, f_l) = \int_{-\infty}^{\infty} \int_{-\infty}^{\infty} \underline{\mathbf{a}}(x, y, f_l) h_i(x - x_{si}, y - y_{si}; \Delta_i) dx dy, \quad (5.13a)$$

$$\underline{\mathbf{a}}(x, y, f_l) = \left[\frac{1}{d_{i,1}} \exp(-j2\pi f_l \tau_{i,1}), \dots, \frac{1}{d_{i,M}} \exp(-j2\pi f_l \tau_{i,M}) \right]^\top. \quad (5.13b)$$

$\tau_{i,m}$ and $d_{i,m}$ denote the time travel and the distance from the source i to the sensor m , respectively. $d_{i,m}$ is function of $\underline{\mathbf{p}}_i$ and is expressed by:

$$d_{i,m} = \sqrt{(x_{cm} - x_{si})^2 + (y_{cm} - y_{si})^2 + (z_c - z_0)^2}, \quad (5.14)$$

where x_{cm} , y_{cm} and z_c (5,3 meter) denote the coordinates of sensor m . In the uniform and isotropic medium (without wind consideration) $\tau_{i,m}$ is given by:

$$\tau_{i,m} = \frac{d_{i,m}}{c_0}. \quad (5.15)$$

The $q \times 1$ vector $\underline{\mathbf{s}}_j(f_l) = [s_{j,1}(f_l), \dots, s_{j,q}(f_l)]^\top$ represents the DFT of the source signals, where $s_{j,i}(f_l)$ is the DFT of the i -th signal source for the j -th sampling segment. The $M \times 1$ vector $\underline{\mathbf{n}}_j(f_l) = [n_{j,1}(f_l), \dots, n_{j,M}(f_l)]^\top$, where $n_{j,m}(f_l)$ denotes the i.i.d additive Gaussian white noise for sensor m in the j -th sampling segment.

The source signal and noise time samples are modeled by random, complex, centered and independent processes. We assume that the noise and the sources are uncorrelated. Considering the previous assumptions, the correlation matrix of the array output $\mathbf{R}_x(f_l)$ for the J segments at the frequency f_l is given by:

$$\mathbf{R}_x(f_l) = E[\underline{\mathbf{x}}(f_l) \underline{\mathbf{x}}(f_l)^H] = \mathbf{C}(\mathbf{P}, f_l)\mathbf{R}_s(f_l)\mathbf{C}(\mathbf{P}, f_l)^H + \sigma_n^2(f_l)\mathbf{I}, \quad (5.16)$$

$\mathbf{R}_s(f_l)$ is the sources correlation matrix with the ij -th component defined as $E[s_i s_j^*]$, $\sigma_n^2(f_l)$ is the noise variance at f_l and \mathbf{I} is the $M \times M$ identity matrix. The sources are assumed to be uncorrelated, so that $\mathbf{R}_s(f_l)$ is a diagonal matrix with elements $\sigma_{s_i}^2 = \mathbb{E}[|s_i|^2]$. The correlation matrix $\mathbf{R}_x(f_l)$ can be estimated from the J segment snapshots by:

$$\hat{\mathbf{R}}_x(f_l) = \frac{1}{J} \sum_{j=1}^J \mathbf{x}_j(f_l) \mathbf{x}_j^H(f_l). \quad (5.17)$$

5.3 Classical Estimators

In this section we recall the two beamforming approaches for point and CD source localization, the CBF [34] and GBF along with the high resolution NFE [18, 20] approach, formulated in the Cartesian coordinates.

5.3.1 Near Field-CBF (NF-CBF)

For a given frequency f_l , the NF-CBF relies on maximizing the 2D cost function defined as:

$$S_{\text{NF-CBF}}(x, y; f_l) = \bar{\mathbf{a}}^H(x, y; f_l) \hat{\mathbf{R}}_x(f_l) \bar{\mathbf{a}}(x, y; f_l), \quad (5.18)$$

where $\bar{\mathbf{a}}(x, y; f_l)$ denotes the normalized CBF steering vector given by:

$$\bar{\mathbf{a}}(x, y; f_l) = \frac{\mathbf{a}(x, y; f_l)}{\|\mathbf{a}(x, y; f_l)\|^2}, \quad (5.19)$$

with $\mathbf{a}(x, y; f_l)$ is the point source steering vector at the (x, y) position for the frequency f_l defined in Eq. (5.13).

5.3.2 Near Field-GBF (NF-GBF)

When dealing with CD sources, the GBF [40] (given in its angular far-field form in Eq. (2.37)) is generalized to the near-field, NF-GBF, consists in searching the maxima of the following cost function:

$$S_{\text{NF-GBF}}(x, y, \Delta; f_l) = \frac{\underline{\mathbf{c}}^H(\underline{\mathbf{p}}, \Delta; f_l) \hat{\mathbf{R}}_x(f_l) \underline{\mathbf{c}}(\underline{\mathbf{p}}, \Delta; f_l)}{\|\underline{\mathbf{c}}(\underline{\mathbf{p}}, \Delta; f_l)\|^2}, \quad (5.20)$$

where $\underline{\mathbf{c}}^H(\underline{\mathbf{p}}, \Delta; f_l)$ denotes the GS vector for the CD sources defined in Eq. (5.13).

5.3.3 Near Field Estimator

To obtain the estimated parameters \hat{x} and \hat{y} for the q sources, the estimator consists of searching the q peaks of the two dimensional cost function $S_{\text{NFE}}(x, y)$:

$$S_{\text{NFE}}(x, y; f_l) = \frac{1}{\underline{\mathbf{a}}^H(x, y; f_l) \hat{\mathbf{E}}_n \hat{\mathbf{E}}_n^H \underline{\mathbf{a}}(x, y; f_l)}. \quad (5.21)$$

The noise basis $\hat{\mathbf{E}}_n$ is constructed with the $M - q$ eigenvectors $\hat{\mathbf{e}}_i$ associated with the lowest $M - q$ eigenvalues of $\hat{\mathbf{R}}_x(f_l)$.

5.4 Proposed Estimators

In the following section, we present the methods proposed previously in the thesis re-parametrized with Cartesian coordinates system for the localization of the 2D distributed near-field source. The first one is the NF-DSPE considering a 2D spread. As seen previously, this method highly depends on the shape distribution $h_n(x - x_s, y - y_s; \Delta)$. The second one is the JADSSE in the Cartesian coordinates version called: Joint Position, Spread and Shape Estimator (JPSSE).

5.4.1 Near Field-DSPE

The proposed estimator minimizes the norm of the product between the estimated noise subspace $\hat{\mathbf{E}}_n$ and the analysis vector $\underline{\mathbf{c}}(\underline{\mathbf{p}}, \Delta; f_l)$. To estimate the parameters \hat{x} , \hat{y} and $\hat{\Delta}$ for the q sources, the estimator searches the q prominent peaks of the three dimensional cost function $S_{\text{NF-DSPE}}(x, y, \Delta; f_l)$:

$$S_{\text{NF-DSPE}}(x, y, \Delta; f_l) = \frac{1}{\underline{\mathbf{c}}^H(\underline{\mathbf{p}}, \Delta; f_l) \hat{\mathbf{E}}_n \hat{\mathbf{E}}_n^H \underline{\mathbf{c}}(\underline{\mathbf{p}}, \Delta; f_l)}, \quad (5.22)$$

and

$$\underline{\mathbf{c}}(\underline{\mathbf{p}}, \Delta; f_l) = \int_{-\infty}^{\infty} \int_{-\infty}^{\infty} \underline{\mathbf{a}}(x, y; f_l) h(x - x_s, y - y_s; \Delta) dx dy. \quad (5.23)$$

In the sequel, we denote NF-DSPE(G) for the Gaussian distribution and NF-DSPE(U) for the uniform one. As discussed before drawback of this method is that the computation of $\underline{\mathbf{c}}(\underline{\mathbf{p}}, \Delta; f_l)$ in Eq. (5.23), requires *a priori* information about the shape of the spatial spread distribution h . Indeed, the performance simulations in chapter three have shown the high sensitivity of the method to the shape mismodeling.

5.4.2 Joint Position Spread Shape Estimator (JPSSE)

The proposed JPSSE minimizes the norm of the product of $\hat{\mathbf{E}}_n$ and the vector $\underline{\mathbf{c}}(\underline{\mathbf{p}}, \Delta, \beta; f_l)$. The estimator relies on searching for the q maxima of the four-dimensional cost function:

$$S_{\text{JPSSE}}(x, y, \Delta, \beta; f_l) = \frac{1}{\|\underline{\mathbf{c}}^{\text{H}}(\underline{\mathbf{p}}, \Delta, \beta; f_l) \hat{\mathbf{E}}_n\|^2}, \quad (5.24)$$

where:

$$\underline{\mathbf{c}}(\underline{\mathbf{p}}, \Delta, \beta; f_l) = \int_{-\frac{\Delta}{2}(1+\beta)}^{\frac{\Delta}{2}(1+\beta)} \int_{-\frac{\Delta}{2}(1+\beta)}^{\frac{\Delta}{2}(1+\beta)} \underline{\mathbf{a}}(x, y; f_l) h(x - x_s, y - y_s; \Delta, \beta) dx dy. \quad (5.25)$$

Introducing a general function family $h(x - x_s, y - y_s; \Delta, \beta)$ and estimating the shape parameter β , the proposed JPSSE makes it possible to reconstruct the two dimensional spatial distribution without *a priori* information about its shape. This blind approach allows to increase the robustness of the estimation with respect to the shape of the spatial 2D spread distribution.

5.5 Power Source Estimators

In practice, when dealing with distributed sources whereas assuming point sources, this mismodeling implicitly underestimates the power and discriminates low power sources. Exploiting the distributed source model offers an access to a more accurate power estimation. Here, we present two methods for the signal source power estimation $\hat{\sigma}_s^2$. The first technique relies on the CBF (respectively the GBF) spectrum with the estimated source parameters \hat{x} , \hat{y} (respectively $\hat{\Delta}$ for CD sources). The second approach is a least square method that requires the estimation of the array correlation matrix $\hat{\mathbf{R}}_x$.

5.5.1 CBF and GBF Power Estimators

For the i -th point source with the estimated (\hat{x}_i, \hat{y}_i) position, the power estimation is given by the CBF spectrum:

$$\hat{\sigma}_{s_i}^2 \text{CBF}(f_l) = \frac{\underline{\mathbf{a}}^{\text{H}}(\hat{x}_i, \hat{y}_i; f_l) \hat{\mathbf{R}}_x(f_l) \underline{\mathbf{a}}(\hat{x}_i, \hat{y}_i; f_l)}{\|\underline{\mathbf{a}}(\hat{x}_i, \hat{y}_i; f_l)\|^4} \quad (5.26a)$$

$$= \frac{\underline{\mathbf{a}}^{\text{H}}(\hat{x}_i, \hat{y}_i; f_l) \hat{\mathbf{R}}_x(f_l) \underline{\mathbf{a}}(\hat{x}_i, \hat{y}_i; f_l)}{M^2}. \quad (5.26b)$$

Distributed sources and especially CDs are characterized by their spread Δ and their spatial distribution h . The GBF power estimation method relies on the Generalized Steering Vector

$\underline{\mathbf{c}}(\underline{\mathbf{p}}, \Delta; f_l)$. The GSV expression is indexed by " h_G ", " h_U " and " h_{RC} " for the Gaussian, Uniform and Raised Cosine shape, respectively. Once the shape distribution $h(x, y; \underline{\mathbf{p}}, \Delta)$ is defined and the estimated i -th source parameters $\hat{\underline{\mathbf{p}}}_i, \hat{\Delta}_i$ are obtained, the GSV is computed as following:

$$\underline{\mathbf{c}}_h(\hat{\underline{\mathbf{p}}}_i, \hat{\Delta}_i; f_l) = \int_{-\infty}^{\infty} \int_{-\infty}^{\infty} \underline{\mathbf{a}}(x, y; f_l) h(x - \hat{x}_{si}, y - \hat{y}_{si}; \hat{\Delta}_i) dx dy. \quad (5.27)$$

Therefore, the GBF power estimator is defined as follows:

$$\hat{\sigma}_{s_i}^{2 \text{ GBF}}(f_l) = \frac{\underline{\mathbf{c}}_h^H(\hat{\underline{\mathbf{p}}}_i, \hat{\Delta}_i; f_l) \hat{\mathbf{R}}_x(f_l) \underline{\mathbf{c}}_h(\hat{\underline{\mathbf{p}}}_i, \hat{\Delta}_i; f_l)}{\|\underline{\mathbf{c}}_h^H(\hat{\underline{\mathbf{p}}}_i, \hat{\Delta}_i; f_l) \underline{\mathbf{c}}_h(\hat{\underline{\mathbf{p}}}_i, \hat{\Delta}_i; f_l)\|^2}. \quad (5.28)$$

5.5.2 Least Square (LS) Subspace Based Power Estimators

Using the assumption of the uncorrelated 2D-CD sources, we collect on the diagonal values of $\hat{\mathbf{R}}_s$ where $[\hat{\mathbf{R}}_s(f_l)]_{ii} = \hat{\sigma}_{s_i}^2$ presents the i -th source power. First, considering point sources, we obtain the power by estimating the source correlation matrix $\hat{\mathbf{R}}_s^{\text{LS-point}}(f_l)$ using the estimate of the steering matrix $\mathbf{A}^\dagger(\hat{\mathbf{P}}, f_l)$, the array correlation $\hat{\mathbf{R}}_x(f_l)$ and the noise power $\hat{\sigma}_n^2(f_l)$. So the point source power estimation is $\hat{\sigma}_{s_i}^{2 \text{ LS-point}}(f_l) = [\hat{\mathbf{R}}_s^{\text{LS-point}}(f_l)]_{ii}$.

$$\hat{\mathbf{R}}_s^{\text{LS-point}}(f_l) = \mathbf{A}^\dagger(\hat{\mathbf{P}}, f_l) \left[\hat{\mathbf{R}}_x(f_l) - \hat{\sigma}_n^2(f_l) \mathbf{I}_{M \times M} \right] \mathbf{A}^{\dagger H}(\hat{\mathbf{P}}, f_l), \quad (5.29)$$

where, $\mathbf{I}_{M \times M}$ denotes the $M \times M$ identity matrix and $\mathbf{A}^\dagger = \left(\mathbf{A}^H \mathbf{A} \right)^{-1} \mathbf{A}^H$ represents the Moore-Penrose pseudo-inverse matrix. The noise power $\hat{\sigma}_n^2(f_l)$ is determined using the mean value of the $M - q$ lowest eigenvalues of the correlation matrix eigen analysis and given by:

$$\hat{\sigma}_n^2(f_l) = \frac{1}{M - q} \sum_{i=1}^{M-q} \hat{\lambda}_i. \quad (5.30)$$

Next, for the CD sources the main change in the method will occur by replacing the common steering matrix of the point sources by the GS matrix for the 2D-CD sources. So the 2D-CD i -th source power estimation is $\hat{\sigma}_{s_i}^{2 \text{ LS-h}}(f_l) = [\hat{\mathbf{R}}_s^{\text{LS-h}}(f_l)]_{ii}$. Herein, two cases for the GS matrix that contains the q vectors $\underline{\mathbf{c}}_h(\hat{\underline{\mathbf{p}}}_i, \hat{\Delta}_i; f_l)$ are considered: the NF-DSPE in Eq. (5.23) and the JPSSE in Eq. (5.25). Once we select h and we provide the suitable GS matrix, the approach is as follows:

$$\hat{\mathbf{R}}_s^{\text{LS-h}}(f_l) = \mathbf{C}_h^\dagger(\hat{\mathbf{P}}, f_l) \left[\hat{\mathbf{R}}_x(f_l) - \hat{\sigma}_n^2(f_l) \mathbf{I}_{M \times M} \right] \mathbf{C}_h^{\dagger H}(\hat{\mathbf{P}}, f_l), \quad (5.31a)$$

$$\mathbf{C}_h^\dagger(\hat{\mathbf{P}}, f_l) = \left(\mathbf{C}_h^H(\hat{\mathbf{P}}, f_l) \mathbf{C}_h(\hat{\mathbf{P}}, f_l) \right)^{-1} \mathbf{C}_h^H(\hat{\mathbf{P}}, f_l), \quad (5.31b)$$

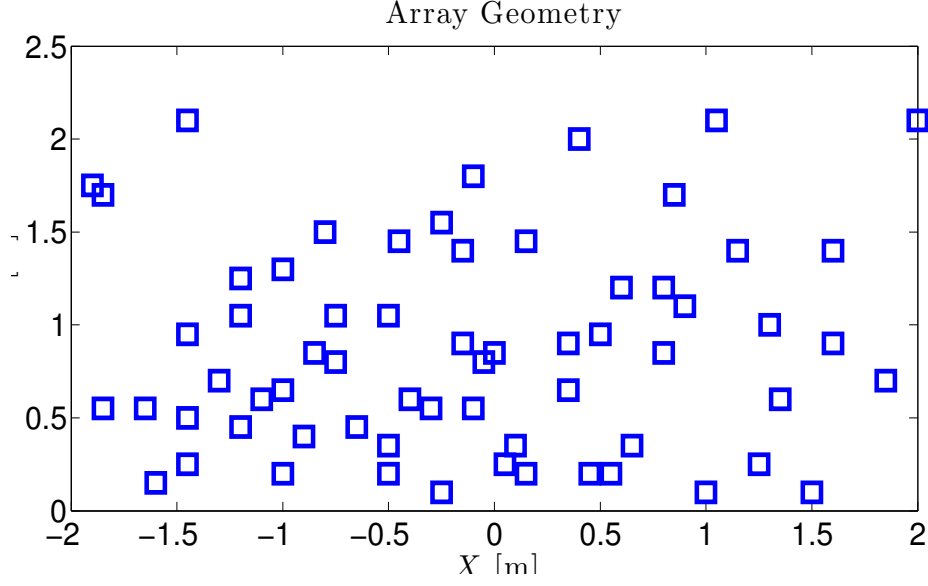


Figure 5.7: Array geometry in the the plane $z_0 = 4.5\text{m}$

5.6 Synthetic Data for Source Imaging

In the upcoming section, performance evaluation is conducted on synthetic data to compare the classical and the proposed methods. Multiple sources scenario are considered with various patterns of 2D-CD sources with different extensions widths Δ and powers σ_s^2 . The simplex based method (*fminsearch* in "Matlab") is used to find the maximum² of each cost function of the methods in sections 5.3 and 5.4. For the localization estimator, we assume that the method fails to localize the source when the error ($|\underline{\mathbf{p}} - \hat{\underline{\mathbf{p}}}|$) is larger than 20cm. We also assume a failure in the power estimation for the methods that provide an error value ($|\sigma_s^2 - \hat{\sigma}_s^2|$) greater than 3.66 dB.

5.6.1 Simulation Parameters

To meet the same setup of the car in the wind tunnel (see Fig.5.1), the simulation conditions are the same as the experiment carried out by Renault SAS [4, 5].

- The Non-Uniform Array (NUA) consists of $M = 64$ microphone sensors located on the $2 \times 4 \text{ m}^2$ vertical plane, where the important aperture of the array is the horizontal one as shown in Fig.5.7. The average aperture of sensor array is $A_p = 2\text{m}$. The NUA presents the advantage of ensuring almost the same performance as an ULA, where

²For synthetic data, initialization values for *fminsearch* are set to $x_s + \delta_x$, $y_s + \delta_y$, $\Delta + \delta_\Delta$ and $\beta + \delta_\beta$ where $\delta_x = \delta_y = 10\text{cm}$, $\delta_\Delta = 5\text{cm}$ and $\delta_\beta = 0.3$

the NUA has fewer sensors compared to the large number of sensors for the ULA case. This feature can decrease computation loads as discussed in [17].

- The distance between the array sensor plane and the source plane is $D=4.5\text{m}$. The aero-acoustic propagation speed in the open air is given by $c_0 \simeq 340\text{m/s}$. To estimate the correlation matrix given in Eq. (5.17), the total number of samples is $T = 1000$ snapshots.
- Concerning the simulated sources in Fig.5.8a and Fig.5.9a, we have considered six 2D-CD sources with different shapes. One Gaussian source overlaps a uniform source and the rest of the sources are in the surrounding (for the exact source parameters refer to Tab.5.2 and Fig.5.9a). Original source powers are in the range of $[0.14, 1]$ ($[-7.8, 0.65]\text{dB}$) which consists approximately in 8.5dB dynamic range (exact source powers are given in Tab.5.1).
- For the noisy background, we consider an i.i.d AGWN with $\sigma_n^2 = 0.86$ (-0.65 dB) as the noise power.
- For the synthetic data we do not consider the multipath propagation effects (ground reflection and wind refraction) but these physical effects will be considered in the wind tunnel application of the next chapter. Here, we focus on the comparison of the proposed methods.

5.6.2 Methods Comparison and Reconstruction of Shape Distributions

Methods comparison and reconstruction of the shape distribution h for the synthetic data at $f_0 = 1000\text{Hz}$ and $\text{SNR}=-0.65\text{ dB}$ are shown in Fig.5.8 for a three dimensional representation and in Fig.5.9 for a two dimensional representation.

Two parts are plotted in Fig.5.9. The first part is the image that shows the true sources positions in black thick cross (+) and the spatial distributions $h(x, y; \underline{\mathbf{p}}, \Delta)$ for each corresponding source. Meanwhile, the other colored markers ($\diamond, \times, \times, \bullet, \circ, \square, \triangle$) refer to the estimated position for different estimators. The second part, on the right of the image, is the color-map that shows the dynamic range of the estimated source powers³. Fig.5.9a shows the power spatial distributions $\sum_i \sigma_{s_i}^2 h(x, y; \underline{\mathbf{p}}_i, \Delta_i)$ with the true source parameters. For the others sub figures in Fig.5.9, h is plotted with the estimated parameters ($\hat{\underline{\mathbf{p}}}, \hat{\Delta}, \hat{\beta}$ and $\hat{\sigma}_s^2$) of each corresponding method.

It is important to note that, for the results discussion, we have associated the power and the localization estimators having the same distribution shape h like the GBF(U) and GBF – \mathbf{h}_{Unif} or using JPSSE and LS – \mathbf{h}_{RC} . Nevertheless, this association is an optional

³The colorbar values indicate the source power weighted by the 2D-CD source distribution $h(x, y; \underline{\mathbf{p}}, \Delta)$

choice and not an obligation. Example we can use the JPSSE for the localization and $\mathbf{GBF} - \mathbf{h}_{\text{RC}}$ for the power estimation like we are going to do in the next chapter.

First, in Fig.5.9b the CBF method provides erroneous localization of three sources (values can be compared in Tab.5.2). Indeed, assuming the point source model, the CBF seems to localize only the spatially spaced sources. Meanwhile, in Fig.5.9c the GBF with a Gaussian distribution only localizes one 2D-GCD source with an error estimation. It fails to localize the overlapped Gaussian and the rest of the sources. In Fig.5.9d the GBF with a uniform distribution only localizes two sources. The GBF method with Gaussian and uniform distribution is limited. The reason behind this behavior is the poor spatial resolution of such estimator in a multi-source scenario where the wide beam of the maximum and the important side-lobes in the cost function affects the other sources.

Next, in Fig.5.9e, the NFE method localizes the 2D-CD sources surrounded by the overlapping sources by providing good estimation of the parameter $\hat{\mathbf{p}}$ as shown in Tab.5.2. Meanwhile, for the overlapped case, NFE fails to accurately localize the 2D-GCD source while it provides a good estimation for the 2D-UCD source.

Then, in Fig.5.9f, the NF-DSPE(G) localizes the Gaussian distribution sources by providing a reliable estimation of the position ($\hat{\mathbf{p}}_1, \hat{\mathbf{p}}_3$ and $\hat{\mathbf{p}}_5$) and spread parameters ($\hat{\Delta}_1, \hat{\Delta}_3$ and $\hat{\Delta}_5$). NF-DSPE(G) is unable to localize the uniform distribution sources in the overlapped case and the 2D-RCCD source.

Next, in Fig.5.9g, NF-DSPE(U) shows a reliable estimation (Tab.5.2) for all the sources present in the simulation with a slight difference in localizing the 2D-GCD source in the overlapping case. Concerning the spread estimation, we can't make a fair comparison with sources of different types than the uniform. The reason is that Δ does not model the same extension in each type of distribution. Furthermore, NF-DSPE(U) does not reconstruct well the source shape because it uses the uniform shape with $\hat{\mathbf{p}}$, $\hat{\Delta}$ and $\hat{\sigma}_s^2$ to reconstruct the distribution.

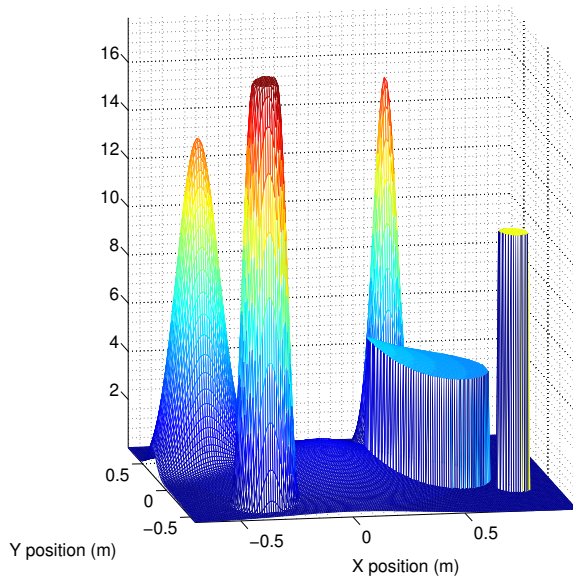
Finally, the proposed JPSSE method in Fig.5.9h allows an accurate localization for all the sources including the overlapped 2D-GCD and 2D-UCD sources. We can also note the shape distribution reconstruction delivered by the JPSSE for the uniform and Gaussian sources.

Concerning the power estimation, Tab.5.1 shows the values given by each method for all the sources. The CBF provides source power estimation with a large error. Meanwhile, the $\mathbf{GBF} - \mathbf{h}_{\text{Gaus}}$ and $\mathbf{GBF} - \mathbf{h}_{\text{Unif}}$ methods fail to provides accurate estimation. $\mathbf{LS} - \mathbf{point}$ reconstructs the sources power values for the sources that present a relatively minor spread and gives significant error for the other sources. $\mathbf{LS} - \mathbf{h}_{\text{Gaus}}$ presents serious deterioration of the power estimation especially for the localized 2D-GCD sources. For the power estimator that uses the uniform and the RC shape, estimation values are provided

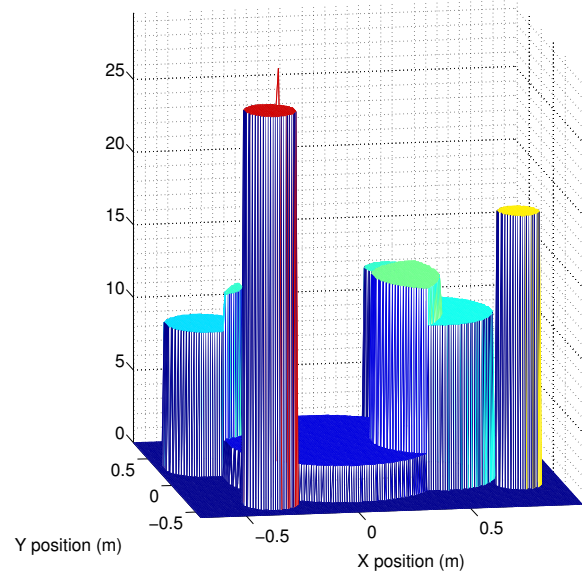
True & Estimated Sources Power						
	2D-GCD	2D-RCCD	2D-GCD	2D-UCD	2D-GCD	2D-UCD
	$\sigma_{s_1}^2$	$\sigma_{s_2}^2$	$\sigma_{s_3}^2$	$\sigma_{s_4}^2$	$\sigma_{s_5}^2$	$\sigma_{s_6}^2$
True Parameters	0.69	0.57	1	1	0.24	0.14
Estimated parameters						
	$\hat{\sigma}_{s_1}^2$	$\hat{\sigma}_{s_2}^2$	$\hat{\sigma}_{s_3}^2$	$\hat{\sigma}_{s_4}^2$	$\hat{\sigma}_{s_5}^2$	$\hat{\sigma}_{s_6}^2$
CBF	0.57	0.57	-	0.55	-	-
GBF – h_{Gaus}	1.23	-	-	-	-	-
GBF – h_{Unif}	1.12	-	-	1.34	-	-
LS – point	0.68	0.73	0.13	0.8	0.38	0.36
LS – h_{Gaus}	-	-	-	-	-	-
LS – h_{Unif}	0.91	1.13	1.74	2.51	0.48	0.51
LS – h_{RC}	0.9	1.1	2.13	2.3	0.49	0.49

Table 5.1: True and estimated parameters of Multi-sources.

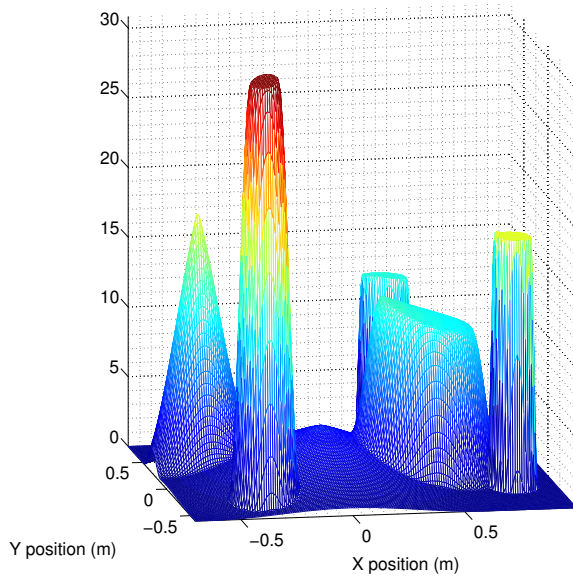
with a considerable error.



(a) True spatial power distribution



(b) Estimation of spatial power distribution with NF-DSPE(U)



(c) Estimation of spatial power distribution with JPSSE

Figure 5.8: The sum of spatial distribution of 2D-CD sources weighted by the power for each source. Each sub-figure represents the plot with true or estimated positions and powers.

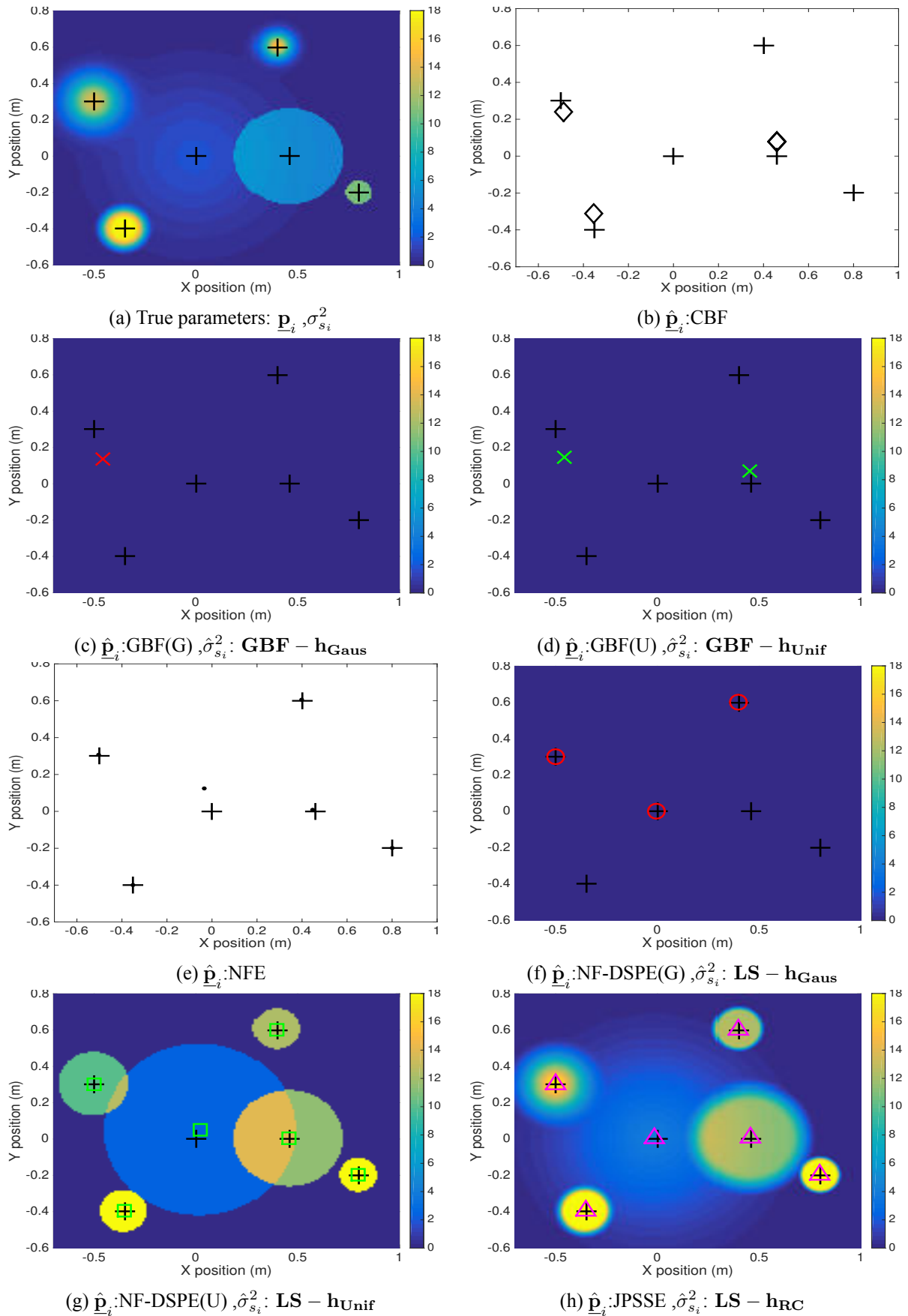


Figure 5.9: Spatial power distribution of 2D-CD sources with true and estimated positions and powers.

True & Estimated Positions Values (m)											
2D-GCD		2D-RCCD		2D-GCD		2D-UCD		2D-GCD		2D-UCD	
$\underline{\mathbf{p}}_1$	Δ_1	$\underline{\mathbf{p}}_2$	Δ_2	$\underline{\mathbf{p}}_3$	Δ_3	$\underline{\mathbf{p}}_4$	Δ_4	$\underline{\mathbf{p}}_5$	Δ_5	$\underline{\mathbf{p}}_6$	Δ_6
True Parameters	0.09	(-0.35,-0.4)	0.2	0.5	(0,0)	0.3	0.53	(0.4,0.6)	0.05	(0.8,-0.2)	0.13
Estimated parameters											
	$\hat{\underline{\mathbf{p}}}_1$	$\hat{\Delta}_1$	$\hat{\underline{\mathbf{p}}}_2$	$\hat{\Delta}_2$	$\hat{\underline{\mathbf{p}}}_3$	$\hat{\Delta}_3$	$\hat{\underline{\mathbf{p}}}_4$	$\hat{\Delta}_4$	$\hat{\underline{\mathbf{p}}}_5$	$\hat{\Delta}_5$	$\hat{\Delta}_6$
CBF	(-0.48,0.24)	-	(-0.35,-0.31)	-	-	-	(0.46,0.07)	-	-	-	-
GBF(G)	(-0.45,0.13)	0.16	-	-	-	-	-	-	-	-	-
GBF(U)	(-0.45,0.14)	0.57	-	-	-	-	(0.45,0.06)	0.58	-	-	-
NFE	(-0.5,0.3)	-	(-0.35,-0.39)	-	(-0.03,0.12)	-	(0.44,-0.00)	-	(0.39,0.6)	-	(0.8,-0.19)
NF-DSPE(G)	(-0.49,0.3)	0.09	-	-	(0,0)	0.3	-	-	(-0.39,0.6)	0.05	-
NF-DSPE(U)	(-0.49,0.3)	0.34	(-0.35,-0.39)	0.23	(0.02,0.04)	0.93	(0.45,0)	0.53	(0.39,0.6)	0.22	(0.79,-0.19)
JPSSE	(-0.49,0.3)	0.17	(-0.35,-0.39)	0.21	(-0.01,0)	0.56	(0.45,0)	0.52	(-0.39,0.6)	0.22	(0.79,-0.19)
	$\hat{\beta}_1$	2	$\hat{\beta}_2$	0.45	$\hat{\beta}_3$	2	$\hat{\beta}_4$	0.27	$\hat{\beta}_5$	0.14	$\hat{\beta}_6$
											0.15

Table 5.2: True and estimated parameters for the synthetic Multi-sources scenario (position, spread and shape). All sources frequencies are equal to $f_0 = 1\text{KHz}$ and $\text{SNR} = -0.65\text{dB}$. The color is used to provide a better values examination (red:2D-GCD, green:2D-UCD and magenta:2D-RCCD). However, symbols near estimator are also used to a better referring for the estimator in Fig.5.9.

Summarized remarks:

1. Beamforming presents serious limitations for the localization of the 2D-CD sources even with the distributed version (GBF). As cited earlier in previous chapters, this issue highly motivates us to use high resolution methods. Meanwhile, CBF and GBF provide good power estimation in spaced multi-source applications.
2. The NFE estimator that relies on the point source assumption has limited results for localizing sources with important spatial extension. It also fails in separating overlapped sources.
3. NF-DSPE with uniform distribution succeeds in localizing all the sources whereas with Gaussian distribution it fails in localizing the uniform sources. Therefore, the shape presents an essential element in the localization of the coherently distributed source. Methods that need to choose *a priori* the shape present some handicap to localize sources (like NF-DSPE).
4. Concerning the proposed JPSSE that considers multiple shapes. It tries to adapt the source shape by providing an additional shape parameter β . For this reason, JPSSE provides good parameters estimation of the source $\hat{\underline{p}}$. The proposed estimator presents good separation capability and accurately localizes sources in a complex case like the overlapped one.
5. Concerning the power estimation, the least square estimator provides better estimation than CBF and GBF power estimators. The reason relies in missing the localization of the majority of the sources. Source power estimators that are based on the source spread with different distributions, $\text{LS} - \mathbf{h}_{\text{Gaus}}$ and $\text{LS} - \mathbf{h}_{\text{Unif}}$ induce inaccurate power estimation in case of an *a priori* error selection of the shape.

5.7 Performance Analysis

In this section, we compare the performance of the three methods JPSSE, NF-DSPE and NFE presented in the subsections 5.3 and 5.4. For JPSSE, Raised Cosine 2D symmetrical distribution is used and the NF-DSPE performance is evaluated using two distributions : the Gaussian and the uniform ones. Here, the performance study is similar to the one studied in the third chapter. Meanwhile, in this chapter, we consider the two dimensional spread of the CD source parameterized in the Cartesian coordinates and we use a different array geometry of the one used in chapter three.

To investigate the performance, the root mean square error (RMSE) of the estimates is evaluated with a Monte-Carlo simulation of 20 independent executions. The simplex based

method is used to find the maximum of the cost function in equations (5.21), (5.22) and (5.24). Concerning the array geometry, the same NUA is used as described in 5.6.1. The snapshots number is fixed at 1000 for estimating the correlation matrix in equation (5.17).

5.7.1 Performance Versus SNR and Snapshots

For the first simulation, we consider: two 2D-CD sources and one point source presented in the parallel plane to the sensors plane and the configurations given in section 5.6. The sources are located in the plane z_0 for the following coordinates ($x_1 = 0.75m$, $y_1 = 0.75m$), ($x_2 = 1m$, $y_2 = 1m$), ($x_3 = 0.3m$, $y_3 = 0.6m$) and spreads of $\Delta_1 = 0m$, $\Delta_2 = 0.1m$, $\Delta_3 = 0.17m$.

The source at (0.75, 0.75) is a point whereas, the source at (1, 1) is a 2D Gaussian CD (2D-GCD) with the spread distribution given in Eq. (5.6) for $\Delta_x = \Delta_y = \Delta_2$. The source at (0.3, 0.6) is a 2D Uniformly CD (2D-UCD), with symmetrical distribution given by:

$$h(x, y; \Delta_3) = \begin{cases} 1/(\frac{\pi\Delta_3}{2})^2 & \text{if } r_3 \leq \frac{\Delta_3}{2}, \\ 0 & \text{Otherwise,} \end{cases} \quad (5.32)$$

r_3 represents the radius of the distribution and is expressed by: $r_3 = \sqrt{(x - x_3)^2 + (y - y_3)^2}$. We recall that the definition of the spread parameter Δ depends on the shape of the spread distribution. Concerning the RC function, Δ is the width of the function at half amplitude whereas it is the standard deviation for the Gaussian function.

The RMSE of the source coordinate x estimate is plotted in Fig.5.10a for the point source, in Fig.5.10b for the 2D-GCD and in Fig.5.10a for the 2D-UCD source.

When comparing the different estimators, the estimator based on the point source model (NFE) and as expected presents bad performance for locating distributed sources. Recalling the error analysis versus SNR performed in the chapter three where sources possess 1D spread distributions, we can adopt or find similar conclusions for the sources presenting a 2D spread distributions. The conclusions can be summarized by:

- NF-DSPE performance is highly dependent on the spread distribution. This estimator presents the best performance when the distribution used by the estimator is the same as the distribution of the source, but when the distributions are different, the performance has serious degradation. NF-DSPE presents high sensitivity to the mis-modeling of the spread distribution.
- For a given distribution of the source belonging to the 2D-RC family, the JPSSE with symmetrical distribution performance reaches that of NF-DSPE using the true

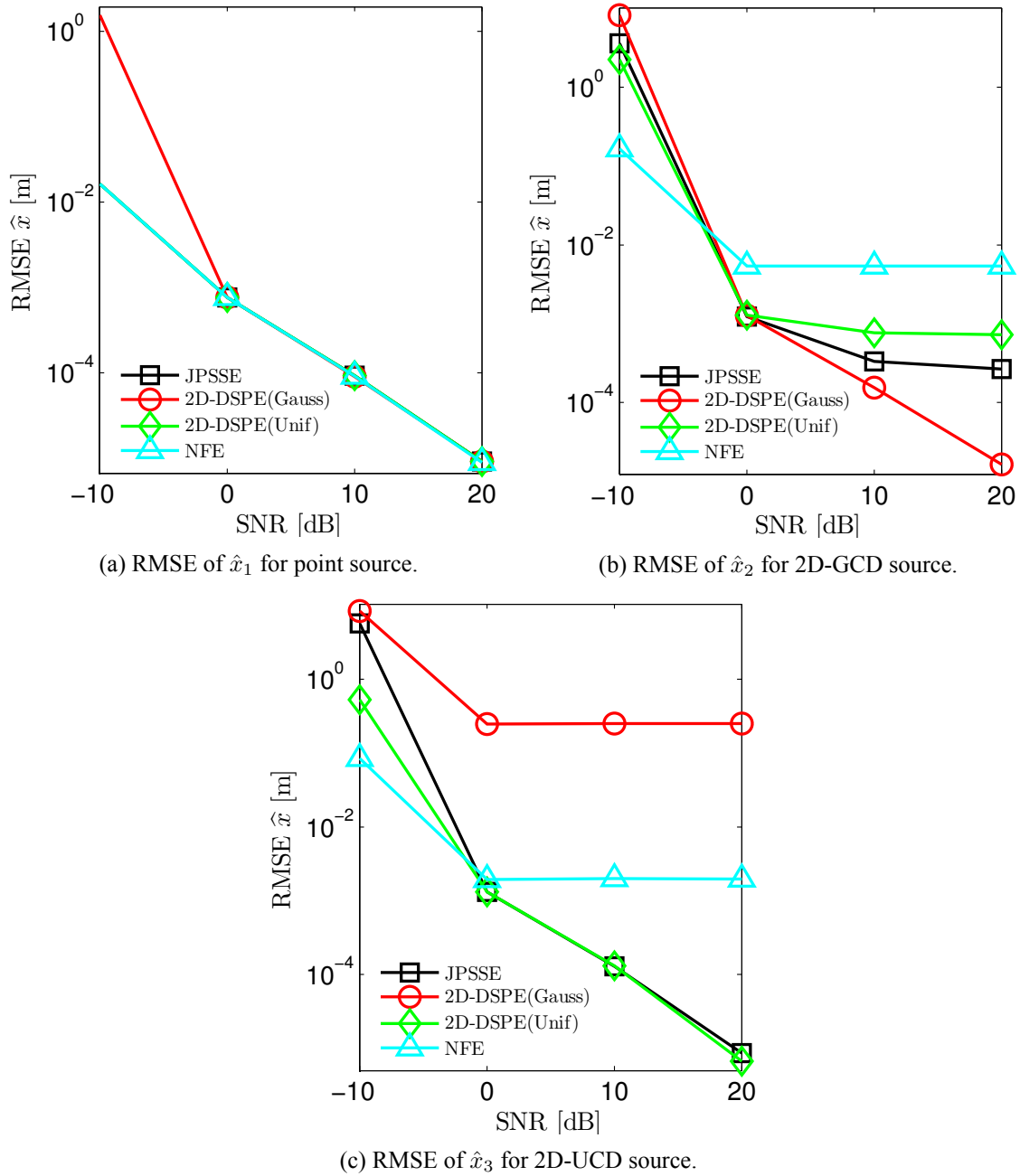
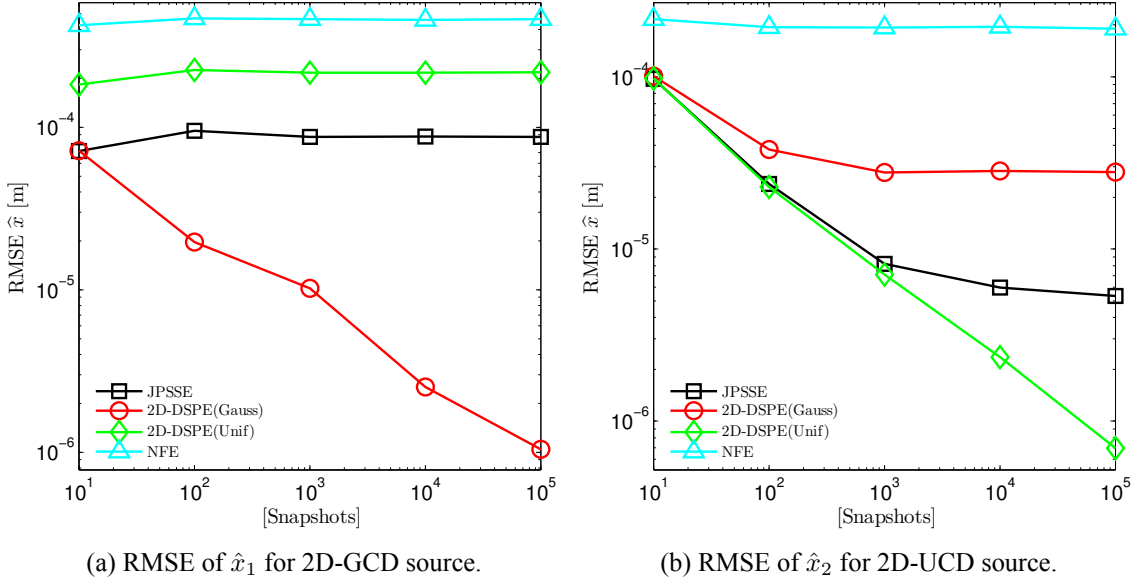


Figure 5.10: Root Mean Square Error of \hat{x} versus SNR for the three sources. True positions $x_1 = 0.75m$, $x_2 = 1m$ and $x_3 = 0.3m$.

Source	x (m)	y (m)	Δ	Shape	f_0
2D-GCD	1	1	0.1	-	1000 Hz
2D-UCD	0.3	0.6	0.17	symmetrical	1000 Hz

Table 5.3: Sources configurations considered for the performances analysis versus the snapshots.

Figure 5.11: Root Mean Square Error of \hat{x} versus snapshots for the three sources. True positions $x_1 = 1m$ and $x_2 = 0.3m$.

distribution (see UCD source in Fig. 5.10c). Consequently, estimating the fourth parameter (the shape parameter β) does not penalize the proposed estimator.

- JPSSE provides reliable estimation even when the distribution of the source does not belong to the RC family (see 2D-GCD source in Fig. 5.10b). This result shows that JPSSE using an RC family is quite robust to the shape of the 2D spread distribution of the source.
- NF-DSPE and JPSSE performance perfectly fit those of NFE when dealing with the point source (see Fig. 5.10a). It follows that JPSSE becomes particularly more interesting in multi-source scenarios where point and distributed sources with unknown shape distributions are mixed.

For the second simulation, a multi-source scenario is considered with one 2D-GCD source and another 2D-UCD source. The same parameters, as the first simulation, are considered and resumed in the following table 5.3.

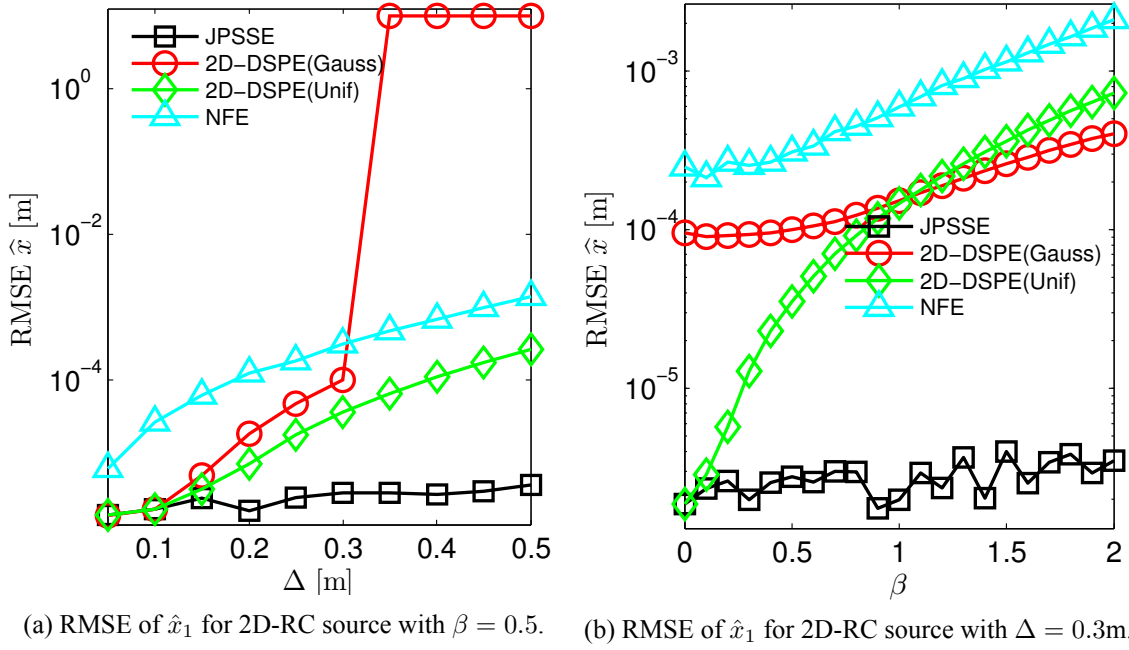


Figure 5.12: Root Mean Square Error of \hat{x} versus spread Δ and shape β for the 2D-RC source. True positions $x_1 = 0.3m$ and $y_1 = 0.6m$.

5.7.2 Performance Versus Source Spread Δ and Shape β

For this simulation, one source with a 2D Raised Cosine distribution is simulated for a frequency $f_0 = 1\text{KHz}$ with $x_1 = 0.3m$ and $y_1 = 0.6m$. The SNR value is equal to $20dB$ and $L = 10000$ snapshots. In the first case we show the variation versus Δ where the shape parameter was fixed at $\beta_1 = 0.5$. In the second case we show the variation versus β where the spread parameter was fixed at $\Delta_1 = 0.3m$.

5.8 Conclusion

In this chapter, we propose an appropriate aero-acoustic source modeling based on the CD source for the localization and power reconstruction. First, the CD model is generalized to consider a two dimensional spatial spread distribution and is parametrized following the Cartesian coordinates. We also account the same configuration setup for the wind tunnel application [4, 5]. Then, for localization, the *a priori* shape based estimator NF-DSPE(given in angular coordinates in chapters 2 and 3) is recalled in the two dimensional Cartesian coordinates form. Next, to overcome the unknown or imperfectly known source shape distributions and based on JADSSE, we present the JPSSE method. Conventional point

source methods used in the acoustic imaging like CBF are limited to their spatial resolution, whereas using high resolution methods like NFE provide accurate estimation. These methods do not consider the distributed aspect of the sources, therefore NF-DSPE (multi-dimensional MUSIC version with a priori shape selection) only localizes the corresponding shaped source. Afterwards, the JPSSE shows good results in the localization and provides a good shape reconstruction. In addition and based on the distributed source modeling, we propose two approaches for source power estimation. The first is based on the CBF, GBF pseudo-spectrums and the second is a least square estimator based on the array correlation matrix. Both methods overcome the challenge of reconstructing weak power sources. Then, simulations with synthetic data corresponding to the aero-acoustic wind tunnel application show that the proposed distributed estimators NF-DSPE and JPSSE provide better localization and shape distribution information (only for JPSSE) of these sources. Meanwhile, the beamforming variant (CBF and GBF) are limited in the closed multi-source scenario. Furthermore, the least square power estimator shows better results compared to the CBF and GBF methods. Finally, we investigate the localization estimator performance for the validation of the methods.

A person who never made a mistake never tried anything new.

Albert Einstein

6

Aero-acoustic Source Imaging

In the previous chapters, we have explained that the proposed estimators based on the CD source modeling are going to be used on the real data issued from the application of the car inside a wind tunnel [4, 5]. More precisely, the methods are applied for acoustic source localization and power estimation from microphone sensors measurements.

In this chapter, we firstly explain the configuration setup of the experimentation. Then, the methods proposed earlier are used with the consideration of the multi-path propagation principle [14] which consists in correcting the ground reflection and wind refraction. Next, we discuss the methods comparison considering the impact of a point and a CD source on the localization. Then, we discuss the influence of the spread distribution shape on the localization for the NF-DSPE with two distribution shapes (Gaussian and uniform). We also consider the case of CD source having different spreads over x and y coordinates ($\Delta_x \neq \Delta_y$) which can reveal new shapes.

The contributions of this chapter are the following:

- Improving the localization of the aero-acoustic source using the estimators that rely on the CD source assumption compared to the ones that use the point source.
- Exploring the impact of the source shape distribution on the localization and power estimation.
- Providing new tools to characterize aero-acoustic source by exploring the spread, shape distribution and power estimation.

6.1 Wind Tunnel Experimentation

Figures 6.1 and 6.3 show the representation of the vehicle in the center of the room, the microphone sensor array and the tunnel that simulates a wind flow of 160km/h to the front side of the car. The wind tunnel experiments carried out by Renault SAS [4, 5] is designed to simulate a fast traveling car on the high-way. These experiments aim to localize the aero-acoustic sources on the car body and to measure their powers. Once the sources are detected, decisions can be taken to improve acoustical comfort of the vehicle passengers.

6.1.1 Configuration Setup for Real Data

The parameters configuration and multi-path propagation effects are shown in Figures 6.1 and 6.2 and explained as follows:

- In Fig6.1, the curvature of the car side is relatively small compared to the distance between the car and the array plane. Thus, we suppose that all of the noisy sources are located in the same plane. The surface of the car side is around $160 \times 490 \text{ cm}^2$. This source plane is sampled into 33×99 pixels by using identical grid step of 5cm. For faster and more significant results, the criteria of the methods are only computed in the region of interest. This region consists in computing the criteria only inside the area of the vehicle perimeter.
- The sensor plane is the same as that discussed in chapter 5
- The real data consists of $T = 524288$ samples with the sampling frequency $f_s = 2.56 \times 10^4$ Hz. These samplings are divided into $J = 204$ segments with $L = 2560$ samples per segment as discussed in chapter 5. The working frequency is 2500Hz.
- We consider the ground reflection and wind refraction developed in [14] for the real data. For the actual propagation time $\tau_{i,m}$ and distance $d_{i,m}$ in Eq. (5.13), we consider the effect of equivalent source to make reflection and refraction correction.

Concerning the wind refraction, since the sensors are located outside the wind tunnel flow Fig.6.3, the acoustic medium is not uniform. As a result, the refraction will happen on the interface between the common air and wind flow. Indeed, in Fig.6.2, for sensor m in the array plane, it seems to receive another signal from the equivalent source i' , instead of the original source signal i , following a direct path $d_{i',m}$, during the same propagation time $\tau_{i',m}$, as if there was no wind influence in the tunnel.

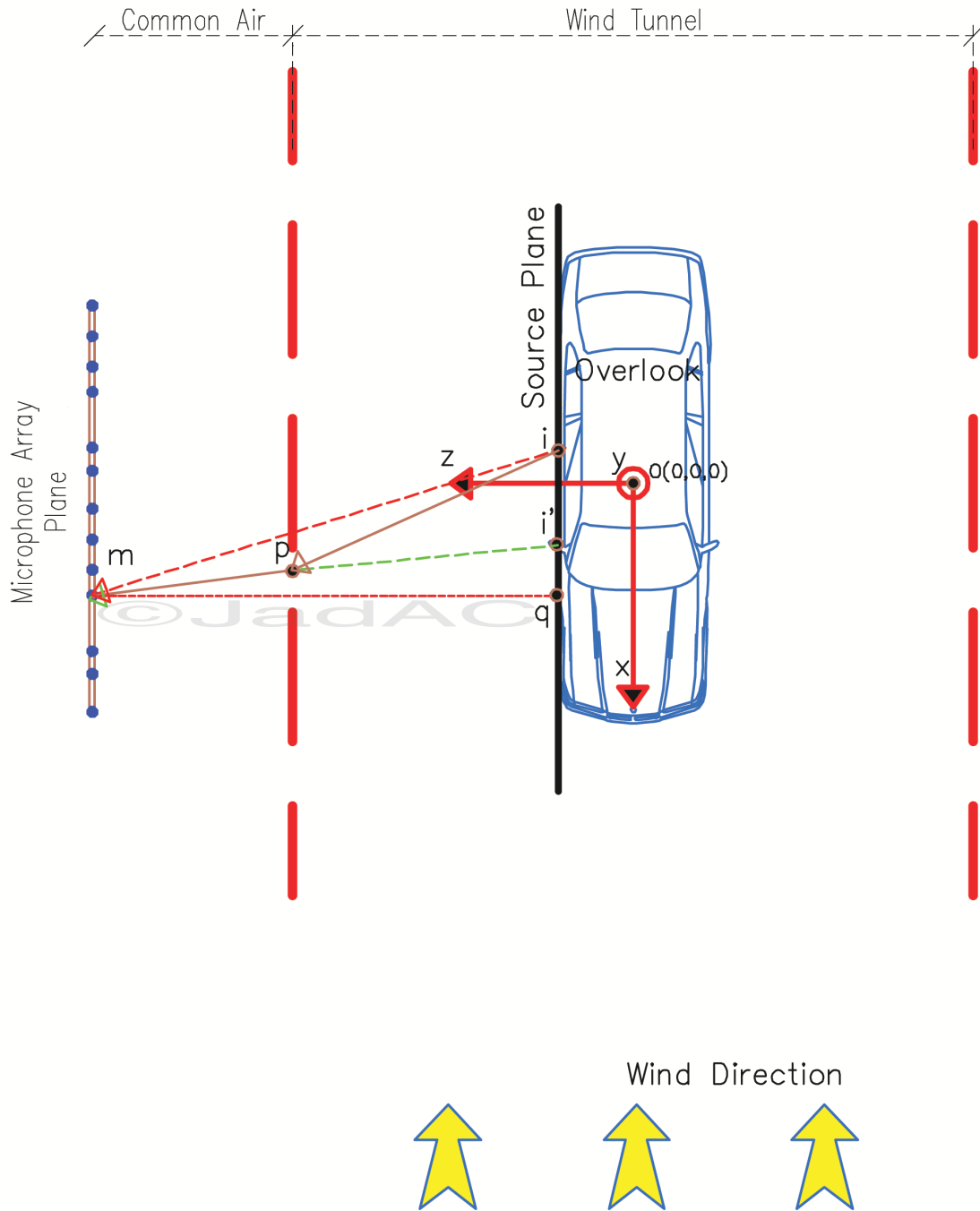


Figure 6.2: Overlook of the experimentation

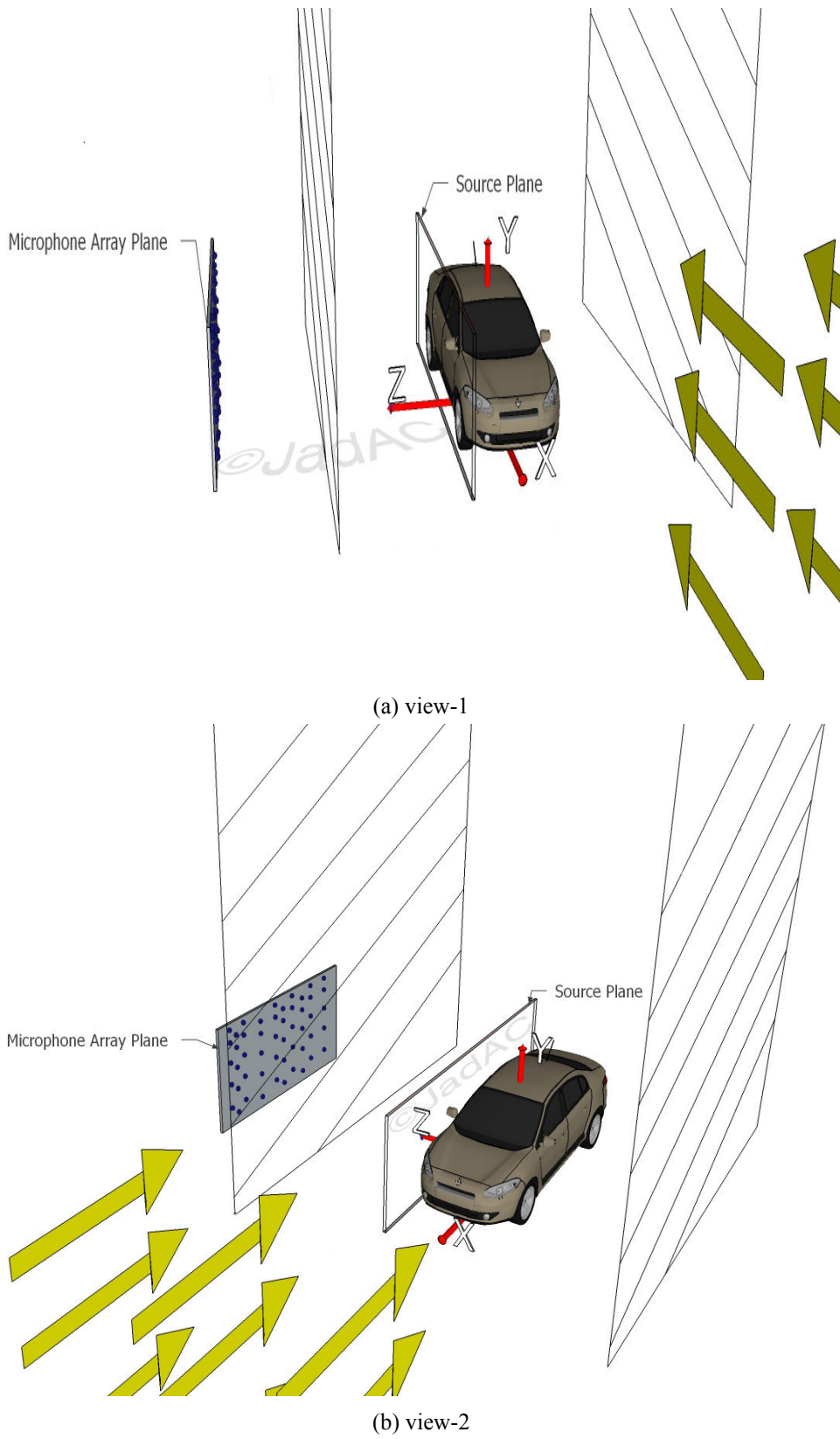


Figure 6.3: 3D Wind tunnel experimentation

Concerning the ground reflection in Fig.6.1, we use the mirror source signal for correction by considering $\tau_{-i,m}$ and $d_{-i,m}$ in the GSV computation Eq. (5.13).

Thus, we define a new GSV based on the GSV of Eq. (5.13) to take into consideration the above effects by summing another GSV with the coordinates of the mirror source $-i$ and accounting the new distance and propagation time within the GSVs (refer to [14] for the exact formulation of $d_{i,m}$, $\tau_{i,m}$, $\tau_{-i,m}$ and $d_{-i,m}$) as follows:

$$\tilde{\mathbf{c}}(\underline{\mathbf{p}}_i, \Delta_i; f_l) = \mathbf{c}(\underline{\mathbf{p}}_i, \Delta_i; f_l) + \varrho \mathbf{c}(\underline{\mathbf{p}}_{-i}, \Delta_{-i}; f_l). \quad (6.1)$$

$\underline{\mathbf{p}}_{-i} = [x_{si}, -y_{si}, z_{si}]$, ϱ represents the reflection coefficient whose value mainly depends on the ground conditions and is set to 0.9 according to [4, 5] in the real data simulations.

6.2 Comparison of The Localization Methods

In this section, first we compare the position estimation for the CBF, NFE and NF-DSPE with Gaussian and uniform shapes. Next, we give a closer look on the criteria of these methods. The aim is to evaluate the interest of: i) high resolution method compared to the standard method and ii) the CD source modeling compared to the source point assumption.

Position Estimation

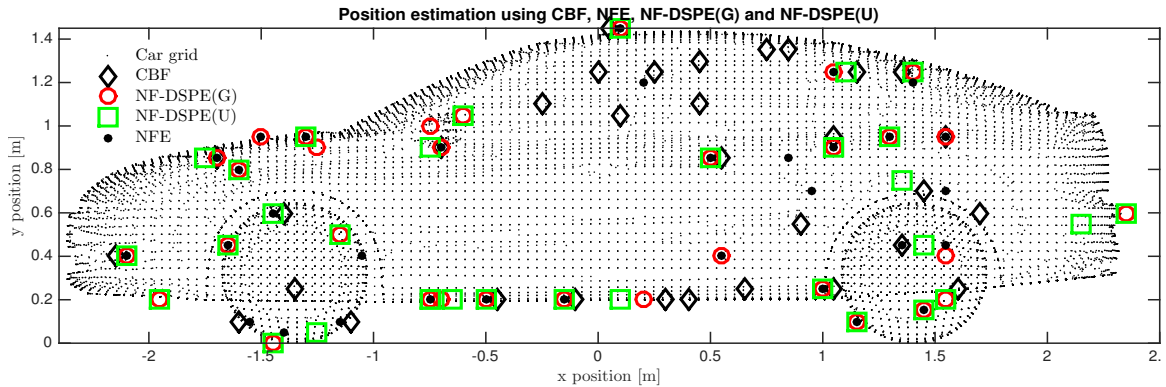


Figure 6.4: The estimated source position are compared on the grid of the car with the methods: CBF, NFE, NF-DSPE with Gaussian shape and NF-DSPE with uniform shape.

Fig.6.4 shows the estimated positions $\hat{\underline{\mathbf{p}}}$ of the 32 sources for the CBF (\diamond), the NFE (\bullet), the NF-DSPE(G) (\circ) and the NF-DSPE(U) (\square) with $\Delta_x = \Delta_y$.

Figure 6.4 shows that the sources are present in the car body area as following: front and back wheel, top front cover, front and back bumper, rear-view mirror, side windows, the lower part between the wheels and finally above the rear-wheel and near the back antenna.

Comparing the two point source estimators: The CBF is limited by its resolution capacity therefore it eliminates some of the relevant sources like around the rear-view mirror and the top front cover. CBF also presents weak source power range. The source located by the CBF in the interval $[-50, 50]$ cm for the x coordinates (in the side windshield area) presents an artifact caused by the important secondary lobes of the CBF method. The high resolution method based on the point source model, NFE, seeks for more relevant sources like the regions where the CBF fails. NFE presents a better resolution in position estimation and is able to depict more closed sources.

However, the estimator based on the distributed source, NF-DSPE, presents approximately the same results as NFE with a slight improvement concerning the estimated positions of the sources. Whereas, the NF-DSPE can also provide the estimated spread information of the source. For example, around the rear-view mirror, NF-DSPE can localize two to three CD sources (depending on the used shape) where the NFE credit is only one source. It is a satisfying matter to notice that certain sources preserve almost the same or shifted positions with NFE and NF-DSPE. On one hand, we can validate the source presence in this location and on the other hand the shifted positions of the sources appears to be more realistic (for example sources around the front wheel, the rear antenna located on the rear windshield and some other nearby sources). It is important to see that NF-DSPE can offer a better source characterization by giving the estimated source position $\hat{\mathbf{p}}$ and the estimated spread $\hat{\Delta}$ for an *a priori* selected source shape.

Criteria Comparison

Here, we compare the criteria computed for 32 sources of the CBF, NFE and NF-DSPE with the uniform shape in Fig.6.5, Fig.6.6 and Fig.6.7, Fig.6.8 respectively.

Comparing the peaks of the CBF and NFE criterion in Fig.6.5 and Fig.6.6, respectively, we notice the following:

- The peaks of the CBF are wider than the ones of the NFE. Also, as explained above, artifacts peaks are present in the side windshield window area caused by the important secondary lobes of the CBF method.
- Comparing the color bar of the two figures, the range of the values are smaller for the CBF than the NFE.

Given the above remarks we can easily review and confirm the selectivity of the NFE cri-

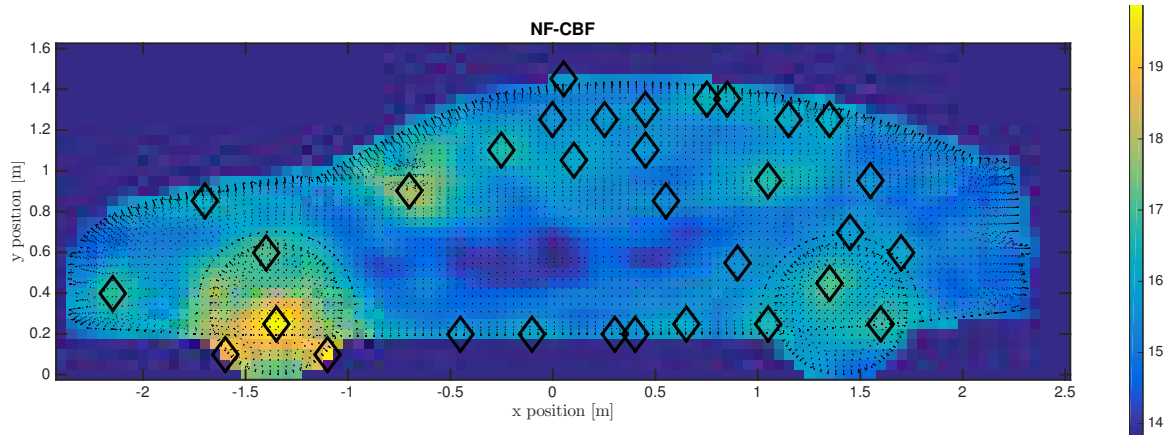


Figure 6.5: The CBF criterion of 32 point sources on the vehicle with the estimated positions depicted with a black diamond marker.

terion compared to the CBF one.

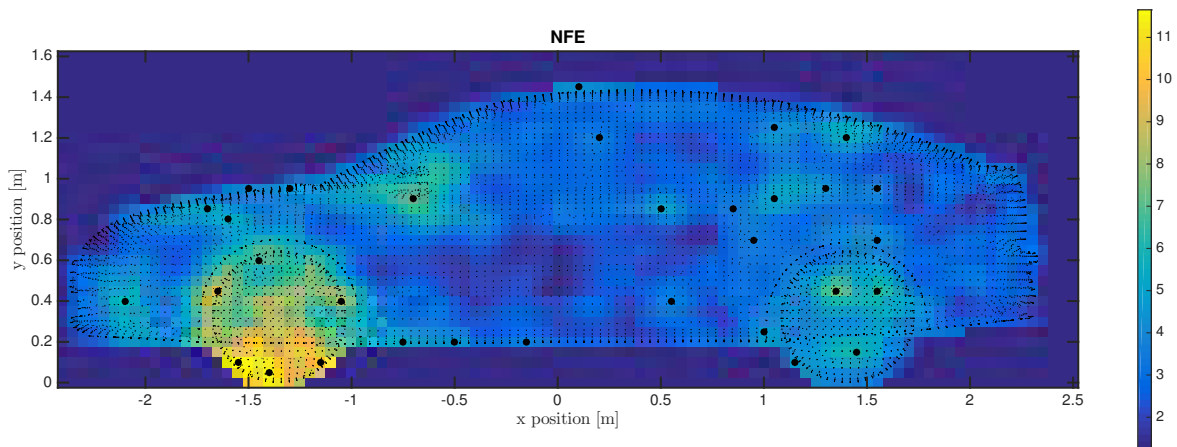


Figure 6.6: The NFE criterion of 32 point sources on the vehicle with the estimated positions depicted with a black point marker.

The NF-DSPE with uniform shape is a three dimensional cost function which consists in estimating the 32 maximum peaks values by maximizing the criterion following the x , y position and the Δ spread. In Fig.6.7 and Fig.6.8, we represent the NF-DSPE criterion for eight spread values in the range of 5 and 40 cm for a grid step of 5cm. The green square marker (\square) represents the source with the estimated location $\hat{\mathbf{p}}$ and spread $\hat{\Delta}$ using the NF-DSPE(U). To note that each set $(\hat{x}, \hat{y}, \hat{\Delta})$ of the estimated parameters locally maximize the NF-DSPE(U) criterion. For example, the estimated spread $\hat{\Delta} = 25$ cm of the rear-view

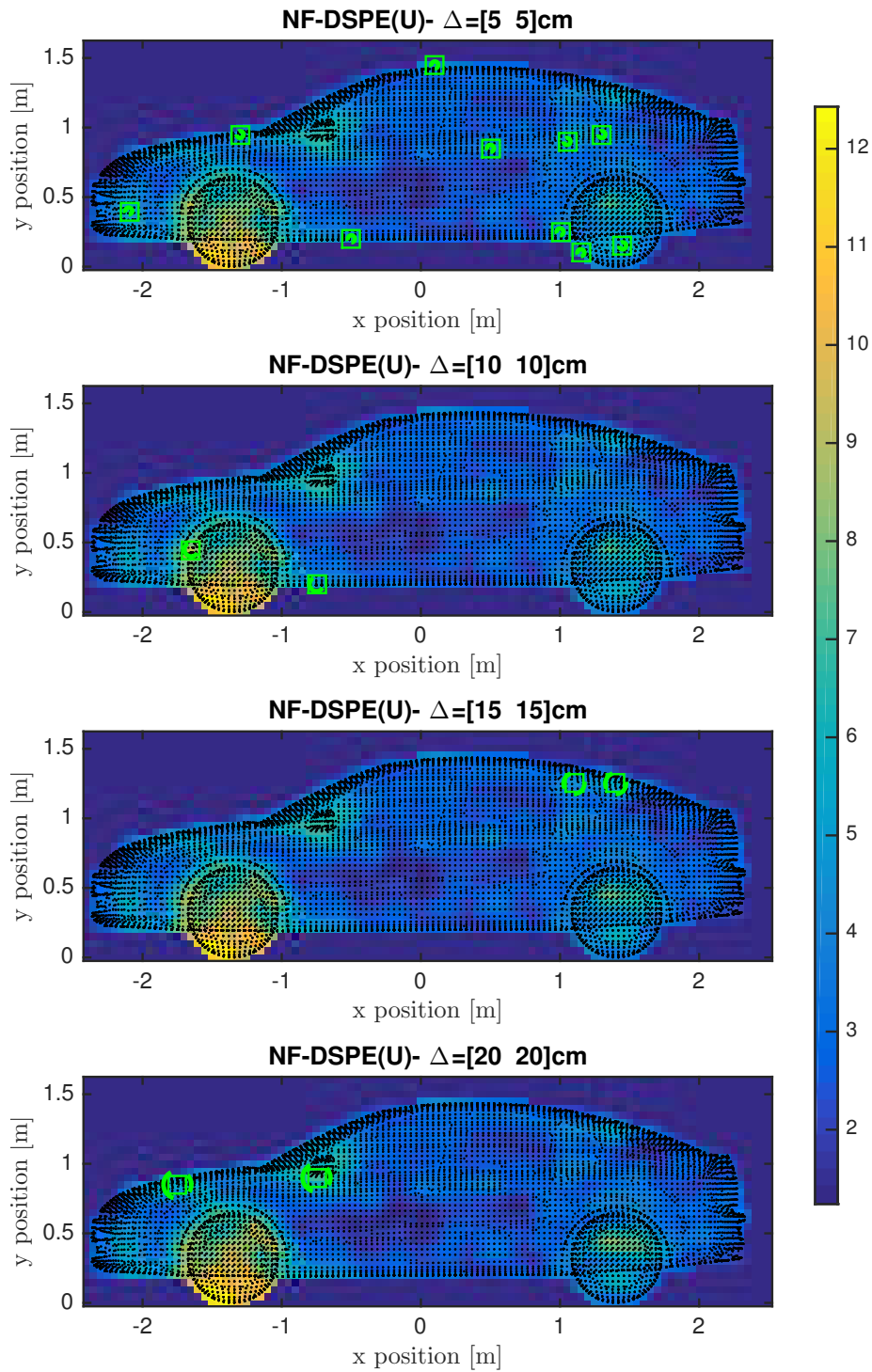


Figure 6.7: The NF-DSPE with uniform shape criterion of 32 CD sources on the vehicle with the estimated positions depicted with a green square marker where the dashed green circle represents the source spread. In this figure we plot the criterion for the spreads 5,10,15,20 cm.

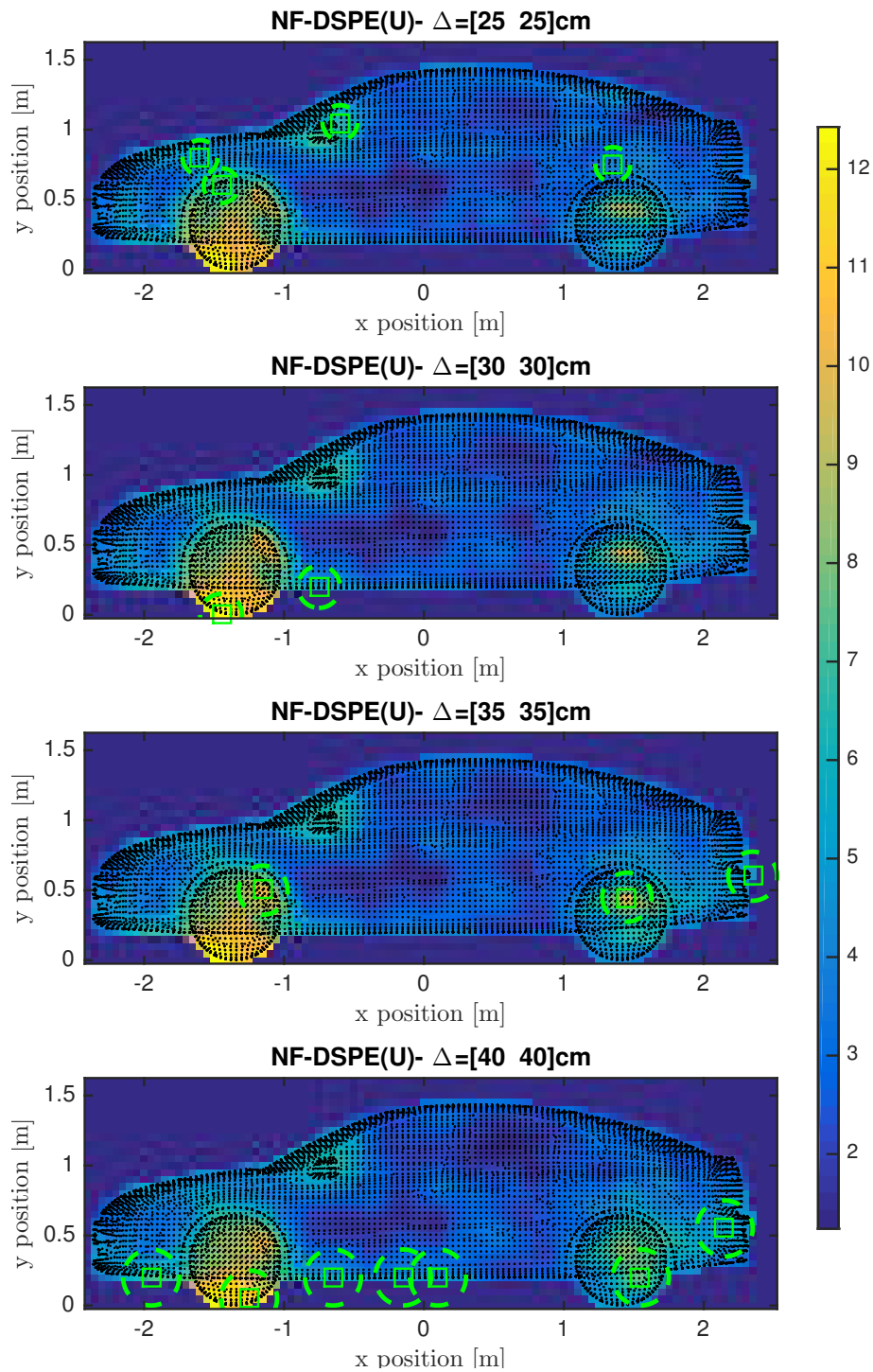


Figure 6.8: The NF-DSPE with uniform shape criterion of 32 CD sources on the vehicle with the estimated positions depicted with a green square marker where the dashed green circle represents the source spread. In this figure we plot the criterion for the spreads 25,30,35,40 cm.

mirror maximizes the NF-DSPE(U) criterion at this position. The diameter of the circle drawn with a thick dashed green line gives a visual representation of the spread $\hat{\Delta}$.

The important comments from the NF-DSPE criterion can be summarized as follows:

- The spread information taken into account as a third dimension to the NF-DSPE criterion provides a more selective cost function compared to the NFE criterion. Indeed, we can confirm this selectivity of the NF-DSPE criterion by showing peaks with more relevant values compared with the NFE criterion for example the rear-wheel of the vehicle. Moreover, we see this effect by retrieving the location of the main sources with approximately a unique spread.
- We see the presence of the sources having adjacent spreads. For example, the rear-view mirror which consists of one of the relevant noisy source in this application appears to be detected for the spread values of 20 and 25 cm. Indeed, a diameter of 20-25 cm appears to be physically acceptable for a rear-view mirror. Apparently, two closed sources are present in the region.

6.3 Influence of the Spread Distribution Shape

First, in this subsection, we show the impact of considering the spread distribution shape on the localization by comparing the NF-DSPE with the Gaussian and uniform shapes. Moreover we consider two cases for the spread variations: i) $\Delta_x = \Delta_y$ that consists in the symmetric circular shape and ii) $\Delta_x \neq \Delta_y$ which depicts an elliptical shape. Then, we show the results for the proposed JPSSE with the 2D-RC distribution considering $\Delta_x = \Delta_y$ where the shape parameter β varies between 0 and 2.

Next, we plot the spatial power distribution for each estimator. It consists in plotting the 2D-CD source distribution weighted by the source power estimation: $\sum_i \hat{\sigma}_{s_i}^2 h(x, y; \hat{\mathbf{p}}_i, \hat{\Delta}_i)$ for NF-DSPE and $\sum_i \hat{\sigma}_{s_i}^2 h(x, y; \hat{\mathbf{p}}_i, \hat{\Delta}_i, \hat{\beta}_i)$ for JPSSE.

We remember that the localized source using NF-DSPE and JPSSE are obtained by jointly maximizing these criteria function to x , y , Δ and β respectively. For the first subsection, we are only interested by showing the estimated source position \hat{x} , \hat{y} for method comparison. In the second subsection, the estimated source spread $\hat{\Delta}$ is visually provided and is equal to the diameter of the plotted circle for both the NF-DSPE and the JPSSE. Moreover, the estimated shape parameter $\hat{\beta}$ can be clearly noticed from the filled color in the circle. For example, a unique color represents a uniform shape distribution given for $\hat{\beta} \simeq 0$, a mix between a unique color and a smooth variation represents a particular shape of the RC distribution with $\hat{\beta} \simeq 0.5$, only a smooth color represents the bell shaped distribution for a $1 \leq \hat{\beta} \leq 2$, in particular a Gaussian shape appears for a $\hat{\beta} \simeq 1.5$.

6.3.1 Localization

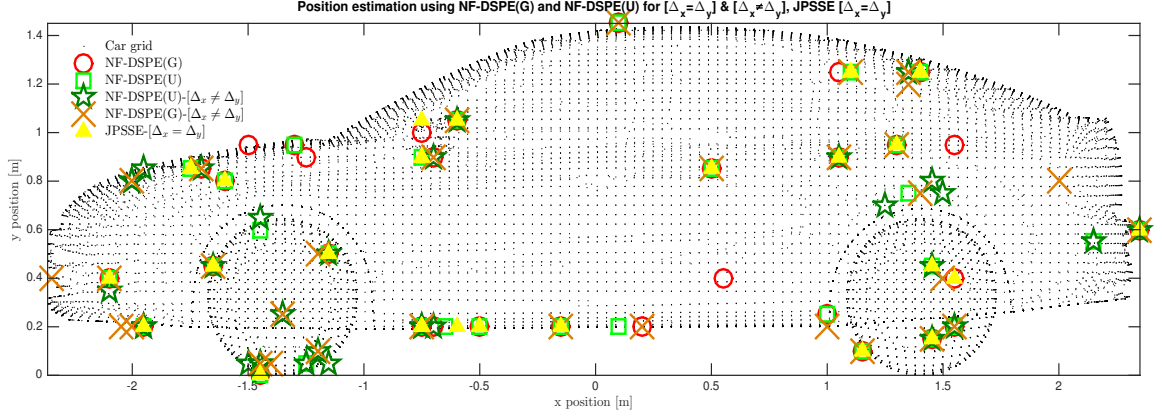


Figure 6.9: The estimated source position are compared on the grid of the car with the following methods: NF-DSPE(G), NF-DSPE(U) and JPSSE. The first NF-DSPE(G) and NF-DSPE(U) methods are used with either equal or different spreads over x and y . For the third JPSSE method, we only considers the equal spreads case.

Figure 6.9 shows the 32 estimated source positions for the NF-DSPE(U) (\square), NF-DSPE(G) (\circ) and JPSSE (\blacktriangle) where the spread over x is equal to the spread over y . We also consider a special case where the spread over x varies independently from the spread over y for NF-DSPE(U) (\star) and NF-DSPE(G) (\times).

Comparing all of the above cited estimators led us conclude that the shape of the spread distribution influence the position estimation. More precisely, if we take NF-DSPE(U) with $\Delta_x = \Delta_y$ and $\Delta_x \neq \Delta_y$ we see that at least nine sources change their positions. The same analysis goes for the NF-DSPE(G) where changing the spread variation changes at least seven sources positions. Now if we consider the JPSSE with NF-DSPE(G) and NF-DSPE(U), we notice that the main contributing sources are localized for all of the used shapes (NF-DSPE with Gaussian or uniform shape or JPSSE). We can also see a slight variation for other sources, indeed new source positions appear to be detected (around the rear-view mirror).

6.3.2 Spatial Power Distribution

Here, we present the spatial power distribution of the estimators NF-DSPE $\sum_i \hat{\sigma}_{s_i}^2 h(x, y; \hat{\mathbf{p}}_i, \hat{\Delta}_i)$ and JPSSE $\sum_i \hat{\sigma}_{s_i}^2 h(x, y; \hat{\mathbf{p}}_i, \hat{\Delta}_i, \hat{\beta}_i)$. We plot the sum of the spatial distributions h weighted by the source power. The spatial power distribution is plotted for NF-DSPE(G) and NF-DSPE(U) in Fig.6.10a and Fig.6.10b for $\Delta_x = \Delta_y$ (named circular) for 32 sources. NF-DSPE(G) and NF-DSPE(U) are plotted in Fig.6.11a and Fig.6.11b for $\Delta_x \neq \Delta_y$ (named

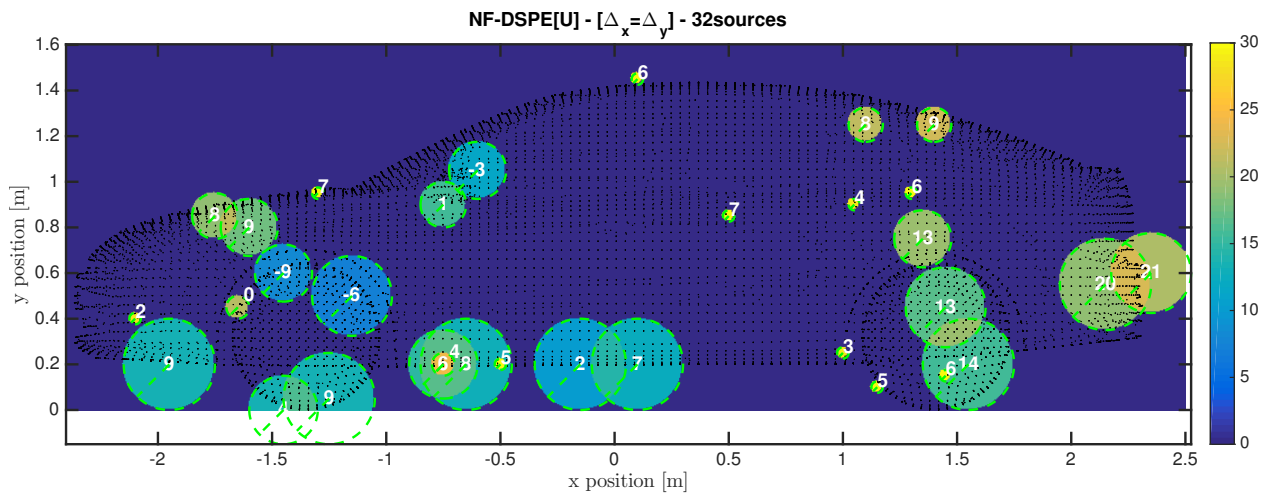
elliptical). The sources power estimates $\hat{\sigma}_s^2$ are obtained with the GBF and plotted in the center of the circle with a white color. Finally, spatial distribution for JPSSE are plotted in Fig.6.12.

The results interpretation:

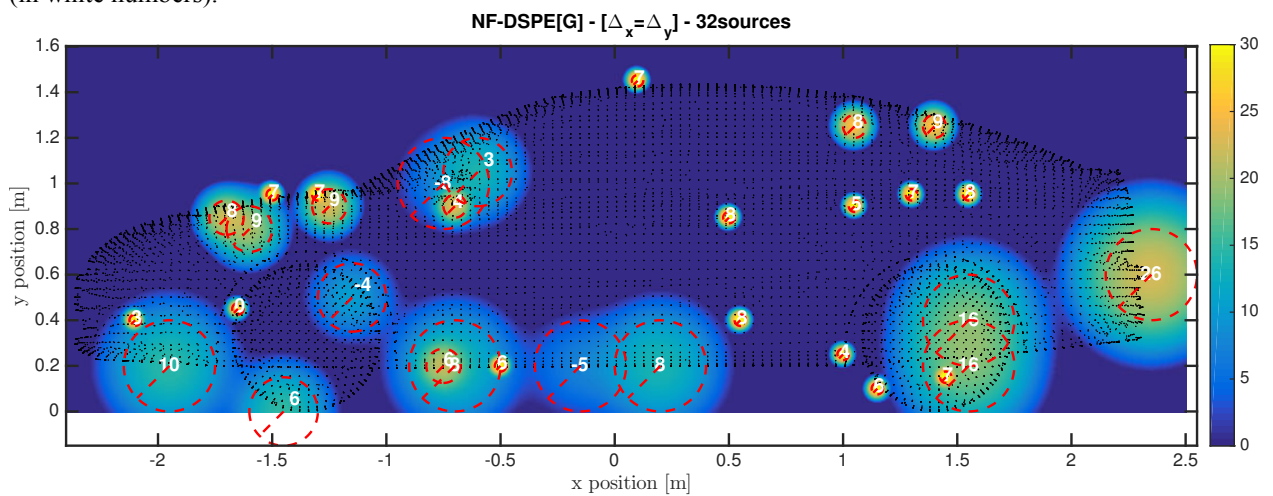
- Location of distributed sources: using the shape of the distributed sources we achieve a higher resolution in spatial position estimation where closed distributed sources are explored.
- Power estimation of the sources: unlike the point based method CBF, the power estimation method that relies on the CD source assumption like GBF with Gaussian or uniform shapes provides a wide dynamic range of source power ($\simeq 30\text{dB}$)
- Extension of the sources and shape of the sources. In the above figures we can clearly see the spatial extension of the aero-acoustic sources and how large they are. We can note that most of the sources are retrieved with the Gaussian or uniform shapes but with different spreads. However, with the JPSSE we can precise the shape of the source given the estimated shape parameter $\hat{\beta}$ where we can find uniform source shapes ($\beta \simeq 0$) and bell shaped source ($\beta \simeq 1, 5$ or $\beta \simeq 2$).

6.4 Conclusions

The previously proposed methods CBF, NFE, NF-DSPE and JPSSE were run on the real data from the wind tunnel application. We consider the effect of multi-path propagation by correcting the ground reflection and wind refraction. First, the results show that the localization can be improved using an estimator based on the distributed source assumption like NF-DSPE and JPSSE compared with a point source estimator like CBF or NFE. In addition, thanks to a higher spatial resolution capacity for the NF-DSPE and JPSSE, these estimators can reveal closed CD sources in some region of the car like the rear-view mirror. Second, concerning the power of the sources we increased for the power range estimation that allows to map both weak and powerful sources. Indeed, we increased the dynamic power range estimation of approximately 20 dB between using a power estimator based on the point source assumption and on the distributed one. We also increased this power range estimation by 8 dB by changing the shape of the sources. In conclusion, the model and the estimators of distributed source provide new tools to better characterize aero-acoustic sources.

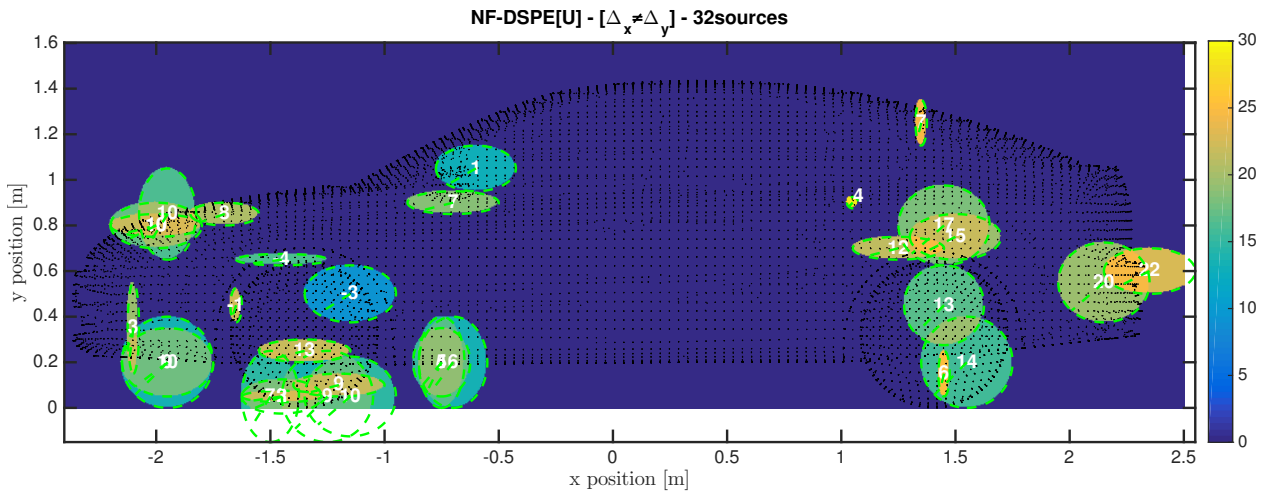


(a) NF-DSPE(U) with estimated positions, spreads (in dashed green line) and powers expressed in dB (in white numbers).

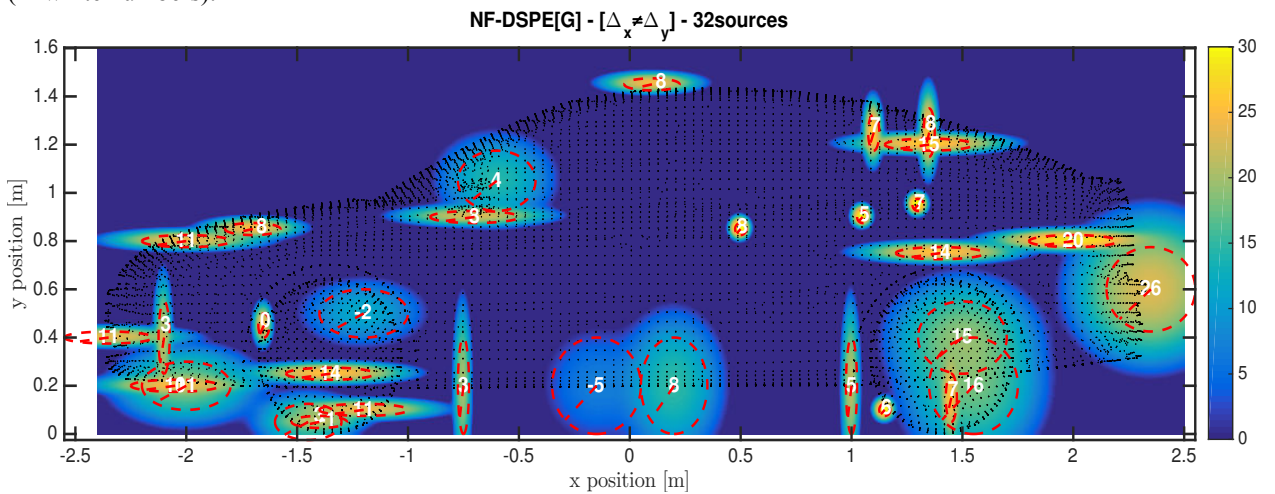


(b) NF-DSPE(G) with estimated positions, spreads (in dashed red line) and powers expressed in dB (in white numbers).

Figure 6.10: Spatial power distribution plots of 32 CD sources using NF-DSPE(U) and NF-DSPE(G) with circular symmetric shape on the vehicle with the estimated positions, spreads and powers expressed in dB (in white numbers).



(a) NF-DSPE(U) with estimated positions, spreads (in dashed green line) and powers expressed in dB (in white numbers).



(b) NF-DSPE(G) with estimated positions, spreads (in dashed red line) and powers expressed in dB (in white numbers).

Figure 6.11: Spatial power distribution plot of 32 CD sources using NF-DSPE(G) and NF-DSPE(G) with elliptical shape on the vehicle with the estimated positions, spreads (in dashed red line) and powers expressed in dB (in white numbers).

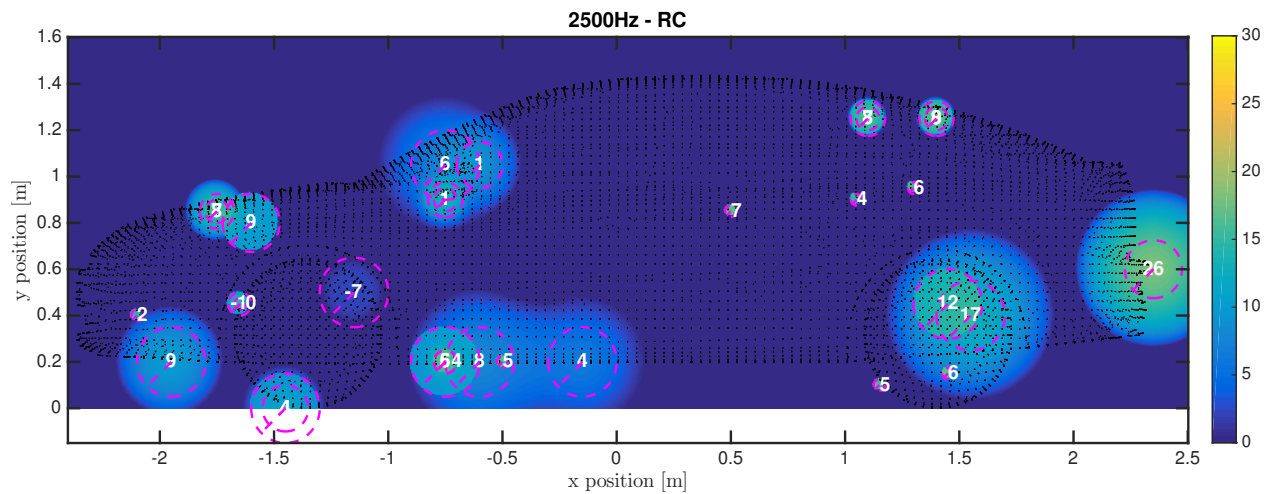


Figure 6.12: Spatial power distribution plots of 32 CD sources using JPSSE on the vehicle with estimated positions, spreads (in dashed magenta line), shapes and powers expressed in dB (in white numbers).

Yesterday is but today's memory, and tomorrow is today's dream.

Gebran Khalil Gebran

7

Conclusions and Perspectives

7.1 Conclusions

The thesis major challenges are the following. Firstly, taking into account the distributed source aspect in the near-field context. Secondly, we investigate the relevance of the source shape distribution where practically this information is not *a priori* provided for the localization. Next, we consider the distributed source aspect and the source shape distribution in a well known application for aero-acoustic source localization. Especially, we see how the spatial extension and the shape of the source can provide a better source localization and characterization.

The main conclusions in this thesis can be summarized as follows:

- In chapter three, we generalize the CD model and the DSPE to the near-field context, named NF-DSPE. We have shown that NF-DSPE is limited to the case where the angular spread distribution is known. Therefore, to deal with the unknown *a priori* shape distribution in practical situation, we propose the JADSSE estimator for the localization of coherently distributed (CD) sources. JADSSE consists in using a generic function family to describe the angular spread distribution so it jointly estimates the angle, the distance and the angular spread with an additional shape parameter. The advantages of JADSSE are summarized by:

- Ability to deal with an unknown angular spread distribution owed to the addi-

tional shape parameter of the generic function family.

- Robustness to various shapes of the angular distribution (RC, Gaussian, uniform and point), where the shape and spread parameters try to fit the source distribution.
 - Improved characterization of the source by providing an estimate of the angular spread distribution (and the shape of the source).
 - Angular resolution capacity in terms of DOA for overlapped sources.
- Chapter 4 was dedicated for proposing a generalized near-field approach for decoupled estimation. DDSPE [37], is generalized to the NF-DDSPE, for localizing CD sources in near-field when their angular shape distribution are unknown. This method is based on the decoupling of the estimation of the DOA and range from the estimation of the angular spread. Two assumptions are required for this method: i) a small angular spread around the DOA so that the Generalized Steering Vector (GSV) can be written as the element-wise product of the steering vector of the point source case and the Fourier transform vector of the angular shape distribution. ii) The second assumptions requires that the components of the Fourier transform vector are such that the first one is equal to one and the others are in decreasing order and positive. Under these assumptions, the NF-DDSPE method allows to estimate the DOAs and ranges of CD sources without knowing their angular shape distribution. However when the angular spread is required, the angular shape distribution must be known to use the NF-DDSPE.

Also, in this chapter we propose the DADSSE. It is the conjunction use of the JADSSE with NF-DDSPE to successively estimate the DOA and range and then their spread and shape estimation. The results show that the performance, in terms of parameters estimation and sources resolution, of these decoupling-based NF-DDSPE and DADSSE degrades when the assumptions are not verified. JADSSE outperforms NFE, NF-DDSPE, DADSSE and NF-DSPE when the assumed angular shape distribution is not the good one, and behaves nearly as NF-DSPE with the known angular shape distribution.

- In chapter 5, based on the CD model, we propose an appropriate aero-acoustic source modeling for the localization and power estimation. The model considers the two dimensional spread distribution of the aero-acoustic sources in a plane with the Cartesian coordinates form. The two dimensional aspect is interesting to reveal special structure of the noisy sources.

Then, for localization, the NFE, NF-DSPE and JPSSE are formulated in the Cartesian

coordinates to account the two dimensional spread distribution. Next, based on the distributed source modeling, we propose two approaches for source power estimation: the first is based on the GBF pseudo-spectrum and the second one is a least square estimator based on the array correlation matrix. We conclude that :

1. Conventional point methods used in the acoustic imaging like CBF are limited by their spatial resolution, and using high resolution methods like NFE fails in detecting overlapped sources. However, these methods do not consider the distributed aspect of the sources, therefore NF-DSPE (multi-dimensional MUSIC version with a priori shape selection) localizes better the corresponding shaped source.
 2. The JPSSE shows good localization results (where an *a priori* mismatch for the shape distribution is resolved) and provides a good shape reconstruction.
 3. Both of the methods overcome the challenge of reconstructing weak power sources and offering a wide dynamic power range.
- The proposed methods were run on the real data from the wind tunnel application in chapter 6 where we take into consideration the effect of multi-path propagation. The main conclusions are summarized as follows:
 - The localization of noisy sources on the car is improved using a distributed estimator (NF-DSPE) or an estimator without an *a priori* on shape selection (JPSSE) instead of using a point source estimator (CBF, NFE). A distributed source estimator like NF-DSPE and JPSSE are able to detect closed aero-acoustic sources.
 - The power range estimation of these noisy sources is increased using an estimator based on the distributed source assumption. Also, accounting the shape parameter for the source power estimation offers a higher dynamic power range compared to the distributed case.
 - The distributed source model and estimators provide new tools for mapping the noisy sources by accessing following source information: position, spread, power and shape.

7.2 Perspectives

To extend the thesis work, we propose the following ideas:

- Shape estimation with other localization methods. Inspired from the JADSSE, estimation of the shape of the angular distribution could be extended to others methods like Capon and ESPRIT to estimate the shape parameter.
-

- Developing a lower bound on the estimation variance for the distributed model in the near-field. We showed, by simulations, the asymptotic decrease of the RMSE for JADSSE in chapter three. It is interesting to develop a lower bound (the Cramer-Rao bound (CRB) for example) on the variance of any estimator of the DOA and the spread, then to compare it to the RMSE of JADSSE. The aim is to express in a closed form the variance bound of the source parameters like DOA, distance, spread and shape.
 - Reducing the computational complexity of JADSSE. This estimator consists of a joint optimization of a four dimensional (if we consider an angular or a one dimensional source spread) criterion, so it is interesting to seek for a lighter computational version of this estimator.
 - Eliminating the *a priori* knowledge on the shape distribution. An alternative way to compensate the unknown *a priori* source shape distribution is to consider a family of elementary predefined distribution shapes with fixed spreads. So the unknown source shape will be reconstructed using a certain number (to be defined depending on the spread) of these elementary distributions. This approach can be also applied for the NF-DDSPE and DADSSE in chapter four. Another approach consists in selecting the appropriate shape from a predefined dictionary using the sparse representation.
-

References

- [1] *Méthodes à haute résolution, traitement d'antenne et analyse spectrale (coll. Traitement du signal) - Sylvie Marcos.*
- [2] T. Abdellatif, P. Larzabal, and H. Clergeot. Performance study of a generalized subspace-based method for scattered sources. In *2000 IEEE International Conference on Acoustics, Speech, and Signal Processing, 2000. ICASSP '00. Proceedings*, volume 5, pages 3101--3104 vol.5, 2000. doi: 10.1109/ICASSP.2000.861193.
- [3] J. Abou Chaaya, J. Picheral, and S. Marcos. Localization of spatially distributed near-field sources with unknown angular spread shape. *Signal Processing*, 106:259--265, January 2015. ISSN 0165-1684. doi: 10.1016/j.sigpro.2014.07.007. URL <http://www.sciencedirect.com/science/article/pii/S0165168414003041>.
- [4] J.L. Adam, D. Ricot, F. Dubief, and C. Guy. Aeroacoustic simulation of automotive ventilation outlets. *The Journal of the Acoustical Society of America*, 123(5):3250--3250, May 2008. ISSN 0001-4966. doi: 10.1121/1.2933531. URL <http://scitation.aip.org/content/asa/journal/jasa/123/5/10.1121/1.2933531>.
- [5] J.L. Adam, D. Ricot, C. Lambourg, and A. Menoret. Correlated beamforming method for relevant aeroacoustic sources identification. SAE Technical Paper 2009-01-2234, SAE International, Warrendale, PA, May 2009. URL <http://papers.sae.org/2009-01-2234/>.
- [6] M. Bengtsson and B. Ottersten. Low-complexity estimators for distributed sources. *IEEE Transactions on Signal Processing*, 48(8):2185 --2194, August 2000. ISSN 1053-587X.
- [7] O. Besson and P. Stoica. Decoupled estimation of DOA and angular spread for a spatially distributed source. *IEEE Transactions on Signal Processing*, 48(7):1872--1882, 2000. ISSN 1053-587X.
- [8] G. Bienvenu and L. Kopp. Optimality of high resolution array processing using the eigensystem approach. *IEEE Transactions on Acoustics, Speech and Signal Processing*, 31(5):1235--1248, October 1983. ISSN 0096-3518. doi: 10.1109/TASSP.1983.1164185.
- [9] Daniel Blacodon and Georges Elias. Level Estimation of Extended Acoustic Sources Using a Parametric Method. *Journal of Aircraft*, 41(6):1360--1369, 2004. ISSN 0021-8669. doi: 10.2514/1.3053. URL <http://arc.aiaa.org/doi/abs/10.2514/1.3053>.

- [10] T. F. Brooks and W. M. Humphreys. A deconvolution approach for the mapping of acoustic sources (DAMAS) determined from phased microphone arrays. *Journal of Sound and Vibration*, 294(4–5):856–879, July 2006. ISSN 0022-460X. doi: 10.1016/j.jsv.2005.12.046. URL <http://www.sciencedirect.com/science/article/pii/S0022460X06000289>.
- [11] J. Capon. High-resolution frequency-wavenumber spectrum analysis. *Proceedings of the IEEE*, 57(8):1408–1418, August 1969. ISSN 0018-9219. doi: 10.1109/PROC.1969.7278.
- [12] J.C. Chen, R.E. Hudson, and K. Yao. Maximum-likelihood source localization and unknown sensor location estimation for wideband signals in the near-field. *IEEE Transactions on Signal Processing*, 50(8):1843–1854, August 2002. ISSN 1053-587X.
- [13] J.C. Chen, K. Yao, and R.E. Hudson. Source localization and beamforming. *IEEE Signal Processing Magazine*, 19(2):30–39, March 2002. ISSN 1053-5888. doi: 10.1109/79.985676.
- [14] N. Chu, A. Mohammad-Djafari, and J. Picheral. Robust Bayesian super-resolution approach via sparsity enforcing a priori for near-field aeroacoustic source imaging. *Journal of Sound and Vibration*, 332(18):4369–4389, September 2013. ISSN 0022-460X. doi: 10.1016/j.jsv.2013.02.037. URL <http://www.sciencedirect.com/science/article/pii/S0022460X13002101>.
- [15] N. Chu, J. Picheral, A. Mohammad-djafari, and N. Gac. A robust super-resolution approach with sparsity constraint in acoustic imaging. *Applied Acoustics*, 76:197–208, February 2014. ISSN 0003-682X. doi: 10.1016/j.apacoust.2013.08.007. URL <http://www.sciencedirect.com/science/article/pii/S0003682X13002016>.
- [16] C. EL Kassis and J. Picheral. Wideband zero-forcing MUSIC for aeroacoustic sources localization. In *Proceedings of the 20th European Signal Processing Conference*, pages 2283–2287, 2012.
- [17] C. El Kassis, J. Picheral, and C. Mokbel. Advantages of nonuniform arrays using root-MUSIC. *Signal Processing*, 90(2):689–695, February 2010. ISSN 0165-1684. doi: 10.1016/j.sigpro.2009.07.014. URL <http://www.sciencedirect.com/science/article/pii/S0165168409003272>.
- [18] E. Grosicki, K. Abed-Meraim, and Y. Hua. A weighted linear prediction method for near-field source localization. *IEEE Transactions on Signal Processing*, 53(10):3651–3660, October 2005. ISSN 1053-587X.
- [19] A. Hassanien, S. Shahbazpanahi, and A.B. Gershman. A generalized capon estimator for localization of multiple spread sources. *IEEE Transactions on Signal Processing*, 52(1):280–283, January 2004. ISSN 1053-587X.
- [20] Y.-D. Huang and M. Barkat. Near-field multiple source localization by passive sensor array. *IEEE Transactions on Antennas and Propagation*, 39(7):968–975, July 1991. ISSN 0018-926X.
-

- [21] H. Krim and M. Viberg. Two decades of array signal processing research: the parametric approach. *IEEE Signal Processing Magazine*, 13(4):67--94, July 1996. ISSN 1053-5888. doi: 10.1109/79.526899.
- [22] J. Lee, I. Song, H. Kwon, and S. Ro Lee. Low-complexity estimation of 2d DOA for coherently distributed sources. *Signal Processing*, 83(8):1789--1802, 2003. ISSN 0165-1684. doi: 10.1016/S0165-1684(03)00103-8. URL <http://www.sciencedirect.com/science/article/pii/S0165168403001038>.
- [23] J. Li, P. Stoica, and Z. Wang. Doubly constrained robust Capon beamformer. *IEEE Transactions on Signal Processing*, 52(9):2407--2423, September 2004. ISSN 1053-587X. doi: 10.1109/TSP.2004.831998.
- [24] J. Liang, X. Zeng, B. Ji, J. Zhang, and F. Zhao. A computationally efficient algorithm for joint range-DOA-frequency estimation of near-field sources. *Digital Signal Processing*, 19(4):596--611, July 2009. ISSN 1051-2004.
- [25] D. Papamoschou. Imaging of directional distributed noise sources. *Journal of Sound and Vibration*, 330(10):2265--2280, May 2011. ISSN 0022-460X. doi: 10.1016/j.jsv.2010.11.025. URL <http://www.sciencedirect.com/science/article/pii/S0022460X1000787X>.
- [26] R. Raich, J. Goldberg, and H. Messer. Bearing estimation for a distributed source via the conventional beamformer. In *Ninth IEEE SP Workshop on Statistical Signal and Array Processing, 1998. Proceedings*, pages 5--8, September 1998. doi: 10.1109/SSAP.1998.739320.
- [27] R. Roy and T. Kailath. ESPRIT-estimation of signal parameters via rotational invariance techniques. *IEEE Transactions on Acoustics, Speech and Signal Processing*, 37(7):984--995, July 1989. ISSN 0096-3518. doi: 10.1109/29.32276.
- [28] R. Schmidt. Multiple emitter location and signal parameter estimation. *IEEE Transactions on Antennas and Propagation*, 34(3):276 -- 280, March 1986. ISSN 0018-926X.
- [29] S. Shahbazpanahi, S. Valaee, and M.H. Bastani. Distributed source localization using ESPRIT algorithm. *IEEE Transactions on Signal Processing*, 49(10):2169 --2178, October 2001. ISSN 1053-587X.
- [30] Pieter Sijtsma. CLEAN based on spatial source coherence. *International Journal of Aeroacoustics*, 6(4):357--374, December 2007. doi: 10.1260/147547207783359459. URL <http://dx.doi.org/10.1260/147547207783359459>.
- [31] D. Storer and Arye Nehorai. Passive localization of near-field sources by path following. *IEEE Transactions on Signal Processing*, 42(3):677--680, March 1994. ISSN 1053-587X.
- [32] T. Trump and B. Ottersten. Estimation of nominal direction of arrival and angular spread using an array of sensors. *Signal Processing*, 50(1-2):57--69, April 1996. ISSN 0165-1684.
-

- [33] S. Valaee, B. Champagne, and P. Kabal. Parametric localization of distributed sources. *IEEE Transactions on Signal Processing*, 43(9):2144 --2153, September 1995. ISSN 1053-587X.
- [34] B.D. Van Veen and K.M. Buckley. Beamforming: a versatile approach to spatial filtering. *IEEE ASSP Magazine*, 5(2):4--24, April 1988. ISSN 0740-7467. doi: 10.1109/53.665.
- [35] A.J. Weiss and Benjamin Friedlander. Range and bearing estimation using polynomial rooting. *IEEE Journal of Oceanic Engineering*, 18(2):130--137, April 1993. ISSN 0364-9059.
- [36] N. Yuen and B. Friedlander. Performance analysis of higher order ESPRIT for localization of near-field sources. *IEEE Transactions on Signal Processing*, 46(3):709 --719, March 1998. ISSN 1053-587X.
- [37] A. Zoubir and Y. Wang. Efficient DSPE algorithm for estimating the angular parameters of coherently distributed sources. *Signal Processing*, 88(4):1071--1078, 2008. ISSN 0165-1684.
- [38] A. Zoubir and Y. Wang. Performance analysis of the generalized beamforming estimators in the case of coherently distributed sources. *Signal Processing*, 88(2):428--435, February 2008. ISSN 0165-1684. doi: 10.1016/j.sigpro.2007.08.010. URL <http://www.sciencedirect.com/science/article/pii/S0165168407002903>.
- [39] A. Zoubir and Y. Wang. Robust generalised Capon algorithm for estimating the angular parameters of multiple incoherently distributed sources. *IET Signal Processing*, 2(2):163--168, 2008. ISSN 1751-9675. doi: 10.1049/iet-spr:20070160.
- [40] A. Zoubir, Y. Wang, and P. Charge. The generalized beamforming techniques for estimating the coherently distributed sources. In *The European Conference on Wireless Technology, 2005*, pages 157--160, October 2005. doi: 10.1109/ECWT.2005.1617679.
-